JPRS L/9542

11 February 1981

USSR Report

ELECTRONICS AND ELECTRICAL ENGINEERING

(FOUO 2/81)

FBIS FOREIGN BROADCAST INFORMATION SERVICE

NOTE

JPRS publications contain information primarily from foreign newspapers, periodicals and books, but also from news agency transmissions and broadcasts. Materials from foreign-language sources are translated; those from English-language sources are transcribed or reprinted, with the original phrasing and other characteristics retained.

Headlines, editorial reports, and material enclosed in brackets [] are supplied by JPRS. Processing indicators such as [Text] or [Excerpt] in the first line of each item, or following the last line of a brief, indicate how the original information was processed. Where no processing indicator is given, the information was summarized or extracted.

Unfamiliar names rendered phonetically or transliterated are enclosed in parentheses. Words or names preceded by a question mark and enclosed in parentheses were not clear in the original but have been supplied as appropriate in context. Other unattributed parenthetical notes within the body of an item originate with the source. Times within items are as given by source.

The contents of this publication in no way represent the policies, views or attitudes of the U.S. Government.

APPROVED FOR RELEASE: 2007/02/08: CIA-RDP82-00850R000300080025-3

JPRS L/9542

11 February 1981

USSR REPORT

ELECTRONICS AND ELECTRICAL ENGINEERING

(FOUO 2/81)

CONTENTS

CERTAIN ASPECTS OF COMPUTER HARD AND SOFT WARE: CONTROL, AUTOMATION, TELEMECHANICS, TELEMETERING, MACHINE DESIGNING AND PLANNING

UDC 621.373.826

IMAGE OUTLINING BY A BINARY FILTER IN PATTERN RECOGNITION SYSTEMS

Moscow RADIOTEKHNIKA I ELEKTRONIKA in Russian Vol 25, No 10, Oct 80 pp 2261-2263
manuscript received 16 Jul 79

[Article by I. I. Sal'nikov]

[Text] Pattern recognition with respect to nonorthogonal features frequently makes use of initial image preprocessing techniques [Ref. 1], one such method being outlining by a binary filter. This method is extensively used because of the simplicity of its realization since the binary filter is nothing more than an opaque screen of radius r placed in the frequency plane [Ref. 2]. In the literature [Ref. 3] it has been shown that preliminary outlining reduces the coefficient of mutual correlation between different classes of images to be recognized, which should lead to an improvement in the effectiveness of recognition. However, if consideration is taken of the noise background of the initial images, the improvement in recognition effectiveness with outlining is not so apparent since one should observe a reduction in signal-to-noise ratio in addition to the reduced mutual correlation coefficient.

Let us determine the conditions under which a reduction is observed in the coefficient of mutual correlation between functions that describe images to be recognized, and also the change in signal-to-noise ratio after outlining by a binary filter.

To simplify the analysis, we will consider the one-dimensional case, and the images to be recognized will be taken as certain signals $s_k(x)$ and $s_j(x)$ with band of the spatial energy spectrum $2\Omega_k$ and $2\Omega_j$ respectively, with $\Omega_k < \Omega_j$. Moreover, we shall restrict ourselves to consideration of simple signals for which the product of the duration multiplied by the band of the spectrum is close to unity $(2X_{k,j})(2\Omega_{k,j})/2\pi = 1$. Let us express the mutual correlation function of $s_k(x)$ and $s_j(x)$ after binary filtration with zero space shift in terms of the mutual energy spectrum $G_{kj}^{(1)}(\omega)$ with band $2\Omega_{kj}$ [Ref. 4]:

$$(1) \qquad B_{kj}^{(1)}(0) = \frac{1}{4\pi}\int_{-\infty}^{\infty} G_{kj}^{(1)}(\omega)\,d\omega = B_{kj}(0) - \frac{1}{4\pi}\int_{-\Omega_f}^{\Omega_f} G_{kj}(\omega)\,d\omega,$$

where $2\Omega_j$ is the elimination bandwidth of the binary filter. Considering the nonnegative nature of energy spectra, and also the relation [Ref. 5] $G_{kj}(\omega) \leqslant [G_k(\omega) \times G_j(\omega)]^{1/2}$, we get the following expression:

$$(2) \qquad B_{kj}^{(1)}(0) \geqslant B_{kj}(0)\left[1 - \frac{1}{4\pi}\int_{-\Omega_f}^{\Omega_f} [G_k(\omega)G_j(\omega)]^{1/2}\,d\omega \Big/ \frac{1}{4\pi}\int_{-\Omega_{kj}}^{\Omega_{kj}} G_{kj}(\omega)\,d\omega\right].$$

We will assume that $\Omega_{kj} = \Omega_k$ for $\Omega_k \leqslant \Omega_j$, and $\Omega_{kj} = \Omega_j$ for $\Omega_k > \Omega_j$. These conditions influence the limits of integration in (2). We then use a Schwarz inequality to replace the integral of the product of spectra with a product of integrals. In integrating $G_j(\omega)$ in elimination band $2\Omega_j$, we assume that $G_j(\omega) = G_{j0}$ since $\Omega_j \leqslant \Omega_k < \Omega_j$, that is

$$\frac{1}{4\pi}\int_{-\Omega_f}^{\Omega_f} G_j(\omega)\,d\omega = \frac{G_{j0}\Omega_f}{2\pi}. \tag{3}$$

In integrating $G_k(\omega)$ in the elimination band where $\Omega_k < \Omega_j$ consideration must be taken of the form of the spectrum $G_k(\omega)$, which will appreciably affect the energy spectrum of the eliminated part. We account for the shape of the spectrum by some shape factor α which we define as the ratio of the band of a rectangular spectrum $2\Omega_{k0}$ with area equal to that above the curve $G_k(\omega)$ and ordinate $G_k(0)$, to $2\Omega_k$ -- the bandwidth of the spectrum on level 0.1:

$$\alpha = \Omega_{k0}/\Omega_k. \tag{4}$$

The shape factor shows the deviation of the shape of the spectrum from rectangular, for which $\alpha = 1.0$ (Fig. 1). For the average signal power in the elimination band, we get a relation that considers the shape of the spectrum:

$$\frac{1}{4\pi}\int_{-\Omega_f}^{\Omega_f} G_k(\omega)\,d\omega = \frac{1}{2\pi}\{G_k(\Omega_f)\Omega_f + [G_k(0) - G_k(\Omega_f)]\Omega_f\alpha\}. \tag{5}$$

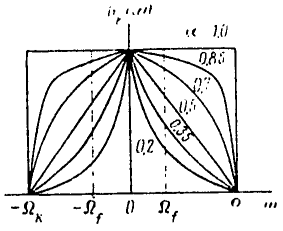

Fig. 1

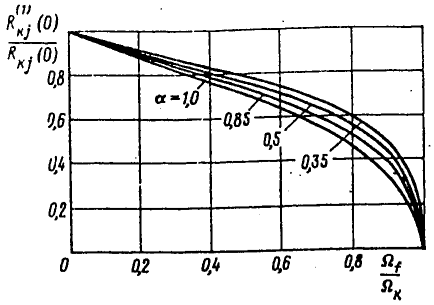

Fig. 2

The difference $G_k(0) - G_k(\Omega_j)$ appearing in (5) was determined with the given assumptions:

$$\frac{G_k(0) - G_k(\Omega_f)}{G_k(0)} = \left(\frac{\Omega_f}{\Omega_k}\right)^{4\alpha^2}. \tag{6}$$

With consideration of (6), expression (5) takes the form

$$\frac{1}{4\pi}\int_{-\Omega_f}^{\Omega_f} G_k(\omega)\,d\omega = \frac{G_k(0)\Omega_f}{2\pi}\left[1 - \left(\frac{\Omega_f}{\Omega_k}\right)^{4\alpha^2}(1-\alpha)\right], \tag{7}$$

at $\Omega_j = \Omega_k$ we will have

$$\frac{1}{4\pi}\int_{-\Omega_k}^{\Omega_k} G_k(\omega)\,d\omega = \frac{G_k(0)\Omega_k\alpha}{2\pi}. \tag{8}$$

Finally we get the following expression for the mutual correlation function:

$$B_{kj}(0) \geqslant B_{kj}(0)\left\{1-\frac{\Omega_f}{\Omega_k}\sqrt{\frac{1}{\alpha}\left[1-\left(\frac{\Omega_f}{\Omega_k}\right)^{4\alpha^2}(1-\alpha)\right]}\right\}. \tag{9}$$

To determine the mutual correlation coefficient $R_{kj}^{(1)}(0)$ it is necessary to normalize (9) with respect to $B_k^{(1)}(0)$ and $B_j^{(1)}(0)$, which we define analogously to $B_{kj}^{(1)}(0)$:

$$\begin{aligned} B_k^{(1)}(0) &= B_k(0)\left\{1-\frac{\Omega_f}{\Omega_k\alpha}\left[1-\left(\frac{\Omega_f}{\Omega_k}\right)^{4\alpha^2}(1-\alpha)\right]\right\}, \\ B_j^{(1)}(0) &= B_j(0)\left[1-\frac{\Omega_f}{\Omega_{j0}}\right], \end{aligned} \tag{10}$$

where $2\Omega_{j0}$ is defined the same as in (4). Then for the mutual correlation coefficient of functions $s_k(x)$ and $s_j(x)$ we can get the relation

$$R_{kj}^{(1)}(0) \geqslant R_{kj}(0)\frac{1-\frac{\Omega_f}{\Omega_k}\sqrt{\frac{1}{\alpha}\left[1-\left(\frac{\Omega_f}{\Omega_k}\right)^{4\alpha^2}(1-\alpha)\right]}}{\sqrt{1-\frac{\Omega_f}{\Omega_k\alpha}\left[1-\left(\frac{\Omega_f}{\Omega_k}\right)^{4\alpha^2}(1-\alpha)\right]}\sqrt{1-\frac{\Omega_f}{\Omega_{j0}}}}. \tag{11}$$

The equality in this expression defines the lower limit of the reduction of the mutual correlation coefficient (Fig. 2). The exact expression depends on the form of functions $s_k(x)$ and $s_j(x)$.

Let us determine the signal-to-noise ratio as the ratio of the signal power to the average noise power after binary filtration: $q_k^{(1)} = P_k^{(1)}/P_N^{(1)} = B_k^{(1)}(0)/B_N^{(1)}(0)$. Let us assume that the signals to be recognized are present against a background of noise with uniform spectral density $G_N(\omega) = N$ limited on the high-frequency side by $\Omega_N = \Omega_{j0}$. Then

$$B_N^{(1)}(0) = \frac{1}{4\pi}\int_{-\Omega_N}^{\Omega_N} G_N(\omega)\,d\omega - \frac{1}{4\pi}\int_{-\Omega_f}^{\Omega_f} G_N(\omega)\,d\omega = B_N(0)\left[1-\frac{\Omega_f}{\Omega_N}\right]$$

and with consideration of (10) we get the expression

$$q_k^{(1)} = q_k\left\{1-\frac{\Omega_f}{\Omega_k\alpha}\left[1-\left(\frac{\Omega_f}{\Omega_k}\right)^{4\alpha^2}(1-\alpha)\right]\right\}\Big/\left(1-\frac{\Omega_f}{\Omega_{j0}}\right). \tag{12}$$

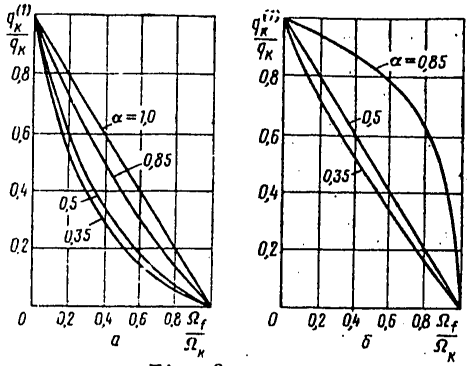

Fig. 3

Fig. 3 shows curves in accordance with expression (13) for the signal-to-noise ratio after binary filtration at different values of α: a--for $\Omega_{j0} \gg \Omega_k$; b--for $\Omega_{j0} = \Omega_k$.

These expressions and graphs give an idea of the possibilities of the method of outlining images in binary filtration, which can be expressed as follows.

1. In systems of pattern recognition by nonorthogonal features based on forming a correlation measure of the closeness of standard and input images, the use of preliminary binary filtration reduces the coefficient of mutual correlation between features that characterize a class. This reduction is more pronounced the less the low-frequency elimination bandwidth differs from that of the signal spectrum. Here only the high-frequency components of the spatial spectrum are singled out, and the slightest differences between images to be recognized are emphasized, which should improve the effectiveness of recognition.

2. Preliminary binary filtration of an additive mixture of signal and noise is detrimental to the signal-to-noise ratio since the signal power is reduced, and this detriment increases with the elimination bandwidth of the binary filter. Besides, noise becomes ever more concentrated, which requires a re-examination of the recognition algorithm with corresponding optimization.

REFERENCES

1. E. I. Krupitskiy, G. Kh. Fridman, "Use of Coherent Optics and Holography in Pattern Recognition Systems" in: "Opticheskiye metody obrabotki informatsii" [Optical Methods of Data Processing], edited by S. B. Gurevich, Nauka, 1974.

2. B. Ye. Krivenkov, Yu. V. Chuguy, AVTOMETRIYA, No 1, 1979.

3. L. M. Soroko, "Osnovy golografii i kogerentnoy optiki" [Principles of Holography and Coherent Optics], Nauka, 1971.

4. B. R. Levin, "Teoreticheskiye osnovy statisticheskoy radiotekhniki" [Theoretical Principles of Statistical Radio Engineering], Book 1, Sovetskoye radio, 1975.

5. Dzh. Bendat, A. Pirsol, "Izmereniye i analiz sluchaynykh protsessov" [Measurement and Analysis of Random Processes], Mir, 1974.

[81-6610]

6610
CSO: 1860

CERTAIN ASPECTS OF PHOTOGRAPHY, MOTION PICTURES AND TELEVISION

UDC 621.397.132.001.33

COLOR IMAGE FILTERING IN DIGITAL TELEVISION SYSTEMS

Leningrad PRIBOROSTROYENIYE in Russian Vol 23, No 9, Sep 80 pp 72-76

[Article by N. V. Ignat'yeva, Yu. M. Titov, K. A. Fedchenkov, Leningrad Electrotechnical Institute imeni V. I. Ul'yanov (Lenin)]

[Text] A study is made of the algorithms for digital color image filtering and the structural principles of digital color filters designed to be used in automatic color image analysis and processing systems and also in broadcast television systems to create complex special effects.

Color image filtering [1] in digital television systems presupposes the use of specialized computers that execute the algorithms that form the standard color fields. The basic operating characteristics of the color television filters -- the color discrimination thresholds and color resolution -- are determined by the parameters of the standard fields, the choice of which is made in accordance with the problems of analyzing and processing the images and also considering a priori information about the statistical characteristics of the standard subjects.

The formation of standard color fields with digitally adjustable parameters during color filtration in digital television systems can be based on the operation of truncating the digital codes of the color coordinates $\hat{m}$ and $\hat{n}$ shaping the quantizing grid lines of the color chart mon (see Figure 1). The position and the dimensions of the standard color fields can in this case be uniquely defined by the coordinates m^{stand}, n^{stand}, for example, the lower left-hand corner of the elementary rectangle on the color chart and the truncation step γ of the binary operands $\hat{m}(n)$, the maximum number of bits of which determines the resolution of the color television filters. The method of color filtration in digital television systems permits recognition of the color of the elements of the color image during comparison of the truncated operands of the current values of the color coordinates $\hat{m}(t)$ and $\hat{n}(t)$ with the digital codes of the points of the quantizing grid of the color chart m_{ξ}^{stand} and $n_{\eta}^{stand}(\xi = \overline{1, L}; \eta = \overline{1, L - \xi})$, where $L = 2^Q$ is the number of points of the quantizing grid with respect to any of the coordinate axes of the color chart with identical word length of the truncated operands $\langle\hat{m}(t)\rangle$ and $\langle\hat{n}(t)\rangle$.

When analyzing the color images in real time with the help of digital television systems, it is necessary to use fast color filtering algorithms which can be executed in digital television color filters of the combination type. In such filters the calculations requiring large expenditures of time (the division operation) are

replaced by the operation of parallel comparison of the corresponding code combinations.

Let us consider one of the possible versions of the construction of television color filters of the combination type, the structural diagram of which appears in Figure 2.

The binary weighted codes $\hat{R}$, $\hat{G}$, $\hat{B}$ from the output of the digital Q-bit video signal sensor:

$$\hat{R}(\hat{G})(\hat{B}) = a_0^{R(G)(B)} \cdot 2^0 + a_1^{R(G)(B)} \cdot 2^1 + \ldots + a_Q^{R(G)(B)} \cdot 2^Q,$$

where $\hat{R}$, $\hat{G}$, $\hat{B}$ are the digital codes of the "red," "green," and "blue" color-discriminated signals, respectively, and $\forall a_i^{R(G)(B)} \{0,1\}$ are subject to addition in the adder (C):

$$\hat{\Sigma} = a_0^{\Sigma} 2^0 + a_1^{\Sigma} 2^1 + \ldots + a_Q^{\Sigma} 2^Q; \quad \forall a_i^{\Sigma} \in [0, 1]; \quad \hat{\Sigma} = \hat{R} + \hat{G} + \hat{B}.$$

Then all of the code combinations are discriminated in the corresponding decoders (DC_R, DC_G, DC_B). The matrices (M) consist of two-input comparison circuits, the number of which is determined by the total number S of permitted and nontrivial code combinations of the results of dividing the input digital signals. Inasmuch as $\hat{m} = 1: \hat{R} = \hat{\Sigma}: \hat{m} = 0$; $\hat{R} = 0$ and always $\hat{R}(\hat{G}) \leq \hat{\Sigma}$, if $\forall a_i^{\Sigma} = 0$ it does not appear possible to determine the color. In this case S can be defined as follows:

$$S = (2^Q - 1)(2^{Q-1} - 1).$$

The code combinations of the results of dividing the digital signals $\hat{R}$ and $\hat{\Sigma}$ are disjunctively combined into 2^Q groups in the matrices of the two-input comparison circuits. If the division result $\hat{m}$ falls in the ξ-th quantization zone of the color x-coordinate Ω_ξ, it is taken equal to $\hat{m}_\xi$. For uniform quantizing of the color chart it is possible to write the combining rule, for example, in the following form:

$$\hat{m} = \frac{\hat{R}}{\hat{\Sigma}} \in \Omega_\xi : f_\xi = 1.$$

In particular,

$$f_1 = a_0^R \overline{a_1^R} \overline{a_2^R} \overline{a_3^R} \wedge a_3^{\Sigma}; \quad f_2 = (\overline{a_0^R} a_1^R \overline{a_2^R} \overline{a_3^R} \wedge a_2^{\Sigma} a_3^{\Sigma}) \vee$$
$$\vee (\overline{a_0^R} a_1^R \overline{a_2^R} a_3^R \wedge a_0^{\Sigma} a_1^{\Sigma} \overline{a_2^{\Sigma}} a_3^{\Sigma}) \vee (a_0^R \overline{a_1^R} \overline{a_2^R} \overline{a_3^R} \wedge a_1^{\Sigma} a_2^{\Sigma} \overline{a_3^{\Sigma}}). \qquad (1)$$

The Q-bit color signal code $\hat{m}(\hat{n})$ is formed in the coders (Sh) in Figure 2, after which the color of the image elements is distinguished in the code comparison circuits (SSK) together with the output comparison circuit (AND) by comparing the codes $\langle\hat{m}\rangle(\langle\hat{n}\rangle)$ with the given standard codes m^{stand} and n^{stand}, and the binary predicate F_1 is formed,

$$F_1 = \begin{cases} 1 : (\langle \hat{m} \rangle = m^{\text{эт}}) \wedge (\langle \hat{n} \rangle = n^{\text{эт}}) \overset{(a)}{} \\ 0 : (\langle \hat{m} \rangle \neq m^{\text{эт}}) \wedge (\langle \hat{n} \rangle \neq n^{\text{эт}}) \overset{(a)}{} \end{cases}$$

Key: a. stand

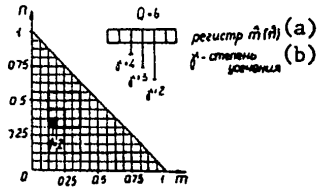

Figure 1. Shaping the color windows in digital filters

Key: a. $\hat{m}(\hat{n})$ register
b. γ truncation step

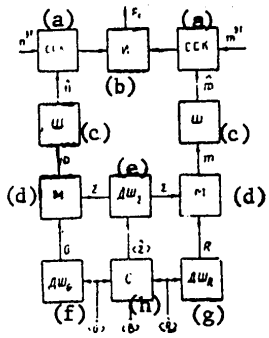

Figure 2. Structural diagram of the first type combination television color filter.

Key:
a. SSK = code comparison circuit
b. AND
c. Sh = coder
d. m = matrix
e. DC_{Σ} = decoder
f. DC_G = decoder
g. DC_R = decoder
h. C = adder

The investigated version of the structure of the television color filter offers the possibility of simultaneous comparison of signals with several standard color fields, that is, the formation of standard color fields of complex shape [2]. If the standard color field is unique and rectangular, the structure of the combination type television color filter is simplified significantly (see Figure 3). In such cases it is assumed that $m^{\text{stand}} = \hat{m}_{\xi}$, and $n^{\text{stand}} = \hat{n}_{\eta}$, and the maximum possible number of nonzero weight coefficients $(Q - \gamma_m)$, $(Q - \gamma_n)$ of the codes $\hat{R}$ and $\hat{G}$ is determined by the given coordinates of the standard color fields m^{stand}, n^{stand}, where γ_m and γ_n are found as follows:

$$\gamma_m = \lfloor -\log_2 m^{\text{эт}} \overset{(a)}{} \rfloor - 1; \quad \gamma_n = \lfloor -\log_2 n^{\text{эт}} \overset{(a)}{} \rfloor - 1. \tag{2}$$

Key: a. stand

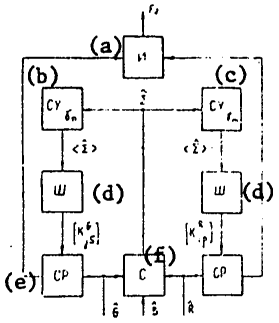

Figure 3. Structural diagram of a second type combination television color filter.

Key:
a. AND
b. SU_{γ_n}
c. SU_{γ_m}
d. Sh = coder
e. SR = equivalence circuit
f. S = adder

The symbol $\lfloor A \rfloor$ denotes the choice of the smallest integer greater than or equal to A, and γ is the truncation step, that is, the number of binary bits by which the code $\hat{\Sigma}$ is shifted to the right.

From the truncated codes $<\hat{\Sigma}>_{\gamma_m}$ and $<\hat{\Sigma}>_{\gamma_n}$, in accordance with the form of the partial predicates f_ξ and f_η, two matrices of weight coefficients of certain standard codes K^R and K^G are formed, the form of which is determined by the choice of m^{stand} and n^{stand} so that each code combination of the truncated codes $<\hat{\Sigma}>_{\gamma_m}$, $<\hat{\Sigma}>_{\gamma_n}$ will correspond to its own column of weight coefficients:

$$K^R = \begin{vmatrix} k^R_{1\gamma_m} & k^R_{2\gamma_m} & \dots & k^R_{M\gamma_m} \\ k^R_{1(\gamma_m+1)} & k^R_{2(\gamma_m+1)} & \dots & k^R_{M(\gamma_m+1)} \\ \dots & \dots & \dots & \dots \\ k^R_{1Q} & k^R_{2Q} & \dots & k^R_{MQ} \end{vmatrix};$$

$$K^G = \begin{vmatrix} k^G_{1\gamma_n} & k^G_{2\gamma_n} & \dots & k^G_{N\gamma_n} \\ k^G_{1(\gamma_n+1)} & k^G_{2(\gamma_n+1)} & \dots & k^G_{N(\gamma_n+1)} \\ \dots & \dots & \dots & \dots \\ k^G_{1Q} & k^G_{2Q} & \dots & k^G_{NQ} \end{vmatrix},$$

where

$$M = 2^{(Q-\gamma_m)}; \quad N = 2^{(Q-\gamma_n)}; \quad \forall k^R_{ip}, \ k^G_{js} \in \{0, 1\},$$

M and N are the total number of code combinations; $p = \overline{1,M}$, $S = \overline{1,N}$ are the numbers of the code combinations of the truncated codes $<\hat{\Sigma}>_{\gamma_m}$, $<\hat{\Sigma}>_{\gamma_n}$, respectively, and $i = \gamma_{m+1}Q$, $j = \gamma_{n+1}$, Q are the numbers of the code bits. For the given Q it is

possible to construct the matrices K^R, K^G for any standard color field. If, for example, Q = 4 and $m^{stand} = 0.375$, the matrix of weight coefficients of the standard codes has the following form:

$$K^R = \begin{bmatrix} 0 & 0 & 1 & 0 \\ 0 & 1 & 1 & 0 \\ 0 & 0 & 0 & 1 \end{bmatrix}.$$

Thus, after shaping the standard codes K^R and K^G in the coders (Sh) (see Figure 3), for recognition of the color of the image elements it is sufficient to form the binary predicate F_2, which is realized by the set of equivalence circuits (SR) and the output comparison circuit (AND). In the investigated case the decision rule is written as follows:

$$F_2 = \begin{cases} 1 : (\forall a_i^R = k_{ip}^R) \wedge (\forall a_j^G = k_{jS}^G) \wedge (\forall a_t^R = 0) \wedge (\forall a_q^G = 0); \\ 0 : (a_i^R \neq k_{ip}^R) \vee (a_j^G \neq k_{jS}^G) \vee (a_t^R \neq 0) \vee (a_q^G \neq 0), \end{cases} \quad (3)$$

where $t = \overline{1, \gamma_m}$, $q = \overline{1, \gamma_n}$ are the numbers of the truncated code bits.

In the special case where the conditions (2) are precisely satisfied, the realization of the digital combination television color filters is simplified still more inasmuch as there is no necessity for the coders (Sh) (see Figure 3). Here $(2Q - \gamma_m - \gamma_n)$ of the conjunctively combined equivalence circuits (SR) must execute a decision rule analogous to (3) under the condition of the substitution:

$$k_{ip}^R \to a_{(i-\gamma_m)}^{\Sigma}; \quad k_{jS}^G \to a_{(j-\gamma_n)}^{\Sigma}.$$

The error δ of the color filtering of digital combination television color filters as a function of the word length of the codes Q, the dynamic range of the total signal D and the degree of truncation γ of the binary operands of the digital codes of the color coordinates is of significant interest. As a result of investigating the accuracy of the color filtering in digital television systems performed on the basis of an error analysis of the determination of the color coordinates on truncation of the operands of the color discriminated signals, the value of δ_m will be determined from the expression:

$$\delta_m = \frac{D_m (1 - \hat{m}) (1 - 2^{\gamma_m})}{\hat{m} [2^Q + D (1 - 2^{\gamma_m})]}.$$

The graphs illustrating the dependence of the color filtration errors on the enumerated factors are presented in Figure 4. The potential accuracy of the combination type digital television color filters is determined by the maximum possible errors which do not depend on the values of the color coordinates and the dynamic range:

$$\delta_{m_{max}} = -\frac{2^{\gamma_m} - 1}{\hat{R}}.$$

In order to decrease the color filtering errors in digital television systems, it is expedient to use truncation with tracking of the filling of the bit grid of the total signal operand. This truncation can be performed with a step $\gamma_m - \gamma_c$, where

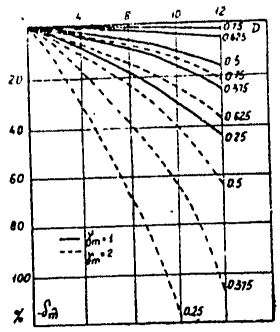

Figure 4. Errors in determining the color coordinates in the dynamic range of the total signal.

γ_c is the number of free high-order bits of the operand Σ. In the general case the number γ_c depends on the magnitude of the dynamic range D and, consequently, if $2^{\gamma_m} \leq D < 2^{\gamma_{m+1}}$, then $\gamma_c = \gamma_m$. The digital filtration errors during tracking truncation are defined by the expression

$$\delta_m = \frac{D(1-\hat{m})\left[1-2^{(\gamma_m-\gamma_c)}\right]}{\hat{m}\left\{2^{Q}+D\left[1-2^{(\gamma_m-\gamma_c)}\right]\right\}}.$$

The investigated method of digital filtration in digital television systems permits the solution of the problems of detection, selection and classification of the image elements in real time, and it can be used effectively for automatic analysis and processing of complex color images.

BIBLIOGRAPHY

1. R. Ye. Bykov, N. V. Ignat'yeva, "Color Filtering during Analysis and Processing of Images," MEZHVUZ. SB./LENINGR. IN-T AVIATS. PRIBOROSTR. (Interuniversity Collection/Leningrad Institute of Aviation Instrument-Making), No 115, 1977, Problems of the Theory and Design of Television Data Transmission, Reception and Display Systems.

2. R. Ye. Bykov, N. V. Ignat'yeva, N. A. Malinkin, et al., "Automated Television Complex for Analyzing Multizonal Movie and Still Photographic Images," TKT, No 4, 1979.

Recommended by the Television Department

Manuscript received 6 June 1979

[8144/0258-10845]

10845
CSO: 8144/0258

COMMUNICATIONS, COMMUNICATION EQUIPMENT, RECEIVERS AND TRANSMITTERS
NETWORKS, RADIO PHYSICS, DATA TRANSMISSION AND
PROCESSING, INFORMATION THEORY

UDC 621.391.2

PROCESSING COMPLEX RADIO SIGNALS BY STROBOSCOPIC METHODS

Moscow RADIOTEKHNIKA I ELEKTRONIKA in Russian Vol 25, No 10, Oct 80 pp 2099-2104
manuscript received 1 Nov 78

[Article by V. D. Zakharchenko]

[Text] The author analyzes a model of a coherent stroboscopic processing system with finite resolution. An asymptotic expression is derived for the output signal in the case of a large stroboscopic sample space.

The use of complex probing signals with different kinds of modulation is quite productive for analyzing either extended objects [Ref. 1-3] or inhomogeneities in a microwave channel that have been identified by methods of pulse reflectometry [Ref. 4]. When periodicity is present in a sequence of signals they can be discretely processed in a radio pulse strobing scheme [Ref. 5] that enables realization of coherent accumulation in addition to transformation of the time scale.

The properties of a stationary reflecting object of finite size can be described by the characteristic h(t) that is analogous to the pulse transfer characteristic (PTC) of a linear circuit with constant parameters [Ref. 3]. In reflectometry problems, detection of the fine structure of the PTC enables exact determination of the location and composition of inhomogeneities in the transmission channel on the basis of their radar portraits. The stroboscopic methods that are extensively used in measurement technology can solve this problem by comparatively simple means. Papers by Naydenov and Chelnokov [Ref. 5, 6] describe the transformation of the time scale of modulated signals of nanosecond duration by strobing with a coherent sequence of short radio pulses. Glebovich [Ref. 4] mentions prospects for using radio pulse strobing in reflectometry of microwave transmission channels. However, the theory of this method has not been adequately worked out in application to problems of location.

The aim of the proposed work is to analyze a radio pulse probing arrangement used to study the fine structure of PTCs that are commensurate in duration with the reference radio signals; to analyze the possibilities of using complex signals in a measurement system with stroboscopic compression of the spectrum. The system of coherent stroboscopic processing of reflected signals differs fundamentally from the superheterodyne receiver of a pulsed radar in the use of a coherent sequence of strobing radio pulses as the reference waveform. The delay of the radio strobe relative to the probing signal increases linearly by an amount ΔT from period to

period. The readout step (ΔT) can be regulated over a range determined by the Kotel'nikov theorem. The recurrence period of the strobing pulses $T_c = T + \Delta T$ (T is the probing period) is shaped by an autoshift circuit used in stroboscopic oscilloscopes [Ref. 5]. Isolation of one of the spectral components by a narrow-band filter gives a time-transformed input signal on a low intermediate frequency Ω (tens or hundreds of kHz) that is convenient for subsequent amplification and registration.

On the basis of the approach developed in Ref. 8, let us consider the mathematical model shown in Fig. 1 for coherent stroboscopic processing, assuming narrow-band probing and reference signals. Using analytical representation, we introduce the notation

$$x(t) = \operatorname{Re} \dot{x}(t), \quad \dot{x}(t) = \dot{X}(t) e^{j\omega_0 t}, \quad \arg \dot{X} = \theta_x(t),$$
$$\mathscr{A}(t) = \operatorname{Re} \dot{\mathscr{A}}(t), \quad \dot{\mathscr{A}}(t) = \dot{A}(t) e^{j\omega_c t}, \quad \arg \dot{A} = \theta_c(t),$$

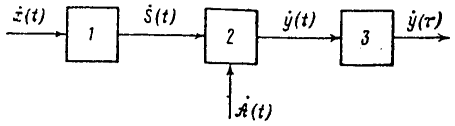

Fig. 1. Model of coherent stroboscopic processing: 1--linear quadrupole network with pulse transfer characteristic h(t); 2--stroboscopic mixer; 3--bandpass filter of stroboscopic system tuned to carrier difference frequency $\Omega = \omega_0 - \omega_c$

where $\dot{X}(t)$, $\dot{A}(t)$ are the complex envelopes of the probing and reference (strobing) signals that are finite on intervals $[0, \tau_X]$ and $[0, \tau_c]$ respectively; $\omega_0 - \omega_c = \Omega << \omega_0, \omega_c$. Periodic sequences

$$\dot{x}(k,t) = \dot{X}(t - kT) e^{j\omega_0 t}, \quad \dot{\mathscr{A}}(k,t) = \dot{A}(t - kT_c) e^{j\omega_c t}, \tag{1}$$

where $k = 0, 1, 2, \ldots, N$ ($N = T/\Delta T >> 1$), $T_c = T(1 + 1/N)$, we will take to be coherent on the observation interval $t \in [0, NT]$. The readout step $\Delta T = T/N$ is determined by the required compression of the spectrum, and can be made arbitrarily small.

Assuming for the sake of definiteness that $T < \pi/\Omega$, we get an asymptotic expression (at $N >> T/\tau_X$) for the stroboscopic system's output signal that is formed by filtering the spectral components of the products of strobing in the vicinity of frequency $\Omega = \omega_0 - \omega_c$. Assuming that small input signals are multiplied by the mixer, we convert the spectral density of the process at the filter input

$$G_y(\omega) = \int_{-\infty}^{\infty} \left\{ \sum_{k=0}^{N} \dot{y}(k,t) \right\} e^{-j\omega t} dt,$$

where $$\dot{y}(k,t) = {}^1/_2 \dot{s}(k,t) \dot{\mathscr{A}}^*(k,t); \quad \dot{s}(k,t) = \int_{-\infty}^{\infty} \dot{x}(k,t') h(t - t') dt',$$

to the form

$$\dot{G}_\nu(\omega)=\sum_{k=0}^{N}\dot{I}_k(\omega)\,e^{-j(\omega-\Omega)k\Delta T_c},$$

$$\dot{I}_k(\omega)=\int_{-\infty}^{\infty}h\left(\frac{kT}{N}-\nu\right)\exp\left\{-j\omega_0\left(\frac{kT}{N}-\nu\right)\right\}\dot{U}(\omega,\nu)\,e^{j(\omega-\Omega)\nu}\,d\nu, \tag{2}$$

$$\dot{U}(\omega,\nu)=\frac{1}{2}\int_{-\infty}^{\infty}\dot{X}(t)\overset{*}{\dot{A}}(t-\nu)\,e^{-j(\omega-\Omega)t}\,dt.$$

Let us single out for consideration the frequency region

$$\Delta\omega=|\omega-\Omega|\ll\frac{1}{\tau_x},\ \frac{1}{\tau_c}.$$

Retaining the first terms of the exponential expansion in functions $\dot{I}_k(\omega)$ and $\dot{U}(\omega,\nu)$ and setting

$$\dot{U}(\omega,\nu)\simeq\dot{\mathcal{K}}_0(\nu)+\delta\dot{U}(\omega,\nu),\quad \dot{I}_k(\omega)\simeq\dot{I}_k+\delta\dot{I}_k(\omega),$$

where $\dot{\mathcal{K}}_0(\nu)=1/2\int_{-\infty}^{\infty}\dot{X}(t)\overset{*}{\dot{A}}(t-\nu)\,dt$ is the complex envelope of the function of mutual correlation of signals x(t) and $\mathcal{A}(t)$,

$$\delta\dot{U}(\omega,\nu)=-j\frac{(\omega-\Omega)}{2}\int_{-\infty}^{\infty}\dot{X}(t)\overset{*}{\dot{A}}(t-\nu)\,t\,dt;$$

$$\dot{I}_k=\int_{-\infty}^{\infty}h\left(\frac{kT}{N}-\nu\right)\dot{\mathcal{K}}_0(\nu)\exp\left\{-j\omega_0\left(\frac{kT}{N}-\nu\right)\right\}d\nu;$$

$$\delta\dot{I}_k=j(\omega-\Omega)\int_{-\infty}^{\infty}h\left(\frac{kT}{N}-\nu\right)\dot{\mathcal{K}}_0(\nu)\exp\left\{-j\omega_0\left(\frac{kT}{N}-\nu\right)\right\}\nu\,d\nu,$$

we disregard the frequency-dependent components of $\dot{I}_k$ and $\dot{U}$ in the given region. The relative error ε of such an approximation can be estimated by the inequalities

$$|\delta\dot{U}|\leqslant\varepsilon_1\max_{\nu}|\dot{\mathcal{K}}_0(\nu)|,\ |\delta\dot{I}_k|\leqslant\varepsilon_2\max_{k}|\dot{I}_k|,$$

$$\varepsilon_1\simeq\Delta\omega\tau_c,\quad \varepsilon_2\simeq\Delta\omega(\tau_x+\tau_c),$$

and at a signal duration of $\sim10^{-8}$ s does not exceed 1% in the frequency band of ~1 MHz. As $N\to\infty$, the difference between successive readouts $\Delta\dot{I}_k=\dot{I}_{k+1}-\dot{I}_k$ of the stroboscopic sample can be asymptotically represented by the integral

$$\Delta\dot{I}_k\to\frac{T}{N}\int_{-\infty}^{\infty}\frac{\partial\dot{\mathcal{K}}_0(\tau)}{\partial\tau}\Bigg|_{\tau=\frac{kT}{N}-t}h(t)\,e^{-i\omega_0 t}dt,$$

where

$$(3) \qquad |\Delta \dot{I}_k| \leqslant \frac{T}{N} \max_{\tau} \left| \frac{\partial \dot{\mathcal{K}}_0(\tau)}{\partial \tau} \right| \int_{-\infty}^{\infty} |h(t)|\,dt.$$

Since the absolute value of the derivative of the analytical function is limited by the upper frequency of its spectrum ω_m

$$(4) \qquad \max_{\tau} \left| \frac{\partial \dot{\mathcal{K}}_0(\tau)}{\partial \tau} \right| \leqslant \omega_m \max |\dot{\mathcal{K}}_0(\tau)|,$$

and for passive reflectors $\int_{-\infty}^{\infty} |h(t)|\,dt$ usually does not exceed unity, in the limit $(N \to \infty)$ $\dot{I}_{k+1} \to \dot{I}_k$ and the second member of inequality (3) can be made arbitrarily small.

The ratio $\Delta \dot{I}_k / T$ has the sense of the derivative of the envelope of stroboscopic samples $\dot{I}_k$, whose value can be estimated by using (3) and (4):

$$\left| \frac{\Delta \dot{I}_k}{T} \right| \leqslant \frac{\omega_m}{N} \max_{\tau} |\dot{\mathcal{K}}_0(\tau)|.$$

Comparing this inequality with (4), we can state that the frequency band of the envelope $\dot{I}_k$ does not exceed the quantity ω_m/N. Passing to the limit in the expression for the spectrum

$$(5) \qquad \dot{G}_v(\omega) = \sum_{k=0}^{N} \dot{I}_k e^{-j(\omega-\Omega)N\tau_k}; \quad \tau_k = \frac{kT_c}{N},$$

as was done in Ref. 8, as $N \to \infty$ (for practical purposes it is sufficient that $N > \omega_m T \sim 10^4$-10^6 for the nanosecond range of durations) by substituting

$$T_c \to T, \quad \tau_k \to \tau, \quad \dot{I}_k \to \dot{I}(\tau), \quad \Delta\tau_k \to d\tau$$

we reduce (5) to a Fourier integral for a complex function

$$(6) \qquad \dot{y}(\tau) = \frac{e^{j\Omega\tau}}{T} \int_{-\infty}^{\infty} h\left(\frac{\tau}{N} - t\right) \dot{\mathcal{K}}_0(t) \exp\left\{-j\omega_0\left(\frac{\tau}{N} - t\right)\right\} dt,$$

represented on the interval $\tau \in [0, NT]$. With consideration of the imposed constraints, (6) defines the analytical form of the output signal of the stroboscopic processing system, this signal being an asymptotically narrow-band process with carrier frequency $\Omega = \omega_0 - \omega_c$.

Practical utilization of the derived relations presupposes specific assignment of the corresponding functions or their approximation. Of considerable interest is the possibility of using the same type of circuit for shaping the probing and reference radio pulses [$\dot{A}(t) \sim \dot{X}(t)$], which will ensure matched filtration in a stroboscopic system of complex signals for any coefficient of spectral transformation N.

As an example, let us consider the case of stroboscopic location of objects whose PTC permits a narrow-band approximation (for example waveguide filters, resonant commutators based on p-n elements and so on):

$$h(t)=H(t)\cos[\omega_0 t+\varphi(t)]=\mathrm{Re}\,\dot{H}(t)e^{j\omega_0 t}.$$

In this case, expression (6) can be rewritten in simplified form

$$\dot{y}(\tau)=\frac{e^{j\Omega\tau}}{2T}\int_{-\infty}^{\infty}\dot{H}\left(\frac{\tau}{N}-t\right)\dot{\mathcal{K}}_0(t)\,dt \qquad (7)$$

and treated as a generalization of the envelope method of Ref. 7 to stroboscopic processing systems. The influence that the duration of the correlation function of the reference signals has on reproduction of the envelope and phase structure of narrow-band PTCs is shown in Fig. 3. Calculations were done for the models of $\dot{\mathcal{K}}_0(t)$

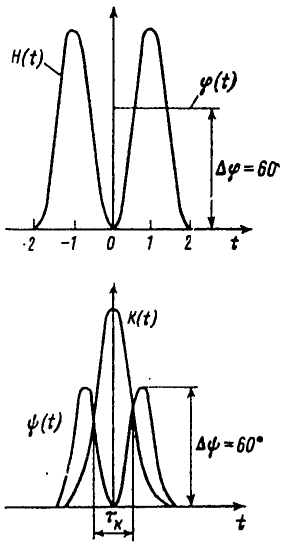

Fig. 2. Models of investigated PTC and complex envelope of the mutual correlation function of signals x(t) and $\mathcal{H}(t)$ $\dot{H}(t)=H(t)e^{j\varphi(t)}$; $\dot{\mathcal{K}}_0(t)=K(t)e^{j\psi(t)}$

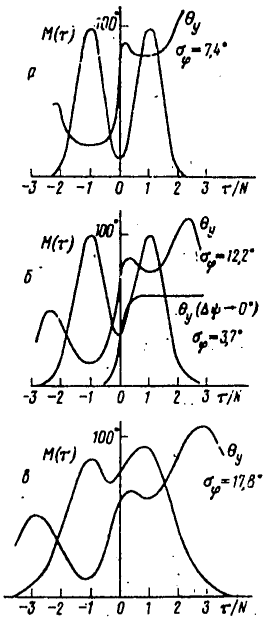

Fig. 3. Evolution of output signal $\dot{y}(\tau)$ with expansion of the aperture of the stroboscopic processing system: *а*--$\tau_к=0.5$; *б*--$\tau_к=1.0$; *в*--$\tau_к=2.0$

and the complex envelope of the PTC that are shown in Fig. 2. The proposed model of the correlation function corresponds to even reference signals, which are characteristic when using semiconductor microwave modulators. Fig. 3 also shows the values of the mean-square error of reproduction of the phase structure of the PTC:

$$(8)\qquad \sigma_\varphi^2 = \frac{\int_{-\infty}^{\infty} M(\tau)\left[\theta(\tau) - \varphi\left(\frac{\tau}{N}\right)\right]^2 d\tau}{\int_{-\infty}^{\infty} M(\tau)\,d\tau},$$

where $M(\tau)$ is the envelope of the output signal

are the mean-square values of the corresponding functions:

$$\theta_{cp} = \frac{\int_{-\infty}^{\infty} M(\tau)\theta_v(\tau)\,d\tau}{\int_{-\infty}^{\infty} M(\tau)\,d\tau}; \quad \varphi_{cp} = \frac{\int_{-\infty}^{\infty} H(\tau)\varphi(\tau)\,d\tau}{\int_{-\infty}^{\infty} H(\tau)\,d\tau}.$$

As can be seen from the figure, expansion of the aperture of the processing system leads to an increase in the error. It should be noted that phase resolution can be considerably improved by reducing the level of phase modulation in the correlation function (Fig. 3б, $\Delta\psi \to 0$) by raising the requirements for the phase-amplitude responses and identity of the reference signal shapers.

The author thanks B. V. Kagalenko and V. A. Korneyev for support and interest in the work.

REFERENCES

1. Blau, "Introduction to the Theory of Partial Coherence in Radar," ZARUBEZHNAYA RADIOELEKTRONIKA, Izd. Sovetskoye radio, No 5, 1967, p 15.

2. B. A. Varentsov, N. P. Krasyuk, "On Using Methods of Linear Electronics to Calculate a Scattered Electromagnetic Field," in "Prikladnyye zadachi rasseyaniya i difraktsii radiolokatsionnykh signalov" [Applied Problems of Scattering and Diffraction of Radar Signals], Northwest Polytechnical Correspondence Institute, Leningrad, No 3, 1974, p 2.

3. Kenno, Moffat, "Approximation of Transfer and Pulse Transfer Characteristics," TIIER, Vol 53, 1965, p 8.

4. G. V. Glebovich, "Determination of Parameters of Wide-Band and Narrow-Band Distributed Systems by Pulse Methods. Up-to-Date Methods and Equipment for Measuring the Parameters of Radio Circuits," Reports of the All-Union Symposium, Siberian Scientific Research Institute of Metrology, Novosibirsk, Vol 127, 1974.

5. A. I. Naydenov, "Transformatsiya spektra nanosekundnykh impul'sov" [Transformation of a Nanosecond Pulse Spectrum], Izd. Sovetskoye radio, 1973.

6. A. I. Naydenov, B. A. Chelnokov, "Problems of Electronics," RADIOIZMERITEL'NAYA TEKHNIKA, Vol 4, 1973.

7. I. S. Gonorovskiy, "Radiotekhnicheskiye tsepi i signaly" [Electronic Circuits and Signals], Izd. Sovetskoye radio, 1977.

8. V. D. Zakharchenko, IZVESTIYA VUZov: PRIBOROSTROYENIYE, No 10, 1976, p 5.

6610
CSO: 1860

UDC 621.391.2:519.217.2

AVERAGED ENERGY SPECTRA OF PULSED RANDOM PROCESSES CONTROLLED BY AN ARBITRARY FINITE ERGODIC MARKOV CHAIN

Moscow RADIOTEKHNIKA I ELEKTRONIKA in Russian Vol 25, No 10, Oct 80 pp 2115-2125
manuscript received 12 Mar 79

[Article by S. D. Eydel'man, T. G. Pletneva and G. N. Rozorinov]

[Text] A solution is found for the problem of calculating the averaged energy spectrum of a pulsed random process controlled by a finite ergodic Markov chain. The procedure of generalized functions is used to substantiate the computational formulas. The effectiveness of the method is illustrated by examples of finding the spectra of signals used in digital magnetic recording.

Introduction

The present investigation arose in finding the energy spectra of highly informative digital magnetic recording signals. In this study it was found that the recommendations of Ref. 1, 2 and the article of Ref. 3 need to be made specific, while the results of Ref. 4, 5 need to be made much more general. Methods of calculating the averaged energy spectra of a broad class of signals, especially electrical communication signals, are given in the book of Ref. 6, and also in the articles of Ref. 7 and 8.

This paper deals with complete solution of the problem of calculating the averaged energy spectrum of a pulsed random process controlled by an arbitrary ergodic Markov chain. Considerable use is made of facts of the theory of finite Markov chains as presented in the book of Ref. 9. Mathematical substantiation of all passages to the limit is based on the theory of generalized functions. The presentation is accompanied by cases in which calculation of the averaged energy spectrum can be substantiated within the framework of classical analysis.

The resultant formulas can be used for fairly efficient calculation of averaged signal spectra.

An information sequence to be transmitted over a communications channel is usually transformed by encoders and modulators [Ref. 15] in such a way that the resultant signal has certain predetermined properties such as high interference immunity. In the most extensively used binary systems the encoder is a synchronous sequential finite Mili automaton, and modulation is accomplished by the action of binary information symbols on any of the parameters that characterize the carrier waveform (a

time function assigned on segment (0,T)). Digital data transmission systems use a square-wave carrier, and therefore the signal in such a system is a sequence of square pulses regardless of which of the parameters of the carrier wave is modulated. In this case the clock interval can be taken as deterministic, and the information signal can be described by pulse "bursts" that alternate in a specific pattern. Then it is natural to consider the relations between different pulse bursts as Markovian. If it is necessary to consider the correlation of bursts that are rather far apart with respect to time of arrival, then the duration of the initial set of bursts can be increased. Such a Markov model is readily calculable, and while it cannot be considered exact, it can nevertheless be used as a fairly satisfactory approximate description of a real process.

1. Mathematical Model

The given random process $\xi(t)$ is a set of square pulses with amplitudes C_1, C_2,... ..., C_p that lasts for time T. The amplitude changes or remains the same at times kT, $k = 0, 1, \ldots$

Hypotheses that describe the process $\xi(t)$:

1.1. There exists an integer r such that only certain bursts $\xi_1(t)$, $\xi_2(t)$,..., $\xi_q(t)$ can appear on the half-open intervals $[(k-1)rT, krT)$, $k = 1, 2, \ldots$ Each burst $\xi_j(t)$ is a predetermined set of square pulses $\phi_j(t)$ of duration rT; $\phi_j(t) = \varepsilon_{j\nu}$ for $t \in [\nu - 1)T, \nu T]$, $\nu = 1, 2, \ldots, r$, where $\varepsilon_{j\nu}$ takes on some value from the sequence $C_1, C_2, \ldots, C_p$.

1.2. The process $\xi(t)$ can be put into one-to-one correspondence with a finite Markov chain $\eta(\tau)$ with discrete time $\tau = 0$, rT, 2rT,... and states $S_1, S_2, \ldots, S_q$ such that:

a) if $\eta(krT)$ is in state S_j, this means that $\xi(t) = \xi_j(t)$ for $t \in [krT, (k+1)rT)$;

b) $\eta(\tau)$ is an ergodic Markov chain [Ref. 9] with given matrix $P = (p_{ij})$, $i, j = 1, 2, \ldots, q$ of transitional probabilities.

1.3. The mathematical expectation $M\{\xi(t)\}$ of process $\xi(t)$ is equal to zero.

Thus $\xi(t)$ is a random process with deterministic clock intervals that is specified by the following quantities: pulse duration T, amplitudes $C_1, C_2, \ldots, C_p$, number of bursts q, their "size" r, the matrix of the form of the bursts $\Phi = (\varepsilon_{j\nu})_{\substack{j=1,\ldots,q \\ \nu=1,\ldots,r}}$ and the matrix of transitional probabilities P.

The considerations given below are also applicable in those cases where the wave-shape of the carrier of the process $\xi(t)$ is arbitrary and not square.

2. Some Notation

Let us denote by $\vec{A} = (A_1, A_2, \ldots, A_q)$ the steady-state distribution of a finite ergodic Markov chain with matrix of transitional probabilities P. In the case of a cyclic chain

$$\exists \lim_{n\to\infty} \frac{I+P+\ldots+P^{n-1}}{n} = A, \qquad \exists d > 1,$$

such that $\exists \lim_{n\to\infty} p^{dn} = A_0$, where elements of A_0 with indices i and j are equal to zero, if S_i and S_j do not belong to the same cyclic class and are obtained by renormalization from the components of steady-state vector $\vec{A}$ that belong to the corresponding cyclic class, if S_i and S_j belong to the same cyclic class [Ref. 9].

In addition, we introduce the following notation: $e_\mu = (\varepsilon_{1\mu}, \varepsilon_{2\mu}, \ldots, \varepsilon_{q\mu})$; $\tilde{p}^S = p^{dS} - A_0$, $S = 1, 2, \ldots$; $\tilde{P}^0 = I$ is the identity matrix; $\hat{A} = (A_i\delta_{ij})$ $i, j = 1, \ldots, q$; δ_{ij} is the Kronecker delta; $\hat{A}e_\nu = (A_1\varepsilon_{1\nu}, A_2\varepsilon_{2\nu}, \ldots, A_q\varepsilon_{q\nu})$;

$$P^S P^\nu e_\mu \cdot \hat{A}e_\nu = \tilde{m}_{\mu\nu}^{(S,\nu)}; \quad A_0 P^\nu e_\mu \cdot \hat{A}e_\nu = m_{\mu\nu}^{(\nu)};$$
$$A_0 e_\mu \cdot \hat{A}e_\nu = m_{\mu\nu}^{(0)}; \quad e_\mu \cdot \hat{A}e_\nu = m_{\mu\nu}; \quad e_\mu \cdot \hat{A}e_\mu = m_\mu; \quad \tilde{m}_{\mu\nu}^{(S,0)} = \tilde{m}_{\mu\nu}^{(S)};$$
$$\vec{\xi}_q = (\underbrace{1, 1, \ldots, 1}_{q});$$
$$a = \int_0^T e^{i\omega T}\, dT; \quad Q = e^{-i\omega T}; \quad \psi_i(\omega) = a\sum_{\nu=1}^{r} \varepsilon_{i\nu} Q^{\nu-1};$$

π is the vector of initial probabilties of the chain $\eta(\tau)$.

3. Calculation of the Averaged Energy Spectrum

The averaged energy spectrum $P(\omega)$ of process $\xi(t)$ is defined by the following formula [Ref. 4, 6]:

$$P(\omega) = \lim_{N\to\infty} P^{(N)}(\omega), \tag{1}$$

where

$$P^{(N)}(\omega) = \frac{2}{NrT} M\left\{ \left| \int_0^{NrT} \xi(t) e^{-i\omega t} dt \right|^2 \right\}. \tag{2}$$

On the basis of hypotheses 1.1-1.3, $P^{(N)}(\omega)$ is represented by the formula

$$P^{(N)}(\omega) = \frac{2|a|^2}{rT}[E_1^{(N)}(\omega) + E_2^{(N)}(\omega)], \tag{3}$$

where

$$E_1^{(N)}(\omega) = \sum_{j=1}^{q} \frac{\sum_{k=1}^{N} (\vec{\pi}P^{k-1})j}{N} \sum_{\nu,\mu=1}^{r} \varepsilon_{j\mu}\varepsilon_{j\nu} Q^{\mu-\nu}; \tag{4}$$

$$E_2^{(N)}(\omega) = 2\Bigg\{ \sum_{\mu,\nu=1}^{r} \sum_{S=1}^{N-1} \sum_{l=1}^{q} \left(1 - \frac{S}{N}\right) \times$$
$$\times \left[\frac{\sum_{k=1}^{N-S} (\vec{\pi}P^{k-1})_l}{N-S} - A_l \right] (P^S e_\mu)_l \varepsilon_{l\nu} \cos(Sr + \mu - \nu)\omega T +$$
$$+ \sum_{\mu,\nu=1}^{r} \sum_{S=1}^{N-1} \left(1 - \frac{S}{N}\right) P^S e_\mu \cdot \hat{A}e_\nu \cos(Sr + \mu - \nu)\omega T \Bigg\} = 2[E_{21}^{(N)}(\omega) + E_{22}^{(N)}(\omega)]. \tag{5}$$

Using the notation of §2 and passing to the limit in (4), we get

$$E_i(\omega)=\lim_{N\to\infty}E_i^{(N)}(\omega)=\sum_{\nu,\mu=1}^{r}m_{\mu\nu}\cos(\mu-\nu)\omega T. \tag{6}$$

The following is important for the subsequent presentation:

a) $\exists b<1$ [Ref. 9] such that

$$\left|\frac{\sum_{k=1}^{n}(\pi P^{k-1})_i}{n}-A_i\right|\leqslant cb^n,\qquad \forall n;$$

b) if the function $\phi(\omega)\in D$, then its Fourier transform $\tilde{\phi}(\sigma)$ satisfies the inequalities [Ref. 10]

$$|\tilde{\varphi}(\sigma)|\leqslant c_j(1+|\sigma|)^{-j},\ \forall j.$$

Consider $E_{21}^{(N)}(\omega)$ in formula (5). We will treat this function as a regular generalized function of D' [Ref. 10], and understand its limit as $N\to\infty$ in the sense of D'. Let us take any fundamental function $\phi(\omega)\in D$ and consider the sequence

$$\begin{aligned}\alpha_N&=(E_{21}^{(N)},\varphi)=\int_{-\infty}^{\infty}E_{21}^{(N)}(\omega)\varphi(\omega)d\omega=\\&=\sum_{\mu,\nu=1}^{r}\sum_{S=1}^{N-1}\sum_{l=1}^{q}\left(1-\frac{S}{N}\right)\left[\frac{\sum_{k=1}^{N-S}(\vec{\pi}P^{k-1})_l}{N-S}-\right.\\&\left.-A_l\right](P^Se_\mu)_l\varepsilon_{l\nu}\operatorname{Re}\int_{-\infty}^{\infty}e^{i\omega T(Sr+\mu-\nu)}a^2(\omega)\varphi(\omega)d\omega.\end{aligned} \tag{7}$$

In virtue of points a) and b) (at $j=2$) and the fact that $a^2(\omega)\phi(\omega)\in D$, we get

$$\begin{aligned}|\alpha_N|&\leqslant c\sum_{S=1}^{N}b^{N-S}S^{-2}=c\left(\sum_{S=1}^{N/2}b^{N-S}S^{-2}+\sum_{S=N/2+1}^{N}b^{N-S}S^{-2}\right)\leqslant\\&\leqslant c\left(b^{N/2}\sum_{S=1}^{\infty}S^{-2}+\frac{4}{N^2}\sum_{S=0}^{\infty}b^S\right)\xrightarrow[N\to\infty]{}0.\end{aligned} \tag{8}$$

Let us go on to find the limit of the function $E_{22}^{(N)}(\omega)$. We will assume that $N=dn$. We can readily see that the limit of $E_{22}^{(N)}(\omega)$ is the same when $N\to\infty$ in an arbitrary way.

$$(9)\qquad E_{\text{вых}}^{(N)}(\omega)=G_1^{(N)}(\omega)+G_2^{(N)}(\omega)-\sum_{\mu,\nu=1}^{r}e_\mu\cdot\hat{A}e_\nu\cos(\mu-\nu)\omega T,$$

where

$$(10)\qquad G_1^{(N)}(\omega)=\sum_{\mu,\nu=1}^{r}\sum_{\gamma=0}^{d-1}\sum_{S=0}^{n-1}\left(1-\frac{dS+\gamma}{dn}\right)\times$$

$$\times(P^{dS}-A_0)P^\gamma e_\mu\cdot\hat{A}e_\nu\cos[(dS+\gamma)r+\mu-\nu]\omega T,$$

$$(11)\qquad G_2^{(N)}(\omega)=\sum_{\mu,\nu=1}^{r}\sum_{\gamma=0}^{d-1}\sum_{S=0}^{n-1}\left(1-\frac{dS+\gamma}{dn}\right)A_0P^\gamma e_\mu\cdot$$

$$\cdot\hat{A}e_\nu\cos[(dS+\gamma)r+\mu-\nu]\omega T.$$

Since the norm of matrix $(P^{dS}-A_0)$ has order $b^{S/d}$, $b<1$, then $G_1^{(N)}(\omega)$ has the classical limit:

$$(12)\qquad \lim_{N\to\infty}G_1^{(N)}(\omega)=\sum_{\mu,\nu=1}^{r}\sum_{\gamma=0}^{d-1}\sum_{S=0}^{\infty}\tilde{m}_{\mu\nu}^{(S,\gamma)}\cos[(dS+\gamma)r+\mu-\nu]\omega T.$$

It is easily shown that

$$(13)\qquad \lim_{N\to\infty}G_2^{(N)}(\omega)=\sum_{\mu,\nu=1}^{r}\sum_{\gamma=0}^{d-1}A_0P^\gamma e_\mu\cdot\hat{A}e_\nu\cdot$$

$$\cdot\lim_{n\to\infty}\Big[\cos(\gamma r+\mu-\nu)\omega T\sum_{S=0}^{n-1}\left(1-\frac{S}{n}\right)\cos dSr\omega T-$$

$$-\sin(\gamma r+\mu-\nu)\omega T\sum_{S=0}^{n-1}\left(1-\frac{S}{n}\right)\sin dSr\omega T\Big],$$

where the limit again is understood in sense D'. Passing to the limit in (13), we get on the basis of Ref. 11

$$(14)\qquad \lim_{N\to\infty}G_2^{(N)}(\omega)=\sum_{\mu,\nu=1}^{r}\sum_{\gamma=0}^{d-1}m_{\mu\nu}^{(\gamma)}\frac{\sin\left(\frac{dr}{2}-\gamma r-\mu+\nu\right)\omega T}{2\sin\frac{dr\omega T}{2}}+$$

$$+\frac{\pi}{drT}\sum_{\mu,\nu=1}^{r}\sum_{\gamma=0}^{d-1}m_{\mu\nu}^{(\gamma)}\cos(\gamma r+\mu-\nu)\omega T\sum_{n=-\infty}^{\infty}\delta\left(\omega-\frac{2\pi h}{drT}\right).$$

The first term in (14) is understood as canonical regularization in the sense of Gel'fand and Shilov [Ref. 11] of the corresponding generalized function.

Sequentially substituting (12) and (14) in (9), and then (9) in (5), and (5) in (6) and (3), we get

$$(15)\qquad P(\omega)=\frac{4|a|^2}{rT}\Big[\sum_{\mu,\nu=1}^{r}\sum_{\gamma=0}^{d-1}\sum_{S=0}^{\infty}\tilde{m}_{\mu\nu}^{(S,\gamma)}\cos[(dS+\gamma)r+\mu-\nu]\omega T-$$

$$-\frac{1}{2}\sum_{\mu,\nu=1}^{r}m_{\mu\nu}\cos(\mu-\nu)\omega T+\sum_{\mu,\nu=1}^{r}\sum_{\gamma=0}^{d-1}m_{\mu\nu}^{(\gamma)}\frac{\sin\left(\frac{dr}{2}-\gamma r-\mu+\nu\right)\omega T}{2\sin\frac{dr\omega T}{2}}+$$

$$+\frac{\pi}{drT}\sum_{\mu,\nu=1}^{r}\sum_{\gamma=0}^{d-1} m_{\mu\nu}^{(\gamma)}\cos(\gamma r+\mu-\nu)\omega T\sum_{h=-\infty}^{\infty}\delta\left(\omega-\frac{2\pi h}{drT}\right)\Big].$$

4. The Case of a Process Controlled by a Regular Markov Chain

In this case the formula for $P(\omega)$ can be formally derived from (15) if we set $d = 1$, $A_0 = A$. The coefficients $m_{\mu\nu}^{(0)} = Ae_\mu \cdot \hat{A}e_\nu = (A_1\varepsilon_{1\mu} + A_2\varepsilon_{2\mu} + \ldots + A_q\varepsilon_{q\mu})\sum_{\varphi} \cdot \hat{A}e_\nu = a_\mu a_\nu$, where $a_\mu = \sum_{j=1}^{q} A_j\varepsilon_{j\mu}$. Thus matrix $(m_{\mu\nu}^{(0)})_{\mu,\nu=1,\ldots,r}$ is symmetric, and in virtue of the odd sine the third sum in (15) vanishes. Since this circumstance is in fact used up to passage to the limit, the procedure of canonical regularization is redundant for processes controlled by regular Markov chains. On the other hand if we know in addition that $a_\mu = 0$, $\forall\mu$, then there is no term with δ-functions, and passage to the limit is classical. In particular, this is so in the practically important case where the matrix P is doubly stochastic (in which event all coordinates of the vector of final probabilities will coincide), and $\sum_{j=1}^{q}\varepsilon_{j\mu} = 0$, $\forall\mu$.

Thus for a regular Markov chain

$$(16)\qquad P(\omega) = \frac{4|a|^2}{rT}\Big\{\frac{1}{2}\sum_{\mu=1}^{r} m_\mu + \sum_{\mu,\nu=1}^{r}\sum_{s=0}^{\infty}\bar{m}_{\mu\nu}^{(s)}\cos(Sr+\mu-\nu)\omega T + \sum_{\mu,\nu=1}^{r} m_{\mu\nu}^{(0)}\cos(\mu-\nu)\omega T\Big[-\frac{1}{2}+\frac{\pi}{rT}\sum_{h=-\infty}^{\infty}\delta\left(\omega-\frac{2\pi h}{rT}\right)\Big]\Big\}.$$

3. Examples of Calculation of Averaged Energy Spectra

Solution of the problem of increasing the density and interference immunity of digital magnetic recording requires calculation of the averaged energy spectra of a large number of signals; the better the signal spectrum agrees with the transfer

TABLE 1

Binary sequence					
№	Input входная	Output выходная	№	Input входная	Output выходная
1	0000	11001	9	1000	11010
2	0001	11011	10	1001	01001
3	0010	10010	11	1010	01010
4	0011	10011	12	1011	01011
5	0100	11101	13	1100	11110
6	0101	10101	14	1101	01101
7	0110	10110	15	1110	01110
8	0111	10111	16	1111	01111

characteristic of the channel, the greater the density and interference immunity of the recording can be made. From this standpoint, the authors studied some promising high-information digital magnetic recording signals [Ref. 12].

Let us emphasize once again that the proposed method is general in nature and can be used to find the averaged energy spectra any time that the model presented in §1 is sufficiently equivalent (exactly or approximately) to the signal being studied. Let us illustrate the technique by some typical examples.

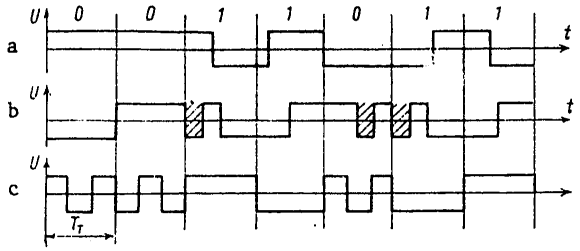

Fig. 1

5.1. One of the most promising signals used in high-density digital magnetic recording is that of narrow-band recording without return to zero (nwrz) [Ref. 12]. The nwrz signal (Fig. 1a) is formed in accordance with the algorithm of Table 1.

In this case in the output binary sequence a succession of more than two zeros running is eliminated, which ensures reliable self-synchronization of the nwrz signal.

The nwrz signal can be represented in the form of 32 repeated bursts (Fig. 2a). The duration of each burst is equal to 5T ($T = 4T_T/5$, T_T is the clock cycle). Since nwrz recording is done with respect to two levels, the amplitudes of the pulses are equal to ±1; q = 32; r = 5;

$e_1 = (F_1, -F_1)$, $F_1 = (1\ 1\ 1\ 1\ 1\ 1\ 1\ 1\ 1\ 1\ 1\ 1\ 1\ 1\ 1\ 1)$;
$e_2 = (F_2, -F_2)$, $F_2 = (-1-1\ 1\ 1-1\ 1\ 1\ 1\ 1-1-1-1-1-1-1-1-1)$;
$e_3 = (F_3, -F_3)$, $F_3 = (-1-1\ 1\ 1\ 1\ 1-1-1-1-1-1-1-1-1\ 1\ 1\ 1\ 1)$;
$e_4 = (F_4, -F_4)$, $F_4 = (-1\ 1-1-1\ 1-1\ 1\ 1\ 1-1\ 1\ 1-1\ 1-1-1)$;
$e_5 = (F_5, -F_5)$, $F_5 = (1-1-1\ 1-1\ 1\ 1-1\ 1\ 1\ 1-1-1-1-1\ 1)$;

$$P = \frac{1}{16}\left(\begin{array}{c|c} 1 & G^* \\ \hline G^* & G \end{array}\right); \quad G^T = (\vec{g}_1\vec{g}_2\vec{g}_2\vec{g}_1\vec{g}_2\vec{g}_1\vec{g}_1\vec{g}_2\vec{g}_1\vec{g}_1\vec{g}_1\vec{g}_2\vec{g}_2\vec{g}_2\vec{g}_2\vec{g}_1),$$

where $\vec{g}_1 = (0000000001110111)$; $\vec{g}_2 = (1111111110001000)$; G* is obtained from matrix G by changing zeros to ones and ones to zeros; G^T is the transpose of matrix G.

It is directly verified that matrix P is doubly stochastic and all elements of P^2 are positive, and therefore the given process is controlled by a regular Markov chain; $\vec{A} = {}^1/_{32}\xi_{32}$; $A = {}^1/_{32}I$;

$$m_\mu = 1; \quad M_1 = (\tilde{m}_{\mu\nu}^{(1)}) = \frac{1}{32}\begin{pmatrix} 0 & -1 & 3 & 2 & -8 \\ 0 & -{}^3/_2 & {}^9/_2 & 3 & -12 \\ 0 & {}^1/_2 & -{}^3/_2 & -1 & 4 \\ 0 & 0 & 0 & 0 & 0 \\ 0 & 0 & 0 & 0 & 0 \end{pmatrix};$$

$\tilde{m}_{\mu\nu}^{(S)} = 0$; $\forall \mu, \nu$; $S > 1$.

Substituting the values found in formula (16), we get

$$P(\omega)=\frac{\sin\frac{2\omega T_т}{5}}{8\omega^2 T_т}\left(80-40\cos\frac{4\omega T_т}{5}-30\cos\frac{8\omega T_т}{5}+\right.$$
$$\left.+14\cos\frac{12\omega T_т}{5}+\frac{5}{2}\cos\frac{16\omega T_т}{5}-3\cos 4\omega T_т+\frac{1}{2}\cos\frac{24\omega T_т}{5}\right).$$

5.2. Among self-synchronized signals that increase recording density is the narrow-band phase-modulated signal (npm) [Ref. 12]. To improve reliability of the process of recording and playback, the shape of the npm signal is considerably modified

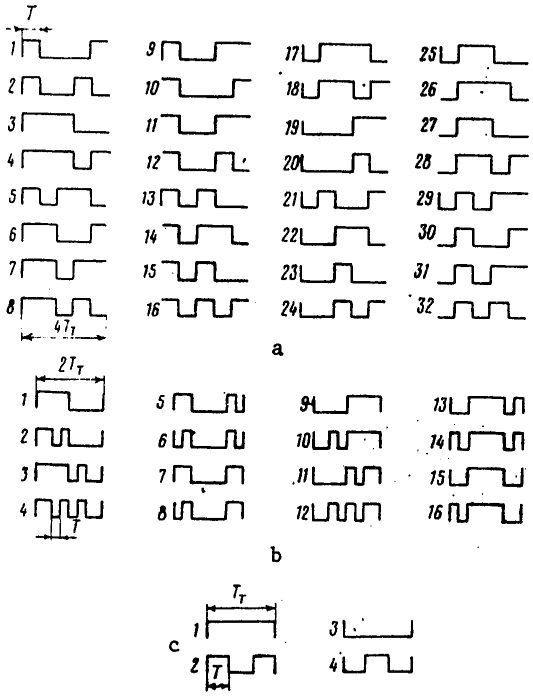

Fig. 2

(Fig. 1b) even before recording on the magnetic medium (i. e. it is predistorted -- pd). The npmpd signal can be represented as 16 bursts (Fig. 2b). The duration of the bursts is equal to 8T ($T = T_T/4$); $q = 16$; $r = 8$.

$e_1=(F_1, -F_1)$, $F_1=(1\,1\,1\,1\,1\,-1\,1\,-1)$;
$e_2=(F_2, -F_2)$, $F_2=(1\,1\,1\,1\,1\,1\,1\,1)$;
$e_3=(F_3, -F_3)$, $F_3=(1\,-1\,1\,-1\,-1\,1\,-1\,-1)$;
$e_4=(F_4, -F_4)$, $F_4=(1\,1\,1\,1\,-1\,-1\,-1\,-1)$;
$e_5=(F_5, -F_5)$, $F_5=(-1\,-1\,-1\,-1\,-1\,-1\,-1\,-1)$;
$e_6=(F_6, -F_6)$, $F_6=(-1\,-1\,1\,1\,1\,-1\,-1\,1\,-1\,-1)$;
$e_7=(F_7, -F_7)$, $F_7=(-1\,-1\,-1\,-1\,1\,1\,1\,1)$;
$e_8=(F_8, -F_8)$, $F_8=(-1\,-1\,-1\,-1\,-1\,-1\,1\,1)$;

$$P=\frac{1}{4}\left(\frac{G}{\widetilde{G^*}}\middle|\frac{G^*}{G}\right);\quad G^T=(\vec{g}_1\vec{g}_1\vec{g}_1\vec{g}_2\vec{g}_2\vec{g}_2\vec{g}_1\vec{g}_1\vec{g}_1\vec{g}_2\vec{g}_2\vec{g}_2),$$

where $\vec{g}_1 = (10100000)$; $\vec{g}_2 = (00000000)$; $\vec{g}_3 = (01011010)$; $G^{*T} = (g_4 g_4 g_3 g_3 g_4 g_4 g_2 g_2)$, where $g_4 = (00000101)$.

This process as well is controlled by a regular chain with doubly stochastic transition matrix P: $\vec{A} = 1/16\,\vec{\varepsilon}_{16}$; $\hat{A} = 1/16\,I$; $m_\mu = 1$.

In the given example, the formula for calculating $P(\omega)$ is theoretically no longer finite, but numerical calculation shows that for the npmpd signal we can limit ourselves to terms $S = 0, 1, \ldots, 5$. Further refinements do not exceed one percent.

TABLE 2

$P^{(1)}_{(\omega)}$	$\frac{\sin^2(\omega T/2)}{2\omega^2 T}$ (16, 4, 8, −8, −16, −4, −16, 2, 0, 2, 10, 2, 4, 0, −2)
$P^{(5)}_{(\omega)}$	$\frac{\sin^2(\omega T/2)}{2\omega^2 T}$ (16, 4, 8, −8, −16, −4, −16, 2, 0, 4, 12, 2, 8, −2, −4, −3, −8, 0, −2, 2, 4, 1, 4, −1/2, 0, −1, −3, −1/2, −2, 1/2, 1, 3/4, 2, 0, 1/2, −1/2, −1, −1/4, −1, 1/8, 0, 1/8, 5/8, 1/8, 1/4, 0, −1/8)

The results of calculations of $P(\omega)$ for the npmpd signal are summarized in Table 2.

In the formulas of $P(\omega)$ (Table 2) the coefficients of $\cos k\omega T$, $k = 0, 1, 2, \ldots$ are given in parentheses.

Also in the category of self-synchronized signals is the frequency-modulated signal with square-wave carrier (fms) shown in Fig. 1c. An interesting feature of this signal is that an odd number of high-frequency half-periods fits in the clock interval. The forms of bursts for the fms signal are shown in Fig. 2c. In this case, $T_T = 3T$; $q = 4$; $r = 3$; $e_1 = e_3 = (1\,1\,-1\,-1)$, $e_2 = (1\,-1\,-1\,1)$;

$$P = \frac{1}{2}\left(\begin{array}{c|c} G & G^* \\ \hline G^* & G \end{array}\right); \quad G = \begin{pmatrix} 0 & 0 \\ 0 & 0 \end{pmatrix}; \quad G^* = \begin{pmatrix} 1 & 1 \\ 1 & 1 \end{pmatrix}$$

Here

$$P^{2m} = \frac{1}{2}\left(\begin{array}{c|c} G^* & G \\ \hline G & G^* \end{array}\right), \quad P^{2m+1} = P.$$

Hence we see that the given process is controlled by a cyclic Markov chain for which $d = 2$. In this case $A_0 = P^2$; $\hat{A} = 1/4\,I$;

$$m_{\mu\nu} = \begin{pmatrix} 1 & 0 & 1 \\ 0 & 1 & 0 \\ 1 & 0 & 1 \end{pmatrix}, \quad m^{(0)}_{\mu\nu} = \begin{pmatrix} 1 & 0 & 1 \\ 0 & 0 & 0 \\ 1 & 0 & 1 \end{pmatrix}, \quad m^{(1)}_{\mu\nu} = \begin{pmatrix} -1 & 0 & -1 \\ 0 & 0 & 0 \\ -1 & 0 & -1 \end{pmatrix},$$

$$\bar{m}^{(s)}_{\mu\nu} = 0, \quad \forall \mu, \ \nu, \ S > 1.$$

Then in the first summand of formula (15) we have non-zero terms at $\gamma = 0$, $S = 0$: $3 + 2\cos 2\omega T - 2 - 2\cos 2\omega T = 1$. The second summand: $-1/2(3 + 2\cos 2\omega T)$. The only components in the singular summand are those at $\gamma = 0$: $1 + \cos 2\omega T$. Passages to the limit are treated in the sense of D'. Substituting the resultant values in formula (15), we find $P(\omega)$ for the fms signal:

$$P(\omega) = \frac{8\sin^2(\omega T/2)}{3\omega^2 T}\left[1 + \frac{8\pi}{3T}\cos^2\omega T \sin^2\frac{3\omega T}{2}\sum_{n=-\infty}^{\infty}\delta\left(\omega - \frac{\pi h}{3T}\right)\right].$$

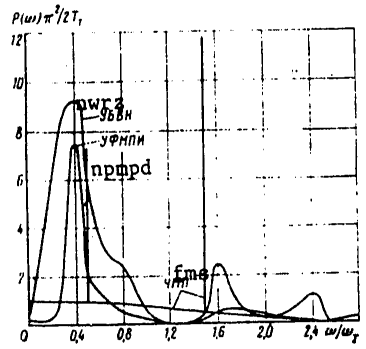

Fig. 3

5.4. The resultant formulas were used for plotting graphs of the averaged energy spectra of the given signals (Fig. 3), where the values of $P(\omega)$ multiplied by the coefficient $\pi^2/2T_T$ are laid out along the axis of ordinates, while the values of the normalized frequency ω/ω_T are laid out along the axis of abscissas.

A comparison was made between the results of calculations and experiment. In the experiment the information signal was simulated by a generator of pseudorandom pulse sequences. The duration of a sequence was taken as equal to 1023 clock cycles and the clock frequency was 1 MHz. Appropriate modulators were used to produce npmpd and fms signals, which were studied on a wide-band spectrum analyzer type S4-25. Photographs on Fig. 4 and 5 [not included in the translation] show the amplitude spectra of these signals taken from the CRT screen of the analyzer in the same scale. A special detector was used to isolate only the envelope of the amplitude spectrum. The error of measurement of the components of the spectrum did not exceed ±1 dB.

The somewhat different shapes of the theoretical and experimental spectra, in particular the slightly higher level of high-frequency components in the theoretical spectra, can be attributed to the fact that in the calculations the rise and fall times were taken as infinitely short, and also to experimental error. However, on the whole the theoretical and experimental spectra correspond fairly satisfactorily.

It can be seen from an examination of the graphs of spectra of the nwrz and npmpd signals that most of the energy of these signals is concentrated in the low-frequency region. Considerable use is made of this fact in optimum matching of signal parameters and the recording-playback channel. The use of signals with the described forms of spectra in digital magnetic recording equipment has made it possible to increase the information density of recording by a factor of 1.5-1.6 without sacrificing high interference immunity [Ref. 13, 14].

The spectrum of the fms signal clearly shows two discrete components corresponding to the zero-level and one-level information digits, which facilitates symbol detection by frequency separation.

REFERENCES

1. B. R. Levin, "Teoreticheskiye osnovy statisticheskoy radiotekhniki" [Theoretical Principles of Statistical Radio Engineering], Book 1, Sovetskoye radio, 1974, p 552.

2. V. I. Tikhonov, M. A. Mironov, "Markovskiye protsessy" [Markov Processes], Sovetskoye radio, 1977, p 488.

3. L. M. Polyak, RADIOTEKHNIKA I ELEKTRONIKA, Vol 17, No 3, 1972, p 626.

4. A. L. Knoll, "Spectral Analysis of Signals Used in Digital Magnetic Recording" in: "Problemy magnitnoy zapisi" [Problems of Magnetic Recording], edited by V. G. Korol'kov, Energiya, 1975, pp 79-91

5. M. Khekt, A. Guida, "Delay Modulation," Trudy Instituta inzhenerov po elektrotekhnike i radioelektronike [Proceedings of the Institute of Electrical and Electronics Engineers], Vol 57, No 7, 1969, p 161.

6. G. V. Konovalov, Ye. M. Tarasenko, "Impul'snyye sluchaynyye protsessy v elektrosvyazi" [Pulsed Random Processes in Electrical Communications], Svyaz', 1973, p 304.

7. Ye. M. Tarasenko, RADIOTEKHNIKA I ELEKTRONIKA, Vol 21, No 2, 1976, p 400.

8. G. L. Cariolaro, G. P. Tronca, IEEE TRANS. COMMUNS, 1974, COM-22, 10, Oct 1955.

9. J. Kemeny, J. Snell, "Konechnyye tsepi Markova" [Finite Markov Chains], Nauka, 1971, p 512.

10. V. S. Vladimirov, "Uravneniya matematicheskoy fiziki" [Equations of Mathematical Physics], Nauka, 1971, p 512.

11. I. M. Gel'fand, G. Ye. Shilov, "Obobshchennyye funktsii i deystviya nad nimi" [Generalized Functions and Operations on Them], GIFML, 1959, p 470.

12. T. G. Pletneva, O. V. Poritskiy, G. N. Rozorinov, S. D. Eydel'man, "Determination of Energy Spectra of Complex Digital Signals by the Method of Associated Markov Chains," OTBOR I PEREDACHA INFORMATSII, No 56, 1979, Naukova dumka, pp 48-59.

13. O. V. Poritskiy, G. N. Rozorinov, S. K. Kachanovskiy, "Magnetic Recording and Playback of Digital Information on a Disk Using Narrow-Band Phase Modulation," VESTNIK KIYEVSKOGO POLITEKHNICHESKOGO INSTITUTA, ELEKTROAKUSTIKA I ZVUKOTEKHNIKA No 1, 1977, pp 45-49.

14. O. V. Poritskiy, G. N. Rozorinov, V. D. Svyachennyy, "High-Voltage Digital Magnetic Recording and Playback of a Continuous Stream of Information," VESTNIK KIYEVSKOGO POLITEKHNICHESKOGO INSTITUTA, ELEKTROAKUSTIKA I ZVUKOTEKHNIKA, No 2, 1978, pp 13-17.

15. M. V. Gitlits, "Magnitnaya zapis' v sistemakh peredachi informatsii" [Magnetic Recording in Data Transmission Systems], Svyaz', 1978, p 304.

6610
CSO: 1860

UDC 621.371

RANGE OF THE DEAD ZONE AND MAXIMUM RECEIVABLE FREQUENCY FOR A HORIZONTALLY NONHOMOGENEOUS IONOSPHERIC LAYER

Moscow RADIOTEKHNIKA in Russian Vol 35, No 10, Oct 80 pp 63-66 manuscript received 28 Jan 80

[Article by M. V. Tinin]

[Text] Among the most important characteristics of a shortwave transmission path is the range of the dead zone (i. e. the distance at which the caustic intersects the surface of the earth) at a given frequency, and also the maximum receivable frequency for a given distance between ground-based communicating parties. Determination of these characteristics involves finding the minimum range of a single hop for beams whose trajectories in the general case of a horizontally nonhomogeneous ionosphere are found by numerical integration of a system of nonlinear ordinary differential equations. In cases where the equations of the beam have an analytical solution, the problem reduces to solution of a rather complex transcendental equation. In this paper, approximate formulas are derived for the range of the dead zone and the maximum receivable frequency in both horizontally homogeneous and horizontally inhomogeneous ionospheric layers with consideration of the smallness in difference between the angle of departure and the critical angle for a beam arriving at the boundary of the dead zone. For the sake of simplicity and clarity of the calculations, we will restrict ourselves to a flat earth and close to flat-layered ionosphere with permittivity assigned as

$$\varepsilon(z', x') = \begin{cases} 1 - \xi^{-1}\left[1 - \left(\frac{z' - y_m}{y_m}\right)^2\right], & 0 \leqslant z' \leqslant 2y_m, \\ 1, & z' \leqslant 0, \end{cases} \qquad (1)$$

where $\xi = f_0/f_c$ is the ratio of the working frequency to the critical frequency; y_m is the half-thickness of the layer. The presence of horizontal inhomogeneity in the ionosphere is accounted for by the slow dependence of parameters ξ and y_m on x' and by the inclination $\alpha = \arctan dh/dx$ of the base of the layer (Fig. 1).

Consider first the case of a horizontally homogeneous ionosphere

$$\xi = \text{const}, \quad y_m = \text{const}, \quad \alpha = 0, \quad z = z', \quad x = x', \qquad (2)$$

where $h_0 = h$, $\psi_0 = \psi_1$, $l_0 = l_1$, $D' = D$, and for the range of a hop of a reflected beam we have [Ref. 1, 2]

$$D = \frac{2hs}{\sqrt{1 - s^2}} + \tau, \qquad (3)$$

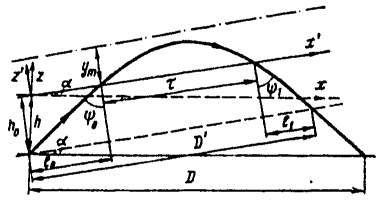

Fig. 1

where

$$\tau = y_m s\xi \ln \frac{1+\xi\sqrt{1-s^2}}{1-\xi\sqrt{1-s^2}} \tag{4}$$

is the range of a hop inside the layer; h is the altitude of the base of the layer; $s = \sin\psi_0$ is the sine of the angle of incidence of the beam on the layer.

The range of the dead zone is determined by substituting in (3) the solution of the transcendental equation

$$\frac{\partial D}{\partial s}(s_m) = 0. \tag{5}$$

It is known [Ref. 2] that the angle of incidence $\psi_{0m} = \arcsin s_m$ of the beam arriving at the boundary of the dead zone is not equal to the critical angle. However, as can be seen from distance vs. angle curves $D(\psi_0)$ [Ref. 1-3] this angle is often quite close to critical. With consideration of this fact, we can solve (3) approximately with respect to $s(\tau)$:

$$s(\tau) = \sin\psi_0 \approx \sqrt{1-\xi^2} + \frac{2}{\xi\sqrt{\xi^2-1}} e^{-\frac{\tau}{y_m\sqrt{\xi^2-1}}}. \tag{6}$$

Substituting (6) in (3), we get an approximate equation for the range of the hop:

$$D = 2h \frac{\sqrt{\xi^2-1} + \frac{2}{\sqrt{\xi^2-1}} e^{-\frac{\tau}{y_m\sqrt{\xi^2-1}}}}{\sqrt{1 - 4e^{-\frac{\tau}{y_m\sqrt{\xi^2-1}}} - \frac{4}{\xi^2-1} e^{-\frac{2\tau}{y_m\sqrt{\xi^2-1}}}}} + \tau \approx 2h\sqrt{\xi^2-1}\left\{1 + \frac{2\xi^2}{\xi^2-1} e^{-\frac{\tau}{y_m\sqrt{\xi^2-1}}}\right\} + \tau. \tag{7}$$

Expression (5) reduces to the equation

$$\frac{\partial D(\tau_m)}{\partial \tau} = -\frac{4h\xi^2}{y_m(\xi^2-1)} e^{-\frac{\tau_m}{y_m(\xi^2-1)}} + 1 = 0. \tag{8}$$

From (8) and (6) we get

$$s_m \approx \sqrt{1-\xi^{-2}}\left\{1 + \frac{y_m}{2h\xi^2}\right\}. \tag{9}$$

Now, substituting (9) in (3)-(4), we get for the range of the dead zone D_m

$$\tilde{D}_m = \sqrt{\xi^2-1}\left\{1 + \frac{\tilde{y}_m}{\xi^2}\right\}\left\{\frac{1}{\sqrt{1-2\tilde{y}_m(1-\xi^{-2})}} + \tilde{y}_m \ln \frac{1+\sqrt{1-2\tilde{y}_m(1-\xi^{-2})}}{1-\sqrt{1-2\tilde{y}_m(1-\xi^{-2})}}\right\}. \tag{10}$$

where $\tilde{D}_m = D_m/2h$, $\tilde{y}_m = y_m/2h$.

With consideration of (8), a transition to the second equality of (7) can be made when

$$\tilde{y}_m < 1. \tag{11}$$

But when condition (11) is met, expression (10) is simplified, becoming

$$\tilde{D}_m \approx \sqrt{\xi^2 - 1}\left\{1 + \tilde{y}_m\left[1 + \ln\frac{2}{\tilde{y}_m(1-\xi^{-2})}\right]\right\}. \tag{12}$$

In order to find the ratio of the maximum receivable frequency to the critical frequency (M-factor), it is necessary for a given range D to solve equation (12) with respect to $\xi = \xi_m$. Assuming a low value of $\tilde{y}_m \ln(1-\xi^{-2})$, let us solve (12) by a method of successive approximations:

$$\xi_m \approx \sqrt{1 + \tilde{D}^2\left\{1 + \tilde{y}_m\left[1 + \ln\frac{2(1+\tilde{D}^{-2})}{\tilde{y}_m}\right]\right\}^{-2}}. \tag{13}$$

A more exact expression for the M-factor can be obtained by solving (10):

$$\xi_m \approx \sqrt{1 + \tilde{D}^2\left\{\left[1 + \frac{\tilde{y}_m}{1+\tilde{D}^2}\right]\left[\eta^{-1} + \tilde{y}_m \ln\frac{1+\eta}{1-\eta}\right]\right\}^{-2}}, \tag{14}$$

where

$$\eta = \sqrt{1 - \frac{2\tilde{y}_m}{1+\tilde{D}^{-2}}}. \tag{15}$$

Comparison with the exact numerical values of ξ_m and $\tilde{D}_m$ has shown that the error of formulas (10), (14) for $\tilde{y}_m = 0.25$, $1.4 \leqslant \xi \leqslant 3.6$ is about 3% or less, and decreases with decreasing $\tilde{y}_m$. The error of formulas (12)-(13) is somewhat higher ($\lesssim 5\%$) on the lower edge of the given range of ξ, but for large ξ (which corresponds to long hop ranges) is also less than 3%.

In the case of a horizontally inhomogeneous ionosphere, conditions (2) are no longer met. Then instead of (3) we have

$$D = \frac{D'\cos\psi_1}{\cos(\alpha+\psi_1)} - \frac{\cos\psi_1}{\cos(\alpha+\psi_1)}\left\{\frac{h_0}{\operatorname{ctg}\psi_0} + \frac{h_0}{\operatorname{ctg}\psi_1} + \tau\right\}. \tag{16}$$

In calculating ψ_0, ψ_1, just as before we use the fact that these angles are close to critical at a sufficiently small $\tilde{y}_m = y_m/2h_0$. Hence

$$\operatorname{ctg}\psi_l = \operatorname{ctg}\psi_0^{(0)} + \underset{l=0,1}{\Delta}\operatorname{ctg}\psi_l, \tag{17}$$

where $\operatorname{ctg}\psi_0^{(0)}(\tau)$ is determined in accordance with formula (6) (i. e. disregarding horizontal gradients), and the corrections for the gradient $\Delta\operatorname{ctg}\psi_i$ are equal to the corresponding corrections to the critical angle found in Ref. 4. Substituting explicit expression (17) in (16), we get an approximate equation for the range of the hop:

$$D \approx [1 - \alpha\sqrt{\xi^2-1}]^{-1}\left\{2h_0\sqrt{\xi^2-1}\left[1 + \frac{2\xi^2}{\xi^2-1}e^{-\frac{\tau}{\tilde{y}_m\sqrt{\xi^2-1}}} - \frac{\tau\xi^2}{4h_0L(\xi^2-1)}\right] + \tau\right\}. \tag{18}$$

where $L = f_c \Big/ \left(2h_0 \frac{\partial f_c}{\partial x}\right)$ is the relative scale of change in critical frequency of the layer. In (18) the values of the parameters $\xi(x)$, $y_m(x)$ are taken at the point where the beam enters the ionosphere. After doing calculations analogous to those done in deriving formulas (8), (11), (12), and expressing the parameters in terms of their values y_{m0}, ξ_0 at the beginning of the transmission path, we get the range of the dead zone for a horizontally inhomogeneous ionosphere

$$\tilde{D}_m = \sqrt{\xi_0^2-1}\left\{1+\tilde{y}_{m0}\left[1+\left(1+a\sqrt{\xi_0^2-1}-\frac{\xi_0^2}{L_f\sqrt{\xi_0^2-1}}+\right.\right.\right.$$
$$\left.\left.\left.+\frac{\sqrt{\xi_0^2-1}}{2L_y}\right)\ln\frac{2}{\tilde{y}_m\left(1-\xi_0^{-2}\right)}\right]-\frac{\xi_0^2}{2L_f\sqrt{\xi_0^2-1}}+a\sqrt{\xi_0^2-1}\right\}, \qquad (19)$$

where $L_y = y_m \Big/ \left(2h_0 \frac{\partial y_m}{\partial x}\right)$ is the relative scale of change in half-thickness of the layer. Using a method of successive approximations, we get an expression for the M-factor from (19):

$$\xi_m = \sqrt{1+(\tilde{D}^*)^2}, \qquad (20)$$

where

$$\tilde{D}^* = \tilde{D}\left\{1+\tilde{y}_{m0}\left[1+\left(1+a\tilde{D}-\frac{1+\tilde{D}^2}{L_f\tilde{D}}+\frac{\tilde{D}}{2L_y}\right)\ln\frac{2(1+\tilde{D}^{-2})}{\tilde{y}_{m0}}\right]-\frac{1+\tilde{D}^2}{2L_f\tilde{D}}+a\tilde{D}\right\}. \qquad (21)$$

The region of applicability of formulas (19), (20) is bounded from below by the condition $\xi > 1$, which in addition to disregarding the magnetic field of the earth takes consideration in the first place of the approximate determination of the extreme angle (9), and in the second place of the approximate calculation of the critical angle in a horizontally inhomogeneous layer by the formulas of Ref. 4. On the other hand, an increase in ξ requires consideration of sphericity in calculations of the range of the dead space [Ref. 5]. Since asymptotic methods were used in deriving (19)-(21), an analytical estimate of their error in the region of applicability is possible only in order of magnitude, very roughly. Some numerical estimates based on comparison with the results of strict calculations show the applicability of these formulas in a range of $1.2 < \xi < 2.0$, the error of the calculations being approximately 5-8% at $\tilde{y}_m = 0.25$, and decreasing as $\tilde{y}_m \to 0$.

It is interesting to note that formulas (19)-(21) can be obtained from (12), (13) for a horizontally homogeneous ionosphere. To do this requires only substitution of the values of the parameters of the layer

$$y_m = y_{m0}\left[1+\frac{D}{2L_y}\right], \quad \xi = \xi_0 - \frac{\xi_0\tilde{D}}{2L_f}, \quad h = h_0(1+a\tilde{D})$$

on the mid transmission path, and expansion of the resultant expressions with respect to powers of the small parameters L_y^{-1}, L_f^{-1}, α, retaining terms of the first order of smallness. This first-approximation equivalence of horizontally inhomogeneous and averaged homogeneous transmission paths reflects the all but obvious fact that in virtue of the duality of the path[1], the results of the calculations

[1]Let us recall that anisotropy of the ionospheric plasma is disregarded in our formulation of the problem.

should not change with reversal of the sign of the horizontal gradient, and consequently the expressions that relate the parameters of the ionosphere at midpath to the maximum receivable frequency, the range of the dead space, the propagation time and several other characteristics should not contain odd powers of L_y^{-1}, L_f^{-1} and α.

The resultant formulas (12)-(13), (19)-(21) enable not only analysis of the way that the range of the dead space and the maximum receivable frequency depend on the parameters of the ionospheric layer, but also dynamic practical calculations of shortwave transmission paths in cases where high accuracy is not a requisite.

REFERENCES

1. K. G. Budden, "Radio Waves in the Ionosphere," Cambridge, Cambridge Univ. Press, 1961.

2. K. Davis, "Radiovolny v ionosfere" [Radio Waves in the Ionosphere], Moscow, Mir, 1973.

3. Ye. M. Zhulina, Ye. M. Kovalevskaya, "Raschet kharaketeristik rasprostraneniya radiovoln s uchetom statisticheskikh svoystv sredy i vozmushchennosti ionosfery" [Calculation of the Characteristics of Radio Wave Propagation with Consideration of the Statistical Properties of the Medium and Disturbance of the Ionosphere], Moscow, IZMIRAN, 1976.

4. M. V. Tinin, in: "Issledovaniya po geomagnetizmu, aeronomii i fizike Solntsa" [Research on Geomagnetism, Aeronomy and Physics of the Sun], No 44, Moscow, Nauka, 1978.

5. M. V. Tinin, in: "Issledovaniya po geomagnetizmu, aeronomii i fizike Solntsa" No 51, Moscow, Nauka, 1980.

[86-6610]

6610
CSO: 1860

UDC 621.372.54

REQUIREMENTS ON METHODS OF SYNTHESIZING DIGITAL FILTERS USED FOR FLAW DETECTION OF ANTENNA SYSTEMS

Moscow RADIOTEKHNIKA in Russian No 9, 1980 pp 56-59

[Article by V. R. Kryuchok, G. P. Lichko]

[Text] One of the basic methods of flaw detection of antenna systems by the results of holographic measurement of the amplitude-phase distribution of the field in the near zone is the method of inverse diffraction [1]. The success in implementing this method depends to a great extent on the level of measurement noise such as the error of the measuring equipment, the nonideal nature of the characteristics of the probes, the disturbance of the conditions of quantification of the measured amplitude-phase distribution (APD) and also the degree of isolation of the variation of the APD caused by the defects in the measurement plane. The given difficulties can be partially surmounted using digital filters having frequency characteristics close to the required characteristics.

Let us define the requirements imposed on the methods of synthesizing digital filters used for flaw detection of antenna systems with the help of general-use digital computers.

The solution of the problem of flaw detection of flat antennas by the measurements of the APD in the near zone and the value of the sealed phase distribution for detection and location of defects require the application of digital filters with two-dimensional frequency characteristic with zero or linear phase characteristic.

The small quantification step used for flaw detection by comparison with the measurement of the APD for other purposes and the large measurement areas lead to an increase in the processed files and the volume of the ready-access memory of the computer used, thus complicating the recursive realization of the digital filters. Under the indicated requirements, considering the stability of the realization of digital filters, the digital filters with restriction by the pulse response (KIKh filters) with nonrecursive realization given by a relation of the following type are the most prospective for application in antenna system flaw detection:

$$y(m, p) = \sum_{k=-K}^{K} \sum_{l=-L}^{L} h(k, l)\, x(m-k, p-l), \qquad (1)$$

where h(k, ℓ) is the pulse response of length (2K+1) (2L+1); x(m, p), y(m, p) are the input and output files, respectively.

Realization of (1) is possible directly or by means of fast Fourier transformations (FFT). The choice of the method of realization depends both on the ratio of the length of the pulse response of the used filter to the magnitude of the processed file of measurement results and the capacity of the ready-access memory of the computer. For a file not contained in the ready-access memory, the filtration time increases significantly as a result of multiple reference to the external memory. For example, the time of realization of the fast Fourier transformation of a 1204x1024 file using the program by the authors realizing the algorithm presented in [2], increases by 50 times by comparison with the time required for the FFT of the 128x128 file in the ready-access memory using the YeS-1022 computer with ready-access memory of 512 kbytes and a magnetic disc storage with a capacity of 29 Mbytes. As a result of the predominant application of digital filters for filtering the results of measuring the APD entered on the intermediate information carrier (punch tape, magnetic tape), on input to the computer it is preferable to use a direct calculation (1) or sectional reduction with the help of the FFT with the known length of the pulse response of the used KIKh-filter. With the possibility of realizing the FFT of the processed file without using the external memory the linear reduction (1) is comparable with respect to speed to the circular reduction for the KIKh-filters with symmetric pulse response up to 24x24 long [3]. Thus, in all of the enumerated cases for predominant use of linear reduction the pulse response length must be minimal. The presence of symmetry has important significance, for if the selected method of synthesizing the KIKh-filter insures symmetry not only of the pulse response, but also symmetry of the frequency characteristic, the time for synthesis and realization of the filter decreases significantly. Restricting the length of the pulse response of the KIKh-filter leads to worsening of the forms of the frequency characteristics obtained with an increase in filtration noise when solving (1). Therefore the choice of the method of synthesizing the KIKh-filter must be matched both to the length of the pulse response and to the characteristics of the measuring equipment such as the dynamic range, the errors in measuring the phase and amplitude. Converting these errors to errors in calculating the APD spectrum, including the radiation pattern (RP) of the antenna system, it is possible to define the initial data for synthesis of the filter in the form of the maximum level of pulsations in the passband D_1 and the elimination band D_2, the width of the intermediate band ΔF.

As an example of synthesis of the KIKh-filter and its application for flaw detection of antenna systems let us consider the following problem. Let it be necessary to detect and locate the variation of APD caused by a defect in the form of violation of the current distribution in 40 elements of a slotted waveguide array consisting of 20x30 elements. A file of 64x64 samples of APD measured with a step of $\lambda/2$ using equipment with dynamic range and measurement error of APD using a probe providing for the calculation of the radiation pattern under the experimental conditions with an error of 5 decibels for a dynamic range of 40 decibels for

$$|\omega_1| \leqslant 0{,}3\pi, \quad |\omega_2| \leqslant 0{,}3\pi, \tag{2}$$

where ω_1, ω_2 are the spatial frequencies.

In order to obtain information about the defects, it is proposed that a method be used analogous to the dark field method [4], which consists in isolation of the upper spatial frequencies with the help of a filter. Thus, as applied to the conditions of the problem solved it is necessary to synthesize a band filter in the form of a ring with the boundaries of the passband satisfying the conditions

$$0{,}0156\pi^2 \leqslant \omega_1^2 + \omega_2^2 \leqslant 0{,}0961\pi^2. \tag{3}$$

In order to obtain the required circular symmetry of the frequency characteristics of the synthesized filter we use the frequency conversion of one-dimensional filters to two-dimensional [3] permitting synthesis of the KIKh-filters with symmetric frequency and zero phase characteristics based on conversion of the frequency coordinates of the type

$$\cos\omega = \frac{1}{2}(\cos\omega_1 + \cos\omega_2 + \cos\omega_1\cos\omega_2 - 1) \tag{4}$$

in minimum time. Synthesizing the required one-dimensional filter and using relation (4) of its frequency coordinate ω to ω_1, ω_2, it is possible to find the corresponding frequency characteristic of the two-dimensional filter. The application of the YeS-1022 computer with characteristics presented above permits realization of cyclic reduction using the FFT in the external memory with a filter 65x65 long with an additional file 64x64. The synthesis of the one-dimensional KIKh-filter is accomplished using the Remez substitution with pulse response length N=65 insuring minimum width of the intermediate band for the given values of the elimination band limit $\omega=0.087\pi$, $D_1=60$ decibels, $D_2=70$ decibels and using optimization with respect to the choice of the value of the elimination limit by the procedure discussed in [3]. The frequency characteristic of the synthesized one-dimensional filter is presented in Figure 1a.

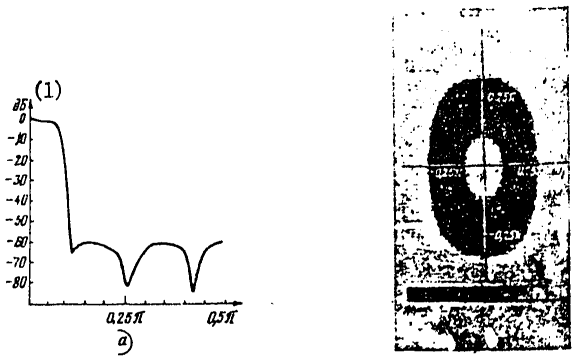

Figure 1

Key:
1. decibels

In order to obtain the required two-dimensional frequency characteristic (Fig 1b), expression (4) was used with a shift of the frequency characteristic of one-dimensional filter by means of multiplying the pulse response by $\cos(2\pi k n_0/N)$, where $n_0=13$ is the magnitude of the required shift.

The filtration time was 4 minutes, the filter synthesis time was 2.5 minutes. Figure 2a, b shows the cartographic images of the initial and filtered radiation patterns, respectively. From the comparison of these images it follows that the application of the KIKh-filter makes it possible to carry out the stated mission of flaw detection without introducing additional distortions in the frequency band of interest.

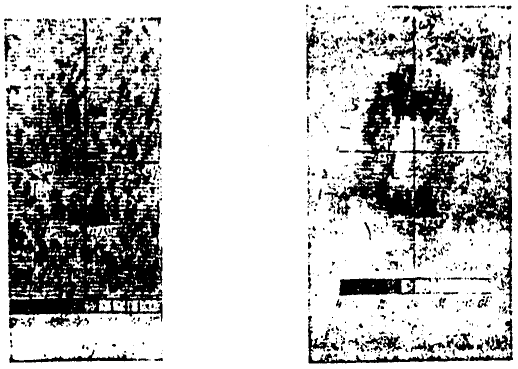

Figure 2

Thus, the class of digital filters used for flaw detection of antenna systems and the means of realizing them are defined in this paper. The necessity for using methods of synthesizing KIKh-filters that insure minimum length of the pulse response when satisfying the parameters of the frequency characteristic is substantiated, and the solution to the practical problem of flaw detection using the synthesized KIKh-filter is presented.

BIBLIOGRAPHY

1. Rensom, Mittra. TIIER, Vol 59, No 6, 1971.

2. Twogood, R. E.; Ekstrom, M. P. TRANS. IEEE, Vol C-25, No 9, 1976.

3. Rabiner, L.; Gould, B. TEORIYA I PRIMENENIYE TSIFROVOY OBRABOTKI SIGNALOV [Theory and Application of Digital Processing of Signals], Moscow, Mir, 1978.

4. Bakhrakh, L. D.; Kurochkin, A. P. GOLOGRAFIYA I MIKROVOLNOVOY TEKHNIKE [Holography in Microwave Engineering], Moscow, Sov. radio, 1979.

Manuscript received 9 Feb 80 after completion

10845
CSO: 1860

UDC 621.372.543.2

PASSBAND LOSSES OF SURFACE SOUND WAVE FILTERS

Moscow RADIOTEKHNIKA in Russian No 9, 1980 pp 17-21

[Article by A. Ye. Znamenskiy]

[Text] Broad possibilities for solving the problem of miniaturization of frequency-selective devices of the meter wave range are opened up as a result of the achievements of acoustoelectronics -- surface sound wave filters -- but they are characterized by a large amount of introduced attenuation. The attenuation of the surface sound wave filters is made up of several components. However, in the surface sound wave filters the losses to mismatch caused by the significant reactive component of the input conductivity of the counter-post converters (CPC). Inasmuch as the Q-factor of the input conductivity increases as the passband expands, the passband losses of the surface sound wave (SSW) filters, in contrast to the other types of filters, also increase with expansion of the passband.

In order to determine the mismatch losses let us use the known expressions [1]:

$$R_п = 1/G_п \approx [1/(n\omega_0 C)]\,(4\pi/9k^2);$$
$$X_п = 1/Y_п \approx 1/(\omega_0 C), \quad R_c \approx (9k^2/4\pi)\,(n/\omega_0 C);$$
$$X_c \approx 1/(\omega_0 C); \quad Q_a = R_п/X_п = X_c/R_c = 4\pi/(9k^2 n),$$

where $R_п$, $X_п$, R_c and X_c are elements of the parallel (Fig 1a) and series (Fig 1b) equivalent input resistance circuits of the CPC; ω_0 is the mean passband frequency; n is the number of posts of the CPC; $C=nC_0$ is the static capacitance of the CPC; C_0 is the capacitance per post equal to 0.55 picofarads/cm in the case of quartz; k is the electromechanical coupling coefficient (the value of k^2 can assume values from 0.0016 for quartz to 0.048 for lithium niobate).

For two identical CPC, the frequency-amplitude characteristic must have the form [1]

$$|H(\omega)| = |\sin\{[(\omega-\omega_0)/2]\tau\}/[(\omega-\omega_0)/2]|^2, \qquad (1)$$

where $\tau=\pi n/\omega_0$ is the duration of the sound pulse formed in the CPC on feeding an electrical δ-pulse to its input. From (1) we determine the value of $n=0.636/w_{1.5}$; $Q_a=(4\pi/9k^2)(0.636/w_{1.5})$, where $w_{1.5}$ is the relative passband width

determined by the 1.5 decibel level for each CPC or 3 decibels for the entire filter. Curve 1 in Fig 2 (the lefthand scale along the y-axis pertains to the solid line, and the righthand scale, to the dotted line) indicates variation of the active resistance of the CPC with parallel equivalent circuit $R_п$ for the case where the aperture (the post length) is taken equal to $40\lambda_0$ (λ_0 is the wave length on a frequency of ω_0) and $k^2=0.0016$. The Q-factor Q_a varies from 7 to 350 in this case. Although the presented relations pertain to the case of absence of apodization all further calculations are also applicable to the SSW filters with apodized CPC. The expressions for the parameters $R_п$, $X_п$, R_c and X_c are only complicated somewhat in this case.

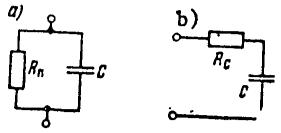

Figure 1

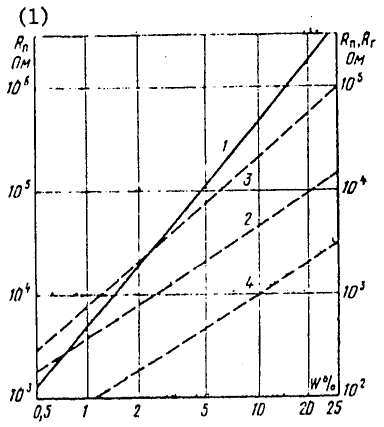

Figure 2

Key:
1. $R_п$, ohms

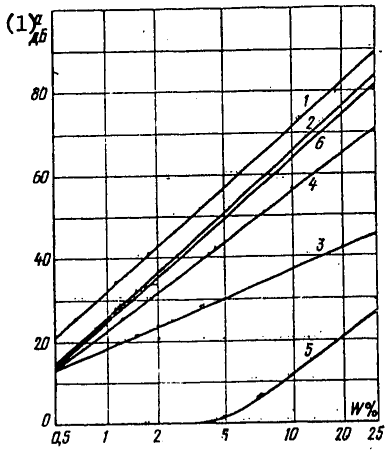

Figure 3

Key:
1. a, decibels

The square of the modulus of the circuit reflection coefficient in Fig 1a will be $|\rho|^2=[(1-\gamma)^2+Q_a^2]/[(1+\gamma)^2+Q_a^2]$ when operating from an oscillator with internal resistance $R_г$, where $\gamma=R_п/R_г$. On the basis of the relation between the losses and the reflection coefficient [2] $10^{-0.1a}=1-|\rho|^2$ the mismatch power losses for one CPC are

$$a = 10 \lg \{[(1+\gamma)^2 + Q_a^2]/4\gamma\}. \qquad (2)$$

If the filter has two identical CPC, then the magnitude of the losses determined by (2) must be doubled. The dependence of the losses defined by (2) on the passband width for filters with the above-indicated aperture included between external circuits with an input impendance equal to R_π is represented by curve 1 in Figure 3; curve 2 corresponds to operation of the same filter between 75-ohm circuits.

For determination of the possibility of lowering the losses as a result of mismatch by selecting the resistance of the external circuits, we find the derivative of the function of the square of the modulus of the reflection coefficient and equate it to zero. The optimal values of γ, the reflection coefficient and losses are as follows:

$$\gamma_{opt} = \sqrt{1+Q_a} \approx Q_a; \quad |\rho| \approx \sqrt{(Q_a-1)/(Q_a+1)}; \quad a = 10\lg[(Q_a+1)/2]. \tag{3}$$

The attenuation as a function of the passband width is represented by curve 4 in Figure 3 which is appreciably lower than curves 1 and 2. In Figure 2, curve 2 characterizes the optimal values of the input impedances $R_\Gamma = R_\pi/\gamma_{opt} \approx X_\pi$ in accordance with (3).

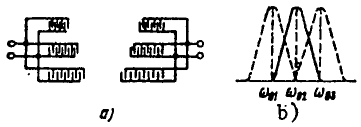

Figure 4

As is obvious from the curves in Figure 2, for wide passbands the input impedances of the external circuits determined from the first condition (3), and the more so in the case of their equality R_π, turn out to be so large that in practice it is impossible to realize them in the investigated frequency band. A reduction in the required values of the input impedances can be achieved on application of multichannel converters with frequency separation of the channels (MCFS), the circuit diagram of which is presented in Figure 4a. Each CPC (input and output) is realized as m channel CPC operating in parallel and designed for a passband m times less than required (Figure 4b), and therefore it has approximately m times larger number of posts. The active radiation resistance of the multichannel CPC within the limits of the required frequency band turns out to be (with the same aperture) m^2 times less than the single-channel CPC would have as a result of an increase in the number of posts on narrowing of the band. If we consider that the multichannel CPC must be realized on a plate of the same width as the single-channel CPC, then the apertures of each of the channel CPC of the MCFS must be executed m times smaller than the aperture of the single-channel CPC. Here R_π of the multichannel CPC turns out to be not m^2 times smaller, but m times smaller than for the single-channel CPC. In connection with the increase in the number of posts, the Q-factor of each of the channel CPC turns out to be m times less by comparison with the single-channel CPC, but if the channel CPC are included in parallel, the total Q-factor of the multichannel CPC as a result of addition of the channel capacitances turns out to be equal to the Q-factor of the single-channel CPC calculated for the same frequency band. The application of the MCFS thus offers the possibility of realizing the less high-resistance CPC and as a result, lowering the magnitudes of the introduced attenuation.

The matching problems are the subject of papers by Bode [3] establishing the limiting relations for circuits with active and reactive components of the input immitance, and Fano [4], who proposed the method of synthesizing matched circuits containing a finite number of lumped circuit elements. Let us note that in [5] it is demonstrated that Fano's solution is not optimal although it is very close to optimal. The Bode ratio for minimum attainable reflection coefficient in the given frequency band, as is known, has the form $|\rho| \geq e^{-\pi/wQ}$; the corresponding dependence of the introduced losses is represented by curve 5 in Figure 3. The application of additional matching circuits, however, leads to the fact that the large-scale LC-elements again appear, elimination of which must be accomplished by the acoustoelectronic SSW equipment. In view of this fact, in practice no more than one additional element (inductance) is used for each CPC. The general frequency-amplitude characteristic of the filter is determined in this case by the product of the transmission coefficients of the input and output circuits of the SSW filter, each of which, in turn, will be the product of the frequency-amplitude characteristic of the oscillatory circuit and the CPC. On the resonance frequency of the circuit, the operating attenuation during energy transmission from the source of emf or current to the radiation resistance of the CPC (R_c or R_π) will be

$$a = 10 \lg [(1 + \gamma + Q_a/Q_L)^2/4\gamma], \tag{4}$$

where $\gamma=R_\Gamma/R_c$ for series inclusion and $\gamma=R_\pi/R_\Gamma$ for parallel inclusion; Q_L is the inductance Q-factor.

With a narrow band of the SSW filter its frequency-amplitude characteristic in practice is completely determined by the characteristics of the CPC. The optimal value of γ is found by the same procedure as above, and it will be $\gamma_{opt}=1+Q_a/Q_L$. In the wide-band filters the electrical Q-factor of the CPC circuit $Q_{e\ell}=1/(1/Q_L+1/Q_a+Q_a/\gamma)$ must be sufficiently low to avoid constriction of the passband of the SSW filter.

Curve 6 corresponding to attenuation of the SSW filter on introduction of the compensating inductances, operation between the 75-ohm circuits and with an aperture of $40\lambda_0$ is constructed in Figure 3. The value of Q_L for small passbands is taken equal to 30; as the band expands, the value of Q_L decreases so that the passbands of the LC-circuits will coincide with respect to the 1.5 decibel level with the passband of the CPC with respect to the same level.

If the filter were connected to external circuits having resistances not equal to 75 ohms, but values following from the Fano relations, then also in the presence of one inductance at the input and one at the output the introduced losses would be characterized by curve 3 in Figure 3, and the required magnitudes of the external circuit resistances, by the curves in Figure 2 (3 -- for the single-channel CPC; 4 -- for the MCFS with m=4).

Inclusion of the SSW filters through the emitter repeater by the schematic in Figure 5a is also used. Using the equivalent diagram in Figure 5b it is easy to see that on the mean passband frequency

$$|U_1/U_2| = 2Q_{a1}(1/Q_{L1} + 1/Q_{a1})(1/Q_{a2} + 1/Q_{L2} + \gamma_2/Q_{a2}), \tag{5}$$

where the subscripts 1 and 2 correspond to the input and output circuits of the SSW filter.

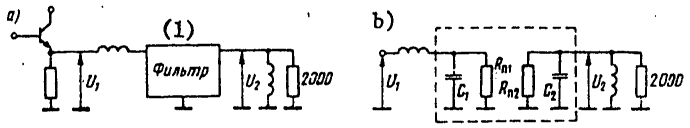

Figure 5

Key:
1. filter

When using both additional inductances and emitter repeaters, the matching of wide-band filters with the external circuits is also complicated as a result of the high resistance of the filters. The application of MCFS even in this case will permit the input impedances of the SSW filters to be reduced and the problem of formation of the required frequency-amplitude characteristics of the wide-band filter to be significantly facilitated. Actually, in the presence of additional inductances at the input and output of the filter there are four elements limiting the passband: two LC-circuits and two CPC. As a result, in order to obtain the required passband of the entire filter, the passband of each of these elements must be significantly broader than the resultant, and the Q-factors of the LC-circuits extremely small, which leads to large losses. When using the MCFS it is easily possible to obtain CPC with passband appreciably wider than the band of the LC-circuits and even to compensate for the nonuniformity of the frequency-amplitude characteristic caused by them.

Let us present the results of measurements of real filters.

1. Two filters matched with square radio pulses for f_0=12 megahertz designed for transmission speeds r_1=64 kbaud and r_2=256 kbaud included with respect to the input in parallel and located on one quartz plate, have the following parameters:

For r_1=64 kbaud with respect to the input: n=78 (the aperture is 0.3 cm without apodization); Q_{a1}=20.2; Q_{L1}=30; $R_{\pi 1}=41\cdot10^3$ ohms; with respect to the output: n=375 (aperture 0.3 cm); Q_{a2}=12; Q_{L2}=30; $R_{\pi}=11.6\cdot10^3$ ohms.

For r_2=256 kbaud with respect to the input: n=65 (the three-channel CPC with apodization, the aperture of each channel is 0.366 cm); Q_{a1}=20.2; Q_{L1}=30 (the inductance coil naturally common to both filters included in parallel with respect to the input); $R_{\pi}=41.2\cdot10^3$ ohms; with respect to the output: n=93 (without apodization, aperture 1.2 cm); Q_{a2}=9.4; Q_{L2}=30; $R_{\pi}=2\cdot10^3$ ohms. The filters operate between the 75-ohm circuits.

The calculation by formula (4) considering the mutual shunting of the filter inputs and the additional losses of 6 decibels as a result of two-way directionalness of the CPC gives 25.5 decibels for the first filter and 36.2 decibels for the second. The measured values of the losses were 23 decibels and 36 decibels.

2. The filter with f_0=12 megahertz calculated for a passband of 1.5 megahertz with respect to the 3-decibel level included by the circuit in Figure 5a executed with four-channel CPC has the following parameters:

With respect to input: n=39 (without apodization, the aperture of the two edge channels of 0.368 cm, two middle channels 0.35 cm); Q_{a1}=87; Q_{L1}=8; $R_{\pi}=38\cdot10^3$ ohms;

With respect to output: n=85 (with apodization, aperture the same); Q_{a2}=63; Q_{L2}=8; $R_{\pi}=29\cdot10^3$ ohms.

The calculation by formula (5) considering the 6-decibel losses as a result of the two-way directionalness of the CPC gave a value of $20\lg|U_1/U_2|$=23 decibels; the measured value was 22.5 decibels. Let us note that for the version of realization of the given filter with two unapodized CPC, the losses, as it is possible to see by using (5), would be 55 decibels.

3. The filter with f_0=70 megahertz calculated for a passband of 6 megahertz with respect to the 3-decibel level included by the scheme in Figure 5a and executed with six-channel CPC has the parameters:

With respect to input: n=72 (without apodization, aperture on the average 2.9 mm); Q_{a1}=72; Q_{L1}=10; R_{π}=2750 ohms;

With respect to output: n=81 (with apodization, aperture the same); Q_{a2}=113; Q_{L2}=10; R_{π}=14500 ohms. The calculation by (5) considering losses as a result of two-way propagation and measurement gave a value of $20\lg|U_1/U_2|$=13 decibels.

BIBLIOGRAPHY

1. TIIER, Vol 64, No 5, 1976, thematic edition, translated from the English, edited by Yu. V. Gulyayev.

2. Beletskiy, A. F. TEORETICHESKIYE OSNOVY ELEKTROPROVODNOY SVYAZI [Theoretical Principles of Electric Wire Communications], Vol III, Moscow, Svyaz'izdat, 1959.

3. Bode, G. TEORIYA TSEPEY I RASCHET USILITELEY S OBRATNOY SVYAZ'YU [Circuit Theory and Calculation of Amplifiers with Feedback], Moscow, GIIL, 1948.

4. Fano, R. M. TEORETICHESKIYE OGRANICHENIYA POLOSY SOGLASOVANIYA PROIZVOL'NYKH IMPEDANSOV [Theoretical Restrictions of the Matching Band of Arbitrary Impedances], Moscow, Sov. radio, 1965.

5. Babkov, V. Yu.; Beletskiy, A. F. RADIOTEKHNIKA I ELEKTRONIKA [Radioengineering and Electronics], Vol XVI, No 8, 1971.

Manuscript received 12 Nov 79

10845
CSO: 1860

UDC 621.372.826.029.65:621.315.61

A GaAs DIELECTRIC WAVEGUIDE FOR THE MILLIMETER BAND

Moscow RADIOTEKHNIKA I ELEKTRONIKA in Russian Vol 25, No 10, Oct 80 pp 2232-2233
manuscript received 24 Jul 79

[Article by S. V. Karmazin, V. Ye. Lyubchenko and B. A. Murmuzhev]

[Text] The problem of developing integrated circuits in the short-wave part of the millimeter band can be successfully solved by using a channeling section that is a dielectric waveguide mounted on the surface of a metal substrate [Ref. 1-3]. A previous report dealt with the feasibility of using a dielectric waveguide of high-resistance germanium or silicon to make both passive and active devices in the 75-300 GHz range. However, the comparatively low resistivity of germanium and silicon attained so far ($\rho \sim 10^7$ $\Omega \cdot$cm) causes considerable losses introduced by such dielectric waveguides in the given range [Ref. 3].

There is a better outlook for making a variety of devices on the basis of dielectric waveguides of semi-insulating gallium arsenide. Studies have shown that individual specimens of this material with resistivity of $\rho \sim 10^7$ $\Omega \cdot$cm have quite small losses in the short-wave part of the millimeter band ($\tan\delta = 2 \cdot 10^{-4}$ on a frequency of f = 150 GHz*). Besides, an epitaxial film of gallium arsenide with predetermined properties can be grown on the surface of a dielectric waveguide of semi-insulating GaAs, and hence devices can be made with operation based on controlling the parameters of the dielectric waveguide by using a constant electric field, illumination, and also by the action of acoustic or electromagnetic fields [Ref. 4-7].

In this research a study was done on a dielectric waveguide of semi-insulating GaAs with cross section of 0.6 x 0.35 mm and length of 1.4 cm. Measurements were made of the total inserted losses, including losses to propagation of the electromagnetic wave in the dielectric waveguide and losses on conversion of the H_{10} wave of a rectangular metal waveguide to the $E_{11}{}^y$ wave of a dielectric waveguide.

Also investigated was the influence that the thickness of an epitaxial film with different concentrations of free carriers (electrons) has on overall losses.

A measurement line and moving shorting piston were used to determine the overall losses by the Deschamps method [Ref. 8] on the setup shown schematically in Fig. 1. GaAs dielectric waveguide 1 with heightwise beveled edges 2 was cemented to the lower side wall of rectangular waveguide 3 with cross section of 3.6 x 1.8 mm. The

*The measurements were made by Ye. F. Ushatkin and Ye. Ye. Chigrya.

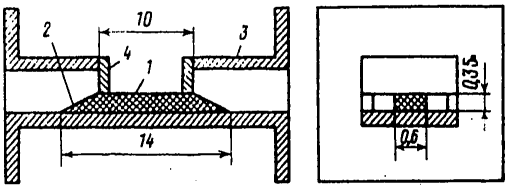

Fig. 1. Placement of the dielectric waveguide in the model

waveguide had no upper or side walls in the region where the dielectric waveguide was located. The open ends of the waveguide were covered with metal screens 4. Decoupling between the input and output ends of the waveguide in the absence of the dielectric waveguide exceeded 30 dB.

The minimum overall losses of the dielectric waveguide of semi-insulating GaAs (1.4 cm long) was 0.9 dB on a frequency of 73 GHz.

A study of the distribution of the wave field in the transverse plane of the dielectric waveguide done by scanning of the magnetic field [Ref. 9] showed that on a frequency of 73 GHz this dielectric waveguide has single-mode operation on the E_{11}^{y} wave.

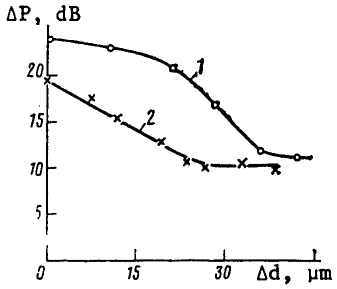

Fig. 2. Behavior of losses in a dielectric waveguide as a function of thickness of an epitaxial film with different conductivities: 1--1.57 $(\Omega \cdot cm)^{-1}$; 2--0.14 $(\Omega \cdot cm)^{-1}$

The results of a study of attenuation in dielectric waveguides that contain epitaxial films of n-GaAs are shown in Fig. 2. The thickness of the films was changed by successive chemical etching and was monitored with respect to etching time. This figure shows that losses in the dielectric waveguide depend appreciably on the conductivity and thickness of the film. This opens up the possibility of effective control of electromagnetic wave propagation in dielectric waveguides.

REFERENCES

1. R. M. Knox, IEEE TRANS., MTT-24, 1976, p 806.

2. V. F. Vzyatyshev, B. A. Ryabov, V. I. Kalinichev, "Transactions of Second All-Union Symposium on Millimeter and Submillimeter Waves," Khar'kov, 1978, No 1.

3. Y. Chang, MICROWAVE J., Vol 19, No 11, 1976, p 26.

4. A. B. Buckman, IEEE TRANS., MTT-25, 1977, p 480.

5. H. Jacobs, M. M. Chrepta, IEEE TRANS., MTT-22, 1974, p 411.

6. Yu. V. Gulyayev, V. V. Proklov, G. N. Shkerdin, FIZIKA I TEKHNIKA POLUPROVODNIKOV, Vol 6, 1972, p 1915.

7. Yu. V. Gulyayev, S. V. Karmazin, V. Ye. Lyubchenko, RADIOTEKHNIKA I ELEKTRONIKA, Vol 23, No 9, 1978, p 1948.

8. V. I. Sushkevich, "Neregulyarnyye lineynyye volnovodnyye sistemy" [Irregular Linear Waveguide Systems], Sovetskoye radio, 1967.

9. S. V. Averin, A. V. Mel'nikov, B. A. Murmuzhev, V. A. Popov, V. V. Salamatin, IZVESTIYA VUZov: RADIOFIZIKA, Vol 21, 1978, p 1028.

[81-6610]

6610
CSO: 1860

UDC 621.396.662.072.6.078

FREQUENCY SYNTHESIZER BASED ON AN ASTATIC ANALOG-TO-DIGITAL PHASE AUTOMATIC FREQUENCY CONTROL SYSTEM

Moscow RADIOTEKHNIKA in Russian No 9, 1980 pp 45-47

[Article by M. I. Drugov, V. L. Karyakin, M. Yu. Solov'yev, N. N. Stepanov]

[Text] At the present time frequency synthesizers based on the phase automatic frequency control system with divider in the feedback circuit are the most prospective from the point of view of standardization and microminiaturization [1]. In order to increase the purity of the spectrum of their output signal, frequently it is necessary to increase the filtering capacity of the phase automatic frequency control system (PAFC), but the lock-on band is unavoidably constricted in this case. In [2] a description is presented of various versions of the analog-to-digital PAFC systems (ADPAFC) permitting the contradiction to be relieved between the effort to expand the lock-on band and increase their filtering capacity. In practice, as a result of the known advantages, for the most part PAFC systems with digital integrator are used (astatic ADPAFC systems).

A frequency synthesizer based on an astatic ADPAFC system is in essence the ADPAFC search system [2], the automatic tuning loop of which includes a frequency divider with variable division coefficient (DVDC) between the tunable oscillator (TO) and the phase detector (PD). The digital integrator of the investigated system consists of a reversible counter (RC), a digital-to-analog converter (DAC), cycle pulse generator and control circuit (CC) of the reversible counter to which the search voltage is fed from the source of constant emf E.

If the frequency of the standard oscillator f_{so} is outside the limits of the lock-on band of the basic ring of the PAFC (without the digital integrator), then the search voltage reaches the controlling element of the TO from the output of the digital integrator. The search speed can be regulated by varying the cycle frequency of the reversible counter, and the direction depends on the polarity of the voltage E. Under the effect of the search voltage, the detuning between the frequency of the standard oscillator and the frequency f_{to}/N decreases (f_{to} is the frequency of the tunable oscillator, N is the division coefficient of the DVDC). When the detuning becomes less than the lock-on band of the basic ring of the PAFC system, the synchrony mode is set up in the system, and the DC voltage from the output of the PD compensates for the search voltage. Here the phase error in the system is proportional to the magnitude of the search voltage E.

During the process of experimental investigation of the frequency synthesizer [3] it was established that the output signal spectrum is determined to a significant degree by the shape of the characteristic of the reversible counter control circuit. The investigation of the dynamic properties of the synthesizer with the relay characteristic of the CC demonstrated that in the steady-state mode periodic changes in the RC code take place with a period that is a multiple of the cycle frequency of the reversible counter. As a result of modulation of the tunable oscillator by a stepped voltage from the output of the digital-to-analog converter corresponding to the RC code, the output signal spectrum will contain intense side components. The use of the CC with characteristic having a dead zone permits the spectrum of the output signal to be improved. In this PAFC system, while the regulation error is within the limits of the dead zone the detuning introduced by the digital integrator does not change. Increasing the zone leads to a decrease in probability of occurrence of periodic or quasi-periodic variations of the phase difference of the standard and tunable oscillators in the steady-state mode and, consequently, to an increase in purity of the output signal spectrum.

A very effective means of improving the spectral characteristics of the astatic ADPAFC system is the use of a control circuit with variable dead zone in the digital integrator. In the going into synch mode, the dead zone is small (or absent in general), which insures the precision of tuning and establishment of the phase difference for which the voltage and the PD output corresponds to the required section of its characteristic. After establishing synchrony the dead zone increases in order to prevent the occurrence of spurious phase modulation of the output oscillation of the tunable oscillator. In practice such a control circuit for the reversible counter is easily realized from threshold elements with hysteresis, for example, using Schmitt triggers.

The structural diagram of the control circuit and the output voltage diagrams are shown in Figures 1a and b. The Schmitt triggers (Fig 1a) TSh_1 and TSh_2 with inverter I have threshold response and release levels of $U_{t.resp\ 1}$, $U_{t.resp\ 2}$, $U_{t.\ rel\ 1}$, $U_{t.\ rel\ 2}$. On investigation of Fig 1b it follows that in the presence of hysteresis on TSh_1 and TSh_2 (that is, for $U_{t.resp\ 1}>U_{t.rel\ 1}$, $U_{t.resp\ 2}>U_{t.\ rel\ 2}$) and satisfaction of the condition $U_{t.rel\ 1}>U_{t.resp\ 2}$, the control circuit insures a variable dead zone. On going into synch (in the search mode) the dead zone is $\nu_{\pi}=U_{t.rel\ 1}-U_{t.resp\ 2}$, and in the steady-state mode, $\nu_{ss}=U_{t.resp\ 1}-U_{t.rel\ 2}$. In the given case (see Fig 1b) the voltage at the output of the PD U_{PD} varies only in the range of positive values, which can occur if PD is of the "access -- storage" type. The dead zone of the control circuit is shifted with respect to the mean value of the voltage at the output of the PD $U_{PD\cdot mean}=(U_{PD\ max}+U_{PD\ min})/2$, which is equivalent to feeding the search voltage to the control circuit. Fig 2 shows the Schmitt trigger circuit K1TSh191 with hysteresis in the region of positive input voltages; its feed is from a unipolar voltage source. The response and release thresholds can be adjusted by means of the mounted R_e and R_k elements.

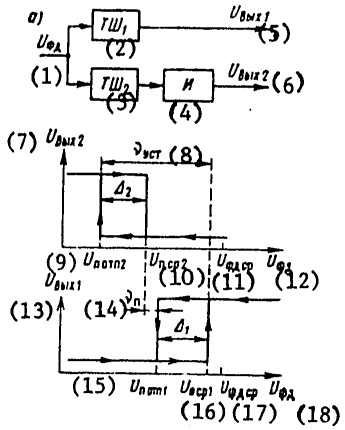

Figure 1

Key:

1. U_{PD}
2. TSh_1
3. TSh_2
4. I
5. $U_{out\ 1}$
6. $U_{out\ 2}$
7. $U_{out\ 2}$
8. ν_{ss}
9. $U_{t.rel\ 2}$
10. $U_{t.resp\ 2}$
11. $U_{PD\ mean}$
12. U_{PD}
13. $U_{out\ 1}$
14. ν_t
15. $U_{t.rel\ 1}$
16. $U_{t.resp\ 1}$
17. $U_{PD\ mean}$
18. U_{PD}

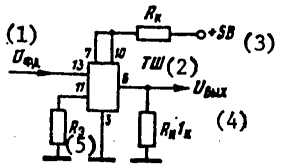

Figure 2

Key:

1. U_{PD}
2. TSh
3. +5 volts
4. U_{out}
5. R_e

When calculating the circuit elements usually the response threshold and the magnitude of the trigger hysteresis are known. The elementary relations for the response threshold and the hysteresis of the Schmitt trigger as a function of the resistance of the resistors R_e, R_k are presented in Figure 3a, b. The graph in Figure 3a permits selection of the resistance of the resistor R_e by the required amount of hysteresis (Δ_1, Δ_2). Then using Figure 3b, it is possible by the given response threshold $U_{t.resp}$ to determine the magnitude of the resistor resistance R_k. By the selected values of R_e and R_k using Figure 3a the value of the Schmitt trigger hysteresis becomes more exact.

The proposed diagram of the control circuit for the reversible counter has high technological nature, low power intake, high reliability, and it is distinguished by simplicity.

Conclusion. 1. When using the PAFC system with digital integrator in frequency synthesizers it is expedient to use the reversible counter control circuit with variable dead zone.

2. The control circuit with the required characteristic, high reliability and low energy intake can be made from Schmitt triggers comparatively simply.

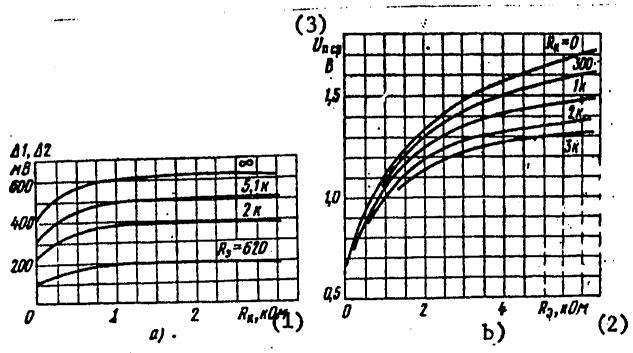

Figure 3

Key:
1. R_k, kilohms
2. R_e, kilohms
3. $U_{t.resp}$

BIBLIOGRAPHY

1. Levin, V. A.; Nisnevich, D. G. ELEKTROSVYAZ' [Electrocommunications], No 4, 1976.

2. Shakhgil'dyan, V. V.; Lyakhovkin, A. A.; Karyakin, V. L.; Petrov, V. A.; Fedoseyeva, V. N. SISTEMY FASOVOY AVTOPODSTROYKI CHASTOTY S ELEMENTAMI DISKRETIZATSII [Phase Automatic Frequency Control Systems with Quantification Elements], Moscow, Svyaz', 1979.

3. Karyakin, V. L.; Solov'yev, M. Yu. TEZISY DOKLADOV VSESOYUZNOY NAUCHNO-TEKHNICHESKOY KONFERENTSII "DAL'NEYSHEYE RAZVITIYE NOVOY TEKHNIKI PRIYEMNYKH USTROYSTV" [Topics of Reports at the All-Union Scientific and Technical Conference on Further Development of New Receivers], Moscow, Gor'kiy, 1977.

Manuscript received 7 Nov 1979

10845
CSO: 1860

ELECTROMAGNETIC WAVE PROPAGATION, ELECTRODYNAMICS

UDC 621.372.018.78

PENETRATION OF AN ELECTRIC FIELD BEYOND THE SHIELDS IN A NONSTEADY CONDUCTING MEDIUM

Moscow RADIOTEKHNIKA in Russian No 9, 1980 pp 64-68

[Article by V. V. Kuznetsov, A. A. Lyubomudrov]

[Text] In a number of cases it is necessary to consider the variation in the effectiveness of the shielding of equipment in a medium with nonsteady conductivity. On the basis of solving the problem of penetration of the electric field (E-field) into a shield located in nonionized air [1], we find the solution in the case of nonsteady state conductivity of the medium cooling the shield.

In the case of a conducting shield, from [1, 2] it is possible to obtain an expression for the resistance of an equivalent oscillator included at the input of a long line characterizing the reflection

$$W = 1\Big/\left(i\omega C_{\text{э}}(t) + \frac{\sigma(t)C_{\text{э}}}{\varepsilon_0}\right), \tag{1}$$

Key: 1. e

where ω is the angular frequency; C_e is the equivalent capacitance of the shield in the air which can be found by solving the electrostatic problem of [3]; $\varepsilon(t)$ is the real part of the dielectric constant of the environment; $\sigma(t)$ is the conductivity of the medium; ε_0 is the dielectric constant of a vacuum. The resistance (1) is realized by a two-terminal network with parallel connected parametric capacitance $C_\pi(t)=\varepsilon(t)C_e$ and parametric resistance $R(t)=\varepsilon_0/\sigma(t)C_e$. Then in the low-frequency case for $\omega\leq\omega_{lim}=1/\mu\sigma_e g^2$ (where μ is the permeability of the shield material, g is the thickness of the shield walls), the equivalent diagram of the shield in the conducting medium has the form of Figure 1a. Let us propose approximately that $\varepsilon(t)\approx 1$; then $C_\pi(t)\approx C_e$. According to the first Kirchhoff's law for the circuit in Figure 1a

$$C_{\text{э}}\frac{dE_1}{dt} + E_1\left[\frac{1}{R(t)} + \sigma_{\text{э}}g\right] = C_{\text{э}}\frac{dE}{dt} + \frac{E}{R(t)}, \tag{2}$$

Key: 1. C_e

where E_1 is the time-dependent field beyond the shield.

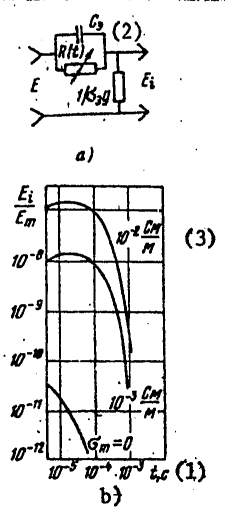

Figure 1

Key:
1. t, sec
2. C_e
3. Siemens/m

Let us write the solution to equation (2):

$$E_i = \exp\left\{-\int\left[\frac{\sigma(t)}{\varepsilon_0}+\frac{\sigma_0 g}{C_e}\right]dt\right\}\times$$
$$\times\left\{\int\left[\frac{dE}{dt}+\frac{E_0(t)}{\varepsilon_0}\right]e^{\int\left[\frac{\sigma(t)}{\varepsilon_0}+\frac{\sigma_0 g}{C_e}\right]dt}dt+b\right\},$$

where θ is the integration constant determined from the initial conditions.

In Fig 1b the relation $E_i(t)/E_m$ is presented beyond the aluminum shield ($\sigma_e=3.5\cdot10^7$ Siemens/m) $g=2\cdot10^{-3}$ meters thick with equivalent capacitance of $C_e=10^{-11}$ farads located in ionized air for

$$E(t)=E_m(e^{-\alpha t}-e^{-\beta t}),\ \alpha=10^8\frac{1}{c}\ (1),$$
$$\beta=10^8\frac{1}{c},\ \sigma(t)=\sigma_m(e^{-\gamma t}-e^{-\eta t}),$$
$$\gamma=10^8\frac{1}{c},\ \eta=10^9\frac{1}{c}\ (1),$$

Key: 1. 1/sec

where α and β are constants characterizing the decay and pulse front of the E-field, and γ and η are the decay and front of $\sigma(t)$. Here the relation $E_i(t)/E_m$ is presented in the absence of ionization. As we shall see, in ionized air the effectiveness of the shielding is one or two orders lower than in the absence of

ionization. In addition, with an increase in the conductivity of the air the pulse of a field penetrating the shield is stretched.

If the function $\sigma(t)$ varies faster than the function $E(t)$, then [4]

$$L[E(t)\sigma(t)] \approx pE(p)\sigma(p),$$

where L is the operator of the Laplace transformation. Therefore from (2) for $\sigma(t)/\varepsilon_0 \leq \sigma_e g/C_e$ we obtain

$$E_1(p) \approx E(p)\, p\left[1 + \frac{\sigma(p)}{\varepsilon_0}\right]\Big/\left(p + \frac{\sigma_0 g}{C_0}\right).$$

For $\sigma_e g/C_e >> \omega$

$$E_1(t) \approx \frac{C_0}{\sigma_0 g}\left[\frac{dE}{dt} + \frac{1}{\varepsilon_0} E(t)\sigma(t)\right]. \tag{3}$$

For the investigated aluminum shield the calculation by (3) gives results that coincide with Figure 1b.

In the more general case of a wide frequency band of the influencing field we use expansion of the input impedance of the four-terminal network equivalent to the absorption shielding [1] in a chain fraction. The chain obtained is presented in Figure 2a where $\delta = \sqrt{\mu\sigma_e g}$. Then in order to determine the field E_s directly on the outside surface of the shield in the conducting medium with two-element and single-element realizations of the input immitance we obtain the equivalent diagrams depicted in Figures 2b and c, respectively. Analysis shows that it is possible to use the diagrams obtained in a quite broad frequency band. Thus, for aluminum shields several millimeters thick the equivalent diagram in Figure 2c is valid from the zero frequency to the frequencies of several hundreds of kilohertz, and in Figure 2b, from zero frequency to frequencies of several megahertz. The operator image of the field on the inside surface of the shield is determined by the product of $E_s(p)$ times the transmission function of the four-terminal absorption network of $1/\operatorname{ch} \delta\sqrt{p}$ [1]

$$E_1(p) = E_s(p)\frac{1}{\operatorname{ch} \delta\sqrt{p}}. \tag{4}$$

The transient processes in the chain in Fig 2c are described by the differential equation

$$\frac{d^2E_s}{dt^2} + \left[\frac{3}{\delta^2} + \frac{\sigma(t)}{\varepsilon_0}\right]\frac{dE_s}{dt} + \left[\frac{1}{\varepsilon_0}\frac{d\sigma(t)}{dt} + \frac{3\sigma(t)}{\delta^2\varepsilon_0} + \frac{3\sigma_0 g}{\delta^2 C_0}\right]E_s = -\frac{3}{\delta^2}\frac{dE}{dt} + \frac{d^2E}{dt^2} + \frac{3}{\delta^2\varepsilon_0}E\sigma(t) + \frac{1}{\varepsilon_0}\frac{dE}{dt}\sigma(t) + \frac{1}{\varepsilon_0}E\frac{d\sigma(t)}{dt}. \tag{5}$$

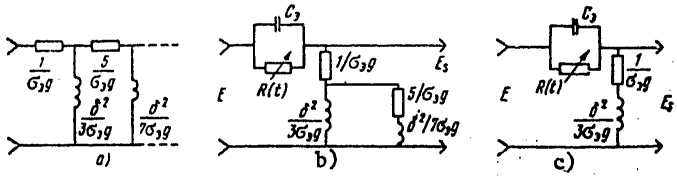

Figure 2

Setting $E_g=uv$, $v=\exp\left\{-\int\left[\frac{3}{2\delta^2}+\frac{\sigma(t)}{2\varepsilon_0}\right]dt\right\}$, from (5) we obtain

$$\frac{d^2u}{dt^2}+\left\{\frac{1}{2\varepsilon_0}\frac{d\sigma(t)}{dt}+\frac{3\sigma_g g}{\delta^2 C_g}-\left[\frac{3}{2\delta^2}-\frac{\sigma(t)}{2\varepsilon_0}\right]^2\right\}u=F(t)\exp\left\{\int\left[\frac{3}{2\delta^2}+\frac{\sigma(t)}{2\varepsilon_0}\right]dt\right\}. \tag{6}$$

where F(t) denotes the righthand side of equation (5). The solution of equation (6) without the righthand side is approximated by the phase integral method [5] by the expression

$$u=\frac{1}{\sqrt{\lambda(t)}}(N\cos\psi+B\sin\psi),$$

where $\lambda=\frac{1}{2\varepsilon_0}\frac{d\sigma(t)}{dt}+\frac{3\sigma_g g}{\delta^2 C_g}-\left[\frac{3}{2\delta^2}-\frac{\sigma(t)}{2\varepsilon_0}\right]^2$, $\psi=\int\sqrt{\lambda(t)}\,dt$; N and B are constant coefficients determined from the initial conditions.

After a series of transformations using the method of undefined Lagrange factors [5] we obtain the solution to equation (5)

$$E_g=\frac{\exp\left\{-\int\left[\frac{3}{2\delta^2}+\frac{\sigma(t)}{2\varepsilon_0}\right]dt\right\}}{\sqrt{\lambda(t)}}\left[\sin\psi\int\frac{h\sqrt{\lambda(t)}\cos\psi}{\dot\psi}dt-\right.$$
$$\left.-\cos\psi\int\frac{h\sqrt{\lambda(t)}\sin\psi}{\dot\psi}dt+N\cos\psi+B\sin\psi\right],$$

where h is the righthand side of (6).

Let us consider some special cases of solving equation (5).

1) For $\frac{3}{\delta^2}\gg\frac{\sigma(t)}{\varepsilon_0}$, $\frac{\sigma_g g}{C_g}\gg\frac{\sigma(t)}{\varepsilon_0}$, $\frac{3\sigma_g g}{\delta^2 C_g}\gg\frac{1}{\varepsilon_0}\frac{d\sigma(t)}{dt}$ we have

$$E_g=e^{st}\left[\cos\varkappa t\int\frac{e^{-st}F_1(t)\cos\varkappa t}{\varkappa}dt-\sin\varkappa t\int\frac{e^{-s}F_2(t)\sin\varkappa t}{\varkappa}dt+C_1\sin(\varkappa t+C_2)\right],$$

where $s=-\frac{3}{2\delta^2}$, $\varkappa\approx\frac{3\sigma_g g}{\delta^2 C_g}$ for $\frac{3\sigma_g g}{\delta^2 C_g}\gg\frac{9}{\delta^4}$; C_1 and C_2 are constant coefficients;

$$F_1(t)=\frac{3}{\delta^2}\frac{dE}{dt}+\frac{d^2E}{dt^2}+\frac{3}{\delta^2\varepsilon_0}E\sigma(t)+\frac{1}{\varepsilon_0}E\frac{d\sigma(t)}{dt}.$$

2) For $(1/\varepsilon_0)(d\sigma(t)/dt)>>3\sigma_e g/\delta^2 C_e$ or also for $(\sigma^2(t)/4\varepsilon_0^2)>>(3\sigma_e g/\delta^2 C_e)$, we obtain the equation of the type

$$\frac{d^2E_s}{dt^2}+(f+q)\frac{dE_s}{dt}+\left(\frac{df}{dt}+fq\right)E_s=F(t), \tag{7}$$

where $f=\sigma(t)/\varepsilon_n$, $q=3/\delta^2$.

The uniform equation (7) has the general solution [5]

$$E_s=\exp\left[-\int\frac{\sigma(t)}{\varepsilon_0}dt\right]\left[C_3+C_4\int e^{\int\frac{\sigma(t)}{\varepsilon_0}dt-\frac{3t}{\delta^2}}dt\right],$$

where C_3 and C_4 are integration constants. One of the partial solutions of the uniform equation (7) is determined by the expression [5]

$$E_s=e^{-\frac{1}{\varepsilon_0}\int\sigma(t)dt}$$

3) For $\frac{\sigma'(t)}{2\varepsilon_0}\gg\frac{3}{\delta^2}$, $\frac{\sigma^2(t)}{2\varepsilon_0}\gg\frac{d\sigma(t)}{dt}$, $\frac{\sigma_0 g}{C_0}\gg\frac{3}{4\delta^2}$ from (6) we obtain

$$\frac{d^2u}{dt^2}+\left[\frac{3\sigma_0 g}{\delta^2 C_0}-\frac{\sigma^2(t)}{4\varepsilon_0^2}\right]u=F_1(t)e^{\int\frac{\sigma(t)}{2\varepsilon_0}dt},$$

where $u=E_s\exp\left[\int\frac{\sigma(t)}{2\varepsilon_0}dt\right]$; $F_1(t)=\frac{d^2E}{dt^2}+\frac{3}{\delta^2\varepsilon_0}E\sigma(t)+\frac{1}{\varepsilon_0}\frac{dE}{dt}\sigma(t)+\frac{1}{\varepsilon_0}E\frac{d\sigma(t)}{dt}$.

We find the solution of the uniform equation in the case of $\sigma(t)=\sigma_m e^{-t/t_0}$.

After substitution of variables $\xi=e^{-t/t_0}$ we have

$$\frac{d}{\xi}\frac{d}{d\xi}\left(\xi\frac{du}{d\xi}\right)+\left(\frac{\nu^2}{\xi^2}-r^2\right)u=0, \tag{8}$$

where

$$\nu=t_0\sqrt{\frac{3\sigma_0 g}{\delta^2 C_0}};\quad r=t_0\frac{\sigma_m}{2\varepsilon_0}.$$

The solution of equation (8) has the form

$$u=C_5 I_\nu(r\xi)+C_6 Y_\nu(r\xi),$$

where $I_\nu(r\xi)$ and $Y_\nu(r\xi)$ are the first and second type Bessel functions, respectively, and C_5 and C_6 are the integration constants.

Case "1" occurs (for in nonmagnetic shields) when $\sigma(t)<<10^{-7}$ Siemenn/m; case "3" occurs for $\sigma(t)>>10^{-7}$ Siemenn/m. If the function $\sigma(t)$ has a pulse nature with front duration much less than $10^{-10}\sigma_m$, then for nonmagnetic shields case "2" is valid for investigation of the process of penetration of the E-field beyond the shield on the front $\sigma(t)$.

Let us discuss the case where one of the functions E(t) or $\sigma(t)$ varies more rapidly than the other. Then from (4) and (5) for

$$\frac{\sigma_0 g}{C_0} \gg \frac{\sigma(t)}{\varepsilon_0},\ \frac{3\sigma_0 g}{\delta^2 C_0} \gg \frac{1}{\varepsilon_0}\frac{d\sigma(t)}{dt} \quad \text{and} \quad \frac{3\sigma_0 g}{\delta^2 C_0} \gg p^2\left[1+\frac{\sigma(p)}{\varepsilon_0}\right]+p\frac{3}{\delta^2} \qquad \text{we obtain}$$

$$E_1(p) \approx \frac{\delta^2 C_0}{3\sigma_0 g} E(p)\,\frac{p\left[1+\frac{\sigma(p)}{\varepsilon_0}\right]}{\operatorname{ch}\delta\sqrt{p}}\left(p+\frac{3}{\delta^2}\right).$$

On high frequencies, when $\omega>>3/\delta^2$,

$$E_1(p) \approx \frac{2}{3}\frac{\delta^2 C_0}{\sigma_0 g} E(p)\, p^2 [1+\sigma(p)/\varepsilon_0]/e^{\delta\sqrt{p}}. \tag{9}$$

Let us consider the passage of the front E(t) through the shield. Approximating the front by the expression $E/E_m=2A\sqrt{t/\pi}$ (where A is a constant coefficient), from (9) we find

$$\frac{E_1}{E_m} \approx \frac{2}{3}\frac{\delta^2 C_0}{\sigma_0 g} A \exp\left(-\frac{\delta^2}{4t}\right)\frac{1}{\sqrt{\pi t}} \times$$
$$\times\left[\frac{1}{2t}\left(\frac{\delta^2}{2t}-1\right)+\frac{1}{\varepsilon_0}\sigma(t)\right].$$

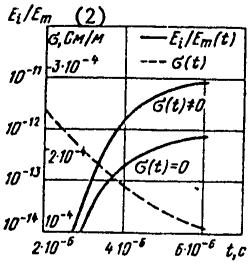

Figure 3

Key:
1. t, sec
2. σ, Siemenns/m

Figure 3 shows the relations for $E_i(t)/E_m$ when $\sigma(t)=0$ and when $\sigma(t)$ is graphically represented in the same figure. The approximation coefficient A is taken equal to 570 $sec^{-1/2}$. From Figure 3 it is obvious that the presence of ionized air on the E-field front leads to an increase in steepness of the front of the field penetrating through the shield.

Thus, the approximate formulas are obtained for determining the field beyond a shield in a conducting medium convenient for engineering calculations.

BIBLIOGRAPHY

1. Lyubomudrov, A. A. ELEKTRICHESTVO [Electricity], No 11, 1977.

2. Nikol'skiy, V. V. ELEKTRODINAMIKA I RASPROSTRANENIYE RADIOVOLN [Electrodynamics and Radiowave Propagation], Moscow, Nauka, 1978.

3. Miller, D. A.; Bridges, I. E. TRANS. IEEE, Vol EMC-10, No 1, 1968.

4. Solodov, A. V. LINEYNYYE SISTEMY AVTOMATICHESKOGO UPRAVLENIYA S PEREMENNYMI PARAMETRAMI [Linear Automatic Control Systems with Variable Parameters], Moscow, GIFML, 1962.

5. Kamke, E. SPRAVOCHNIK PO OBYKNOVENNYM DIFFERENTSIAL'NYM URAVNENIYAM [Reference on Ordinary Differential Equations], Moscow, Nauka, 1971.

Manuscript received 5 Mar 1980

10845
CSO: 1860

UDC 621.311.25:621.039.001.86

FIFTEEN YEARS OF EXPERIENCE IN OPERATING THE NOVOVORONEZHSK NUCLEAR ELECTRIC PLANT COMMEMORATING THE FIFTIETH ANNIVERSARY OF THE USSR

Moscow ELEKTRICHESKIYE STANTSII in Russian No 11, Nov 80 pp 8-12

[Article by V. K. Sedov, N. A. Isakov, I. A. Dmitriyev, V. B. Netesin, V. P. Kruglov, V. D. Dobrynin and V. M. Tsybenko, engineers, Novovoronezhsk Nuclear Electric Plant]

[Text] In 1979, the power engineers at the Novovoronezhsk Nuclear Power Facility [NVAES] marked the fifteenth anniversary since the first generator was put on line. In the ensuing years they have accumulated considerable experience in using the operating generators.

The NVAES has four operating generator units with an overall installed power rating of 1455 MW. Work is now in progress on getting another generating facility ready for production operation with installed capacity of 1000 MW.

It should be pointed out that all the generating facilities at the NVAES are pilot plants that have been the basis for developing and implementing project and design decisions incorporated into the conception of the water-moderated water-cooled nuclear power reactor [VVER]. Experience in using these generating units has convincingly shown that a nuclear electric facility with reactors of the VVER type is a safe, reliable source of electrical energy that makes satisfactorily efficient use of nuclear fuel.

The main parameters of the NVAES reactors are summarized in Table 1, and are also described in Ref. 1, 2.

Technical-economic working indices. Table 2 summarizes the technical-economic indices for 1974-1979 characterizing the qualitative growth and dynamics of development of the NVAES.

We see from Table 2 that the production of electrical energy in the last five years (without any increase in installed capacity) has risen by more than 9%, reaching in excess of 10.5 billion kWh in 1978.

The coefficient of utilization of installed capacity of the NVAES rose from 0.760 in 1974 to 0.825 in 1978 (a relative increase of 8.5%). This increase was due to improvement of the level of operation and quality of repairs.

TABLE 1

Parameter	Generating unit				
	I	II	III	IV	V
Installed electric power, MWt	210	365	440*	440*	1000
Type of reactor	VVER-210	VVER-365	VVER-440	VVER-440	VVER-1000
Thermal power of reactor, MWt	760	1320	1375	1375	3000
In-pile coolant pressure, kgf/cm^2	100	105	125	125	160
Coolant temperature, °C:					
at reactor inlet	252	252	265	267	290
at reactor outlet	271.1	277.8	290.5	295.8	322
Number of turbogenerators in the unit	3	5	2	2	2
Turbogenerator installed power, MWt	70	73	220	220	500
Number of reactor circulating loops	6	8**	6	6	4
Steam generator capacity, met. t/hr	230	325	455	455	1469
Steam pressure, kgf/cm^2	32	33	47	47	64
Main circulating pump capacity, thous. m^3/hr	5.6	7.1	7.0	7.0	20
Power consumption of MCP, MWt	1.53	1.53	2.26	2.26	5.3
Rated gross efficiency, %	27.63	27.65	32.0***	32.0***	33.3
In-house energy expenditures, %	8.0	7.3	7.15	7.15	5.5

*Design data
**Seven circulating loops are operating
***At pressure of 0.035 kgf/cm^2 in the turbine condensers

TABLE 2

Index	1974	1975	1976	1977	1978	1979
Electric energy production, GWh	9664.1	9138.1	9750.8	10080.0	10517.0	9915.8
Release of electric energy into the power system, GWh	8927.5	8427.0	8999.7	9310.0	9723.0	9158.7
In-house energy expenditures, %	7.62	7.78	7.70	7.65	7.55	7.82
Coefficient of utilization of installed power	0.760	0.717	0.763	0.791	0.825	0.789
Gross efficiency, %	28.27	28.37	28.48	28.71	28.88	28.54
Net cost of electric energy production, copeck/kWh	0.644	0.643	0.632	0.634	0.609	0.613

The gross efficiency for the five-year period rose by 0.61% (in relative terms -- by 2.1%), and in 1978 averaged 28.88%. The rise in efficiency was the result of improvement of the vacuum in the turbine condensers and elevation of the temperature of the feed water due to improvement in the quality of utilization of the equipment and in the operation of the circulation systems, in particular through the introduction of thermal and vacuum scavenging of the condensers.

The improvement of all these indices was conducive to lowering the resultant economic indicator, the net cost of electric energy production, over the last five years from 0.644 to 0.609 copeck/kWh, a relative reduction of 5.4%. If the technical-economic indices of the NVAES are compared with those of the best fossil-fuel electric plants, we find that a nuclear facility with VVER reactors is quite competitive, and in some indices surpasses the best fossil-fuel plants.

Somewhat poorer performance in 1979 was due to the increased volumes and times of repair work involved in planned preventive maintenance on the third and fourth generating units.

Utilization of nuclear fuel. Considerable experience on organizing the fuel cycle of the nuclear reactors has been accumulated over a prolonged period of operation of the NVAES reactors.

The reactors are recharged once a year in sequence on all generating units, the annual extensive planned preventive maintenance work being combined with the recharging program. It must be noted that the NVAES has successfully mastered a procedure in which recharging involves complete unloading of the cores for checking the condition of the inside surfaces of the reactor vessel and the equipment inside.

The average burnup of the spent fuel that is unloaded is continually increasing. For example the rated burnup of spent fuel, which was 12.85 kg/met. t for the VVER-210, 27.8 kg/met. t for the VVER-365 and 28.3 kg/met. t for the VVER-440, has been surpassed.

In the reactor of the first generating unit, this was achieved by introducing a core configuration mode close to a zonal mode, and using fuel assemblies with 3% enrichment (up to 30). In the reactor of the second generating unit, the increase in burnup of spent fuel was attained chiefly by introducing fuel assemblies with 3% enrichment without absorbers. The increase in the actual burnup of spent fuel above the planned rating for the VVER-440 reactor in the third generating unit was due mainly to conversion of this reactor to makeup with fuel with the standard enrichment for the VVER-440, i. e. 2.4 and 3.6%.

The use of fuel assemblies of ARK cassettes with 2.4% enrichment on a schedule of two recharges per run of these assemblies had a certain influence on fuel burnup for VVER-440 reactors. In addition, the systematic use of prolonged runs also contributed to some extent to the overall increase of burnup of the spent fuel for all reactors of the NVAES.

The maximum burnup of fuel in the individual spent fuel assemblies, which is equal to 30.98 kg/t for the first generating unit (initial enrichment of the fuel assembly 2.4%), 48.06 kg/t for the second unit (initial enrichment of the fuel assemblies 3% with absorbers), and 50.44 kg/t for the third (initial enrichment 3.3% with absorbers), refers to fuel assemblies that were purposely left in the cores of the reactors to study the behavior of the fuel elements in the case of burnups much greater than the design levels, and to evaluate the service life of these elements.

Experience in operating the NVAES shows that during the operation of fuel charges, the integrity of the cladding of individual fuel elements may be lost, which is accompanied by escape of radioactive fission fragments into the coolant.

Special monitoring methods based on registration of fission products of nuclear fuel in the coolant of the in-pile loop are used to maintain adequately low radioactivity in the coolant, and for timely detection and elimination of fuel assemblies with leaky fuel elements in nuclear facilities with reactors of the VVER type.

On the running reactors, the state of the fuel element cladding is evaluated from the results of radiochemical analysis of the coolant, and additionally by using loop monitoring systems to check for delayed neutrons. The periodicity of analysis is determined by the total radioactivity of the dry residue of water samples from the in-pile loop, which is checked daily. If the total radioactivity is less than 10^{-3} Ci/l, radiochemical analysis is done once a month, otherwise -- more often. The purpose of radiochemical analysis of water samples from the in-pile loop is to evaluate the content of isotopes of iodine, barium, strontium, xenon, krypton, cesium and neptunium. The isotopes are isolated from the coolant specimens by methods of radiochemical deposition on tissue sorbents, distributive chromatography and extraction techniques.

A method of monitoring the isotopic makeup of the coolant without taking samples has been introduced on the third and fourth generating units of the NVAES. By using a gamma spectrometer based on a semiconductor detector, the measurement is made directly in the pipeline on the bypass of a mixed-action filter (in the facility for continuous cleaning of the water in the in-pile loop).

The state of fuel element cladding on the working reactor is continually monitored by loop systems that permit checking the dynamics of development of the process of loss of integrity of the fuel elements and making decisions on the periodicity of radiochemical analysis of the coolant.

During recharging of reactors, extensive use is made of a method based on calculating the radioactivity of a gas sample taken from a sealed can with the fuel assembly to be tested (the so-called "dry" method).

Preliminary experiments were done on determining the rate of warmup of the fuel assembly in the "dry" can. It was found that for a fuel assembly with a burnup of 19.7 kg of slag per metric ton of uranium 100 days after unloading from the reactor the warmup rate is about 3°C/min for the temperature range from 35 to 150°C. For the same fuel assembly 9 days after reactor shutdown the warmup rate was about 6°C per minute. Thus the safe time for holding the cassette in the "dry" can is 5-10 minutes.

The sensitivity of the method is fairly high: the readings of gas activity of leaky fuel elements are a thousand or more times as high as those of tight elements. As a rule, the "dry" method detects all fuel assemblies with leaky fuel elements. The method is quite simple, does not require complex equipment and combines operations on monitoring fuel element cladding with technological operations on recharging the reactor core, thus shortening the down time of the generating units.

To get a more accurate idea of the leakiness of fuel element cladding in fuel assemblies identified as "leaky" by the "dry" method, the radioactivity of iodine-131 is determined in water samples obtained by letting the fuel assembly stand in water -- the "wet" method.

Continuous monitoring of the radiochemical makeup of the in-pile coolant reveals high reliability of the fuel assemblies used in NVAES reactors. At present, the gas-tightness of fuel assembly cladding is not checked every time the reactors are shut down for recharging, and the need for such a check is evaluated from the results of monitoring the radiochemical makeup of the coolant, and from data of the system for checking gas-tightness of fuel element cladding based on delayed neutrons during reactor operation.

Operation and repair of major equipment. The high coefficient of utilization of installed power attained on the first four generating units of the NVAES indicate fairly high reliability of operation of equipment in the nuclear facility. This reliability is supported both by proper use and by timely high-quality repair of equipment.

There are certain peculiarities of repairing radioactive reactor equipment at the nuclear facility as compared with repairing other equipment. The following should be noted first of all:

the limited time that repair personnel can remain on the worksite means that a large number of workers are needed;

before inspection and repair, additional inputs of labor and material are needed for decontamination of equipment;

repair requires formulating special tolerances at the worksite, and monitoring of the radiation environment there, as well as the use of individual and group facilities for shielding from ionizing radiation;

after completing repair work, the tools, equipment and fittings must be decontaminated, and the radioactive wastes must be collected, removed, transported and buried;

because of radioactive contamination or pecularities of construction, some parts and components cannot be handled or restored under factory conditions.

The minimum staff of repair personnel handles the repair of auxiliary equipment in the period between shutdowns for recharging in the restricted areas. On the other hand, the maximum number of repair personnel is required during shutdowns of the generating unit for recharging in combination with planned preventive maintenance. The structure of the NVAES is determined by these requirements, and permits personnel to move about in performance of the work with minimum one-time and annual radiation dosage.

At the Novovoronezhsk Nuclear Facility, considerable attention is given to checking the state of equipment. Initial inspection of the metal of the equipment is done at the NVAES to discover impermissible defects of equipment arriving for installation, and to check on the conformance of equipment to technical specifications. On this stage of inspection, the initial state of the equipment metal is determined, which is necessary for subsequent operational inspection. Operational inspection of equipment metal is done with set periodicity in accordance with the rules in force. The total inspection schedule is carried out at least once every four years. Individual units and equipment of the reactor installation that are most critical

are inspected more frequently, for example the connecting tubing of the reactors, the jackets of the drives in the reactor control system and the like.

The most extensively used methods of equipment inspection at the nuclear facility have been visual-optical, x-ray and gamma radiography, ultrasonic, helium-halogen, eddy-current and luminescent-hydraulic methods and a method of color flaw detection. To check welds in the connecting tubing of reactors and pipelines with diameter of 500 mm, a remote unit with telescoping arm is used. The luminescent-hydraulic method of flaw detection is used in checking the gas-tightness of tube bundles in the steam generators.

In addition to periodic inspection of equipment metal, the NVAES monitors running equipment by the methods and facilities of technical diagnosis.

The operating noise that arises when the equipment is running is registered by an in-house vibroacoustic monitoring system in operational use, and in case anomalies show up the noise is analyzed by a variety of equipment under laboratory conditions. Accelerometers of piezoelectric type are used as the sensors of vibroacoustic noise. The initial data on the number and location of the sensors are obtained during trial runs, and on the basis of experience in using equipment of the in-pile loop.

In addition to the use of vibroacoustic signals, monitoring is also done on hydrodynamic noises, mainly during trial runs. However, this kind of monitoring is limited because of the necessity of installing sensors in direct contact with the coolant, which involves the use of additional flanges and welds in the in-pile loop.

The state of equipment within the reactor shell is monitored by using methods of analysis of core neutron noises that are measured by four conventional ionization chambers arranged with 90° spacing between them in the plan view.

The state of equipment is diagnosed in the following sequence: deviations in the signal are detected by comparison with the initial signal; the point of onset of the anomaly is located; the specific flaw that is the cause of the anomaly is determined.

As a result of using a continuous monitoring system, equipment defects are revealed as a rule on an early stage of development. For example in 1978, weakening of the impeller mounting was detected in time on one of the main circulating pumps of the fourth generating unit. The pump was shut down and repaired. Without the use of diagnostic monitoring, a flaw of this kind as a rule could not have been detected in time, which could have led to prolonged emergency shutdown of the pump.

Neutron noise monitoring revealed vibration of the core cage of the reactor in the third generating unit with amplitude of less than 0.5 mm. A planned inspection of equipment inside the reactor shell revealed considerable wear at the point where the core cage was fixed in the centering sleeve. After elimination of the flaw, the cage vibration dropped to less than 0.1 mm.

It can be concluded that timely information on the state of equipment during operation of the generating units under load considerably improves the reliability and safety of utilization of nuclear electric facilities with reactors of the VVER type.

Radiation safety and environmental protection. More than fifteen years of experience in operating the Novovoronezhsk Nuclear Electric Facility shows that the production of electric energy in a nuclear electric plant with VVER reactors is reliable from the standpoint of radiation safety.

The work of personnel under conditions where exposure to ionizing radiation can act on the human body is strictly monitored by the dosimetry service.

TABLE 3

Year	Mean annual dose of external irradiation of monitored personnel, rem	Mean daily activity of power plant waste	
		Gas, Ci/day	Aerosol, mCi/day
1965	2.03	282.5	-
1966	2.58	578.7	-
1967	2.34	417.5	-
1968	1.97	223	-
1969	2.30	174	-
1970	2.44	2.7	-
1971	1.91	1.1	-
1972	0.70	56.0	0.023
1973	0.64	82.5	0.32
1974	0.85	112.1	2.23
1975	0.95	116.4	2.26
1976	0.93	28.8	1.29
1977	0.78	18.9	1.43
1978	0.61	39.0	0.71
1979	0.60	15.3	1.71
max. per.	5.0	3500	500

Table 3 summarizes data on mean daily exposure of personnel at the MVAES. These data show that there is a trend toward reduction of exposure, and the dose is much lower than the maximum permissible. On no occasion does the dose of external irradiation exceed the maximum permissible dose at the NVAES.

Table 3 also shows the mean daily radioactivity of gaseous emissions over the entire period of operation of this nuclear facility. This parameter does not exceed 1% of the maximum permissible value.

The table also shows that the radioactivity of aerosol waste with four generating units in operation at the NVAES amounts to 0.1% of the maximum permissible value.

The radiation environment in the vicinity of the nuclear electric plant is monitored by the external dosimetry service. Table 4 shows the results of monitoring with respect to major objects of the external environment.

TABLE 4

Concentration of radioactive materials in air, 10^{-17} Ci/l

Year	At the facility			50 km away		
	Total specific radioactivity	Cs-137	Sr-90	Total specific radioactivity	Cs-137	Sr-90
1974	19.3	0.47	0.42	18.0	0.33	0.34
1975	13.0	0.4	0.51	10.0	0.3	0.53
1976	6.46	0.14	0.08	4.63	0.1	0.06
1977	20.4	0.4	0.16	22.8	0.45	0.17
1978	12.6	0.36	0.27	11.1	0.28	0.22
1979	5.9	0.42	0.3	2.5	0.24	0.14

Concentration of radioactive matter in the water of the Don River, 10^{-12} Ci/l

Year	Upstream of the facility			Downstream of the facility		
1974	10.3	2.6	0.63	9.9	1.97	0.55
1975	11.6	1.37	0.46	9.7	1.46	0.52
1976	8.35	0.58	0.36	8.7	0.32	0.4
1977	10.0	0.43	0.47	8.7	0.42	0.6
1978	12.0	0.88	0.48	9.5	1.25	0.42
1979	9.3	0.8	0.54	8.7	0.7	0.54

Concentration of radioactive matter in bottom sediments of the Don, 10^{-9} Ci/l

1974	9.2	0.22	0.1	7.0	0.12	0.14
1975	18.3	0.07	0.18	12.9	0.18	0.22
1976	13.0	0.14	0.07	10.9	0.15	0.03
1977	11.2	0.07	0.14	7.1	0.11	0.9
1978	15.0	0.11	0.18	22.0	0.49	0.15
1979	3.4	0.16	0.1	5.0	0.17	0.1

We can see from this table that the concentration of radioactive materials in air within the limits of measurement error is the same as beyond 50 km away from the facility. Comparison of the concentrations of radioactive matter in the water and bottom sediments of the Don River upstream and downstream of the nuclear plant also shows a lack of environmental impact on the part of the NVAES.

Training personnel at the vocational education center. Present-day nuclear electric facilities are characterized by complexity of equipment, high intensity of ongoing technological processes and elevated requirements for reliability, safety and economy of operation, which necessitates special training of service personnel. A vocational education center was set up at the Novovoronezhsk Nuclear Facility in 1972 for training both Soviet and foreign specialists for nuclear electric plants with VVER reactors. About 2000 specialists for such nuclear facilities have been trained here since that time.

In 1976, the vocational education center began developing standard curricula for instructing three categories of operational personnel: operative, technical and repair. Personnel are now being trained for 44 positions and trades.

In recent years particular attention has been given to practice in controlling both the reactor and the generating unit as a whole on a trainer at the vocational education center. Work on the trainer is necessary for the operative personnel to get practice in starting and shutdown of the generating unit, in controlling the systems of the unit and in maintaining technological conditions, and also to practice sizing up situations and making operative decisions, especially in eliminating troubles that may arise on operating units. When the trainer is finally put into use, it is planned that instruction will be organized not only for operative personnel in newly constructed nuclear facilities, but also for retraining personnel on operating generating units at nuclear facilties.

The plans for development of the nuclear industry in the Soviet Union call for building a large number of nuclear electric plants in the USSR and elsewhere with Soviet technical assistance. In this connection, a trainer is to be built for the VVER-1000 reactor that will handle 180 trainees per year. Plans also call for installing another trainer for the VVER-440 reactor.

REFERENCES

1. F. Ya. Ovchinnikov et al., "Ekspluatatsiya reaktornykh ustanovok Novovoronezhskogo AES" [Operation of Reactor Units at the Novovoronezhsk Nuclear Electric Plant], Moscow, Atomizdat, 1972.

2. F. Ya. Ovchinnikov et al., "Ekspluatatsionnyye rezhimy vodovodyanykh energeticheskikh yadernykh reaktorov" [Operating Conditions of Water-Cooled Water-Moderated Nuclear Power Reactors], second edition, revised and enlarged, Moscow Atomizdat, 1979.

[8144/0309-6610]

6610
CSO: 8144/0309

INSTRUMENTS, MEASURING DEVICES AND TESTERS, METHODS OF MEASURING, GENERAL EXPERIMENTAL TECHNIQUES

UDC 535.317.2

DISPLACEMENT THRESHOLD AS A CHARACTERISTIC OF THE OPERATING QUALITY OF THE MECHANICAL WORKS OF OPTICAL INSTRUMENTS

Leningrad PRIBOROSTROYENIYE in Russian Vol 23, No 9, Sep 80 pp 80-84

[Article by I. V. Knoroz, Leningrad Institute of Precision Mechanics and Optics]

[Text] A study is made of the possibility of using the displacement threshold as a characteristic of the operating quality of the mechanical works of optical instruments as a function of the functions performed by them in the optical instruments.

The most important operating characteristics of optical instruments are the operating precision and ergonomic nature which in many cases are determined by the operating quality of the mechanical works of which they are made. Nevertheless, judging by the published sources, a substantiated system of operating quality characteristics required both for the design of these mechanisms and for their production and control, has still not been developed.

Let us discuss the operating peculiarities of mechanisms as a function of their purpose in the optical instruments. With respect to functions performed, the kinematic circuits of optical instruments can be basically divided into control circuits and measuring circuits.

Let us consider the positioning or focusing control circuits in more detail (see Figure 1). In this case the operation of the mechanical works is characterized by conversion of a relatively large displacement at the input of the circuit to a relatively small displacement of the servoelement at its exit (for example, the mechanisms for focusing and adjustment devices). This positioning control is realized for a broad list of optical instruments in the manual "correcting" [1] movement mode, for which starting with subsequent halt and, frequently, reversing of movement are characteristic. The correcting mode unavoidably arises in practice always when it is necessary to match the servoelement of the mechanism with a reference element of the object being focused on. Here halting or slowing of the servoelement is used to control the precision of this matching, and in the case of insufficient precision of the achieved match, it is obtained as a result of one or several corrective displacements realized in the same or opposite direction.[1] Obviously the

[1] Similar conditions, generally speaking, also arise in automated tracking systems, and not only in manual control systems.

smaller the achieved corrective displacement, the simpler it is to realize the match with precision determined by the control conditions. (We shall discuss the requirements which can be imposed on the focusing process in more detail later). These small displacements which can still be realized at the output of the specific mechanism are determined by its limiting capabilities under the conditions of a transient dynamic regime (in which the corrective movements are made) and also the limiting capabilities of the operator during his interaction with the control element of the given mechanism [1]. Hereafter we shall call the smallest displacement at the output of the mechanism which can be realized when starting it the "displacement threshold" or "threshold displacement" at the output of the mechanism.

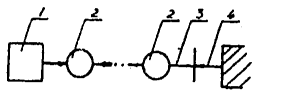

Figure 1. Structural diagram of the positioning control circuit:
1 -- control element; 2 -- elements of the mechanical circuit;
3 -- servoelement; 4 -- reference element of the object focused on.

Let us note that the concept of "threshold" itself does not have a unique interpretation in scientific literature. In each special case the approach to the threshold concept is determined by the peculiarities of the nature of the investigated value, the requirements and the traditions of the specific scientific area [2, 3, 4]. At the same time, the thing in common to all of these approaches can be considered as the most significant; this is the expression of the theoretical limit of some physical process in terms of the threshold concept.

Let us discuss in more detail the differences in positioning control as a function of whether the reference element is discovered or is subject to discovery during the positioning process.

Let the reference element be discovered by some method, for example, let it be observed by the operator (the matching of the image of the object with the cross hair during cross focusing of a microscope). Then the magnitude of the displacement threshold at the output of the mechanism determines the probability of matching the servoelement of the mechanism and the reference element of the object on one attempt at focusing. Under the condition of invariant precision of control of the matching process this probability will be higher the lower the magnitude of the displacement threshold at the output of the mechanism. (A reduction or an increase in the precision of controlling the matching widens or restricts the expedient requirements on the displacement thresholds at the output of the mechanism respectively [5].) Consequently, for the discovered reference element and unregulated number of corrective movements the magnitude of the displacement threshold at the output of the mechanism is an important ergonomic characteristic, for the labor-consumption and duration of the process of matching with given precision depend on it. If it is necessary to match the servo and reference elements with adjustment of the duration of the matching process of a number of corrective displacements (for example, matching with one trial at focusing), then the threshold displacement at the output of the mechanism to a significant degree determines the precision of the realized matching.

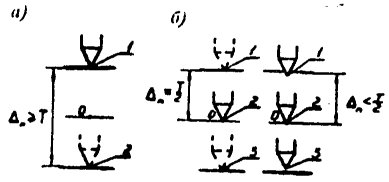

Figure 2. Diagram of the focusing process: $\Delta_п$ — displacement threshold at the output of the focusing mechanism; T — depth of focus zone of the subject's base; 0 — object focused on; 1, 2, 3 — successive positions of the subject point of the objective.

Let us consider the peculiarities of the positioning control for the case where objects subject to discovery in the positioning process (for example, the process of focusing in a microscope) appear in the role of the reference elements. Then the threshold displacement at the output of the mechanism, retaining the ergonomic characteristic or precision, in addition also determines the probability of whether the object of interest to us will be skipped.[1] We see this on considering the focusing process in more detail, which, as is known, consists in displacement of the subject point of the objective depth of focus zone T of the subject's base. Let the magnitude of the displacement threshold at the output of the focusing mechanism exceed the depth of focus for the given microscope objective. If we represent the object in the form of a contrast point[2], then with a displacement threshold at the output $\Delta_п \geq T$, there is a probability of "skipping" through the zone of sharp viewing of the object, and at the same time, skipping it (see Figure 2,a). If the speed of relative displacement of the subject point of the objective on the object is appreciably less than the speed of the sensomotor tracking [6], then the condition

$$\Delta_n \leqslant \frac{1}{2} T \tag{1}$$

guarantees absence of skipping the point object (see Figure 2,b). Here, for the case of $\Delta_п \approx (1/2)T$ the subject point of the objective can be in the zone T 1-3 times during a single one-way pass (considering some small indeterminacy of the physical boundaries of the depth of focus [7]). In the given phase of development of the concepts of the role of the mechanism in the focusing process the expression

$$\Delta_n \leqslant \frac{1}{2} T_{\min}, \tag{2}$$

where T_{min} is the least of the depths of focus for the objectives used in the microscope set, and it can serve as the limiting condition of insuring focusing on the part of the mechanism used.

---

[1] The latter fact is decisive in a number of experiments, and it indicates the functional suitability of the instrument.

[2] This representation of the object permits us to obtain a margin of accuracy when estimating the admissible threshold displacements.

For the investigated cases of use of mechanisms in control circuits, the threshold displacement at the input of the mechanism cannot serve as an independent operating characteristic, but it is of interest for research purposes [1].

Let us consider the peculiarities of the functioning of mechanisms in measuring circuits, and let us discover the role of the displacement thresholds for this case. In the measuring circuits (Figure 3) the mechanisms are used for conversion, as a rule, of a small "signal" displacement to a large one at the output, in accordance with the gear ratio of the mechanism which, in the general case, is a variable. Here the accuracy of realizing the prescribed relation between the displacement at the input and the displacement at the output, that is, the accuracy of realizing the gear ratio, is important. As is known, the values of the gear ratio are calculated without considering friction, the terminal rigidity of the circuit, clearances and dynamic factors which lead to the threshold limit of realizable displacements at the input and output of the mechanism. The displacement thresholds in the mechanisms

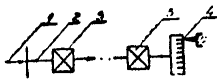

Figure 3. Structural diagram of a measuring circuit: 1 -- signal; 2 -- sensitive element of the measurement circuit; 3 -- measurement circuit elements; 4 -- indicator.

increase the general sensitivity threshold of the measuring instrument which, according to [2], is defined metrologically as a value equal to the zero error, and the relative measurement error in this case is accordingly equal to 100%. Therefore the comparative estimates of the displacement thresholds for different types of mechanisms could serve as the basis when selecting the optimal mechanism for insuring the required operating precision of the measuring circuit of the optical instrument. In the opinion of the author, the displacement thresholds should not have independent significance for production quality control of the mechanisms of measuring circuits.

At the same time it is necessary to note that in many optical instruments the mechanisms simultaneously perform the control function and the measurement function (for example, the precision focusing mechanism of a measuring microscope). For such mechanisms it is important to control both the accuracy of realizing the transfer function and the threshold displacement determining the quality of the mechanism for positioning control.

When substantiating the expediency of using the threshold characteristic for investigation and control of the mechanical works of optical instrument control circuits, the metrological aspects of rating them are not touched on, for this must be the subject of a separate investigation for each case of use of mechanisms depending on the peculiarities of the operating conditions and requirements.

BIBLIOGRAPHY

1. V. V. Kulagin, S. M. Latyyev, "Threshold Sensitivity of the Movement of Precision Mechanisms with Manual Control," OPTIKO-MEKHANICHESKAYA PROMYSHLENNOST' (Optical-Mechanical Industry), No 5, 1973, pp 16, 17.

2. P. V. Novitskiy, OSNOVY INFORMATSIONNOY TEORII IZMERITEL'NYKH USTROYSTV (Fundamentals of the Information Theory of Measuring Devices), Leningrad, Energiya, 1968, p 107.

3. L. A. Ostrovskiy, OSNOVY OBSHCHEY TEORII ELEKTROIZMERITEL'NYKH USTROYSTV (Fundamentals of the General Theory of Electrometering Devices), Leningrad, Energiya, p 101.

4. M. M. Miroshnikov, TEORETICHESKIYE OSNOVY OPTIKO-ELEKTRONNYKH PRIBOROV (Theoretical Principles of Optico-Electronic Instruments), Leningrad, Mashinostroyeniye, 1977, p 19.

5. S. A. Sukhoparov, V. A. Dmitriyev, "Designing Optical Instruments with the Help of Spatial Gear Ratios," TR./LENINGRADSKIY INSTITUT TOCHNOY MEKHANIKI I OPTIKI (Works of the Leningrad Institute of Precision Mechanics and Optics), No 84, 1976, p 18.

6. B. F. Lomov, CHELOVEK I TEKHNIKA (Man and Machine), Moscow, Sov. radio, 1966, p 46.

7. A. N. Zakhar'yevskiy, KONTROL' OPTICHESKIKH SISTEM I PRIBOROV [KONSPEKT LEKTSIY] (Optical System and Instrument Control [Lecture Synopsis]), No 2, izd. LITMO, 1946.

Recommended by Optical Instrument Design and Production Department

Manuscript received 28 Feb 1979

[8144/0258-10845]

10845
CSO: 8144/0258

OPTOELECTRONICS, QUASIOPTICAL DEVICES

UDC 621.372.852.1:621.376.42

QUASIOPTICAL PHASE FREQUENCY SHIFTERS FOR THE MILLIMETER BAND

Moscow RADIOTEKHNIKA in Russian Vol 35, No 10, Oct 80 pp 76-78 manuscript received 11 Jan 80

[Article by B. N. Knyaz'kov, Ye. M. Kuleshov and M. S. Yanovskiy]

[Text] A frequency or frequency spectrum can be shifted by some small amount by using continuous linear phase shifters that produce a time-uniform change of phase displacement. In quasioptical phase shifters for the submillimeter band the frequency displacement is accomplished upon reflection of a circularly polarized wave from a rotating half-wave differential phase section located between reflecting quarter-wave sections, one of which is for linear-to-circular polarization, while the other is for circular-to-linear polarization [Ref. 1].

In the case of oblique incidence of the electromagnetic wave on a rotating half-wave phase section formed by a wire grid backed with a flat reflector, a spectrum of spurious components appears at the output of the device due to spurious phase modulation [Ref. 2]. In this connection, it has been suggested that a 90-degree dihedral corner reflector be used as the half-wave section [Ref. 3], which enables time-linear phase shift of the electromagnetic wave that is reflected.

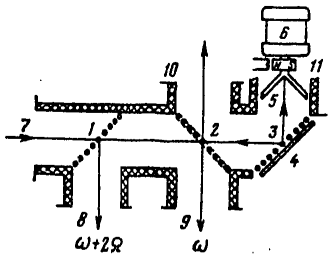

Fig. 1

Fig. 1 shows just such a phase frequency shifter based on a hollow dielectric beam guide [Ref. 4].

Placed in a bend of the beam guide is a reflecting quarter-wave phase section made up of wire grid 3 and stationary flat reflector 4. The grid is made up of parallel wires with a recurrence period much shorter than the wavelength λ. The beam guide is closed by 90-degree dihedral reflector 5 fastened to the shaft of motor 6 with electromagnetic double rotation frequency sensor 11. At the output are two polarization beam splitters with wire grids 1 and 2 in the diagonal planes; the wires of these grids are at an angle of 45° to each other. A wave polarized perpendicularly to the wires of grid 1 enters at input 7. This wave is the fundamental mode of the hollow dielectric beam guide EH_{11} with plane front and axisymmetric amplitude distribution that has a maximum on the axis and falls off toward the periphery of the beam guide in accordance with Bessel law. The wave passes freely through grid 1, and is split on grid 2: half the energy is tapped off to flange 9 and may be sent to the

reference channel of a measurement circuit, while half of the energy passes through grid 2 and enters section 3-4 that produces a quarter-wave path difference between orthogonal components. Produced at the output of the section is a circularly polarized wave that is then incident on corner reflector 5. The phase of the reflected circularly polarized wave is now related to its angle of turn about the axis of the beam guide: rotation of the reflector through angle ψ displaces the phase of the reflected wave by angle 2ψ, and consequently uniform rotation at frequency Ω produces a frequency shift of 2Ω in the reflected signal. When the circularly polarized wave is reflected from the quarter-wave section, it is once more transformed to linear polarization. It passes freely through grid 2, and is split on grid 1: half the power (1/4 the power of the input signal) goes to output flange 8 from which it can be directed to the measurement channel of the circuit.

Imprecision in tuning section 3-4 to the quarter-wave differential phase shift, or frequency dependence of the phase shift for fixed tuning of the section leads to a spurious component in the spectrum of the output signal. When the phase shift deviates from the nominal ($\pi/2$) by an amount δ, an elliptically polarized wave appears at the output of the quarter-wave section that can be represented as two components with orthogonal circular polarization. Upon reflection from the rotating corner reflector the useful component is shifted in frequency by $(\pm)2\Omega$, and the spurious component acquires a "mirror" displacement by $(\mp)2\Omega$. After secondary reflection from the phase section and splitting by grid 1, we get a useful signal at the output (flange 8) of the form $\frac{1}{2}\cos^2\frac{\delta}{2}\sin(\omega(\pm)2\Omega)t$ and a spurious signal on the "mirror" frequency $\frac{1}{2}\sin^2\frac{\delta}{2}\sin(\omega(\mp)2\Omega)t$. In addition, a signal $\sin\delta\cos 2\Omega t\sin\omega t$ is reflected from grid 2 to flange 10 that contains components with frequency $\omega+2\Omega$ and $\omega-2\Omega$. A signal on the difference frequency 4Ω is induced at the output of a detector connected to this flange. Fine adjustment of the phase section to the quarter-wave phase shift in the working device can be conveniently done with respect to the minimum of this signal, or with respect to the minimum of the detected signal on frequency 4Ω at the output 8.

In essence, this device is a phase shifter of the frequency of the reflected wave in which a system of polarization splitters isolates 1/4 of the power on the displaced frequency. If a circulator had been included, it would have been possible to convert all the power to the signal on the shifted frequency. However, there are no circulators for the submillimeter band, and therefore the phase frequency shifter was based on rotating corner reflectors. This device converts all the power that reaches it to signal power on the shifted frequency, i. e. it is a phase shifter of the transmitted wave frequency [Ref. 5] (Fig. 2). In polarization beam splitters 6 and 7 the grid wires form an angle of 45° to one another. The two adjacent arms of splitter 7, lying to either side of the grid, are closed by 90-degree dihedral corner reflectors 3 and 4 placed on the ends of the one-piece shaft of motor 5 and turned through 90° relative to one another. In arms I and II are 45-degree beam guide bends with movable reflectors in front of which are wire grids that form quarter-wave differential phase sections 1 and 2.

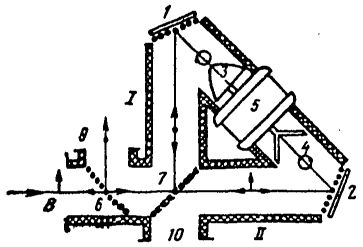

Fig. 2

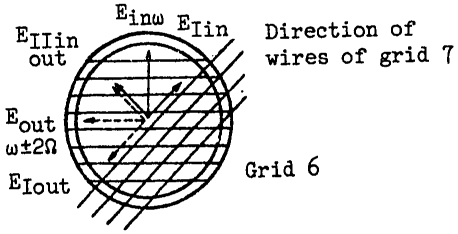

Fig. 3

Input electromagnetic wave E_{in} (Fig. 3) passes through grid 6 without attenuation, and is split by grid 7 equally between the two arms of the splitter E_{Iin} and E_{IIin}. The orientation of grids of sections 1 and 2 is chosen so that if a wave with left-hand circular polarization is excited on the output of section 1, a wave with right-hand polarization is excited at the output of section 2, or vice versa. In this event the waves reflected from corner reflectors 3 and 4 acquire a frequency shift of the same sign (-2Ω or $+2\Omega$), depending on whether the directions of circular polarization and rotation of the corner reflectors do or do not coincide. As a result, two waveforms with orthogonal linear polarization on the displaced frequency show up on the section of beam guide between grids 7 and 6. Waveform E_{Iout} that is produced in arm I is polarized parallel to the wires of grid 7, while E_{IIout} that is formed in arm II is polarized perpendicular to these wires. Since corner reflectors 3 and 4 are turned through 90° relative to one another, one of these waveforms acquires an additional 180-degree phase shift, and the resultant wave E_{out} is polarized parallel to the wires of grid 6, and is reflected by this grid to output flange 9. Thus a transmission frequency shifter circuit can be made by using a rotating system of two reflecting dihedral corner reflectors without the aid of a circulator.

Let us denote deviations of the differential phase shift in sections 1 and 2 from $\pi/2$ by δ_1 and δ_2 respectively. Then in output channel 9 we get useful signal

$$E_c = \frac{1}{2}\left(1 + \cos\frac{\delta_1+\delta_2}{2}\cos\frac{\delta_1-\delta_2}{2}\right)\sin(\omega_{(-)}^{+}2\Omega)t$$

and spurious signal on the "mirror" frequency

$$E_з = \frac{1}{2}\left(1 - \cos\frac{\delta_1+\delta_2}{2}\cos\frac{\delta_1-\delta_2}{2}\right)\sin(\omega(\mp)2\Omega)t.$$

When $\delta_1 = \delta_2 = \delta$, the amplitudes of these signals will be $\cos^2\frac{\delta}{2}$ and $\sin^2\frac{\delta}{2}$ respectively, and the level of the waveform on the "mirror" frequency with respect to the useful signal on the shifted frequency will be $\tan^2\frac{\delta}{2}$. In auxiliary channel 10 we get components: polarized perpendicular to the wires of grid 7 $E_\perp = \sin\delta_1\cos 2\Omega t\sin\omega t$ and parallel to these wires $E_\parallel = \sin\delta_2\cos 2\Omega t\sin\omega t$. By adding a detector to arm 10 that receives one of the polarized signals, we can carry out separate tuning of sections 1 and 2 to the quarter-wave differential phase shift with respect to the minimum on frequency 4Ω.

The described frequency shifters were made on the basis of a hollow dielectric beam guide 20 mm in diameter; wire grids were used with a period of 30 μm and wire 8 μm

in diameter. Frequency shifters with tunable phase sections operated in a wave band of 0.5-2.2 mm. With fixed tuning of the phase sections, the level of the spurious component of the output signal spectrum relative to the useful signal on the shifted frequency was less than -40 dB in the range of ±15% of the tuned frequency of the sections. The speed of rotation of the corner reflectors reached 9000 rpm, where the frequency shift was 300 Hz. Attenuation in the beam guide system of the device was about 1 dB on a 0.5 mm wave, and increased to 3 dB toward the long-wave section of the band.

REFERENCES

1. M. S. Yanovskiy, B. N. Knyaz'kov, IZV. VUZov: RADIOELEKTRONIKA, Vol 13, No 10, 1970.

2. B. N. Knyazkov, M. S. Yanovskiy, RADIOTEKHNIKA, Vol 27, No 9, 1972.

3. B. N. Knyaz'kov, Ye. M. Kuleshov, M. S. Yanovskiy, "A Quasioptical Phase Shifter," USSR Patent No 439866.

4. A. I. Goroshko, Ye. M. Kuleshov, in: "Radiotekhnika" [Radio Engineering, a Collection of Papers], Khar'kov, Khar'kov State Univ., No 21, 1972.

5. M. S. Yanovskiy, B. N. Knyaz'kov, "A Modulator of the Plane of Polarization," USSR Patent No 508895.

[86-6610]

6610
CSO: 1860

UDC 621.383.98

CHOOSING THE LOAD RESISTANCE OF A PHOTODIODE IN PULSED OPTOELECTRONIC SYSTEMS

Moscow RADIOTEKHNIKA in Russian Vol 35, No 10, Oct 80 pp 72-74 manuscript received 10 Apr 80

[Article by F. I. Khaytun and I. Ye. Zamanskaya]

[Text] The ever increasing use of high-resistance photodiodes in pulsed lidar and optical communication systems combined with the current trend toward shortening transmitted signals (to tens of nanoseconds and less) makes it necessary to account for the influence that time lag of the photodetector circuit has on the characteristics of systems, and to use care in choosing the parameters of the photodetector circuit for different signal processing requirements in the reception channel.

Thus the problem arises of rational choice of the load resistance R_H of the photodiode not only for optimum reception [Ref. 1, 2], but also under conditions where the passband of the channel is maintained constant (preset), and may differ considerably from the optimum when $R_H = \text{var}$.

Principal Relations. Notation on the block diagram of the reception channel (Fig. 1): $\Phi_c(t)$--signal flux on the photodetector; ε--current sensitivity of the photodiode; $i_c(t)$, $S(i\omega)$--signal photocurrent and spectrum; $G_1 = 2eI_0 + 4kT^0/R_H$--spectral noise density of the photodetector circuit; I_0--constant component of photodiode current; e--charge of the electron; k--Boltzmann's constant; T^0--absolute temperature; $G_2 = \bar{e}_V^2/R_H^2$--equivalent spectral noise density of the amplifier (with respect to current); $K_1(i\omega)=(1+i\omega T)^{-1}$--transfer function of the photodetector circuit; $T = R_H C$; C--overall capacitance of the input circuit; $K_2(i\omega)$--transfer function of the amplifier.

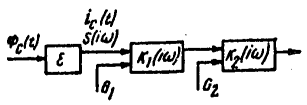

Fig. 1

The transfer function of the channel, which differs from the optimum in scaling conversion, takes the form [Ref. 3]

$$K(i\omega) = K_{opt}(i\omega/n) = \frac{aS^*(i\omega/n)\,e^{-i\omega t_0/n}}{G_1 + G_2|K_1(i\omega/n)|^2},$$

and signal-to-noise ratio μ for symmetric input pulses takes the form

$$\mu = \frac{\left(\frac{2}{\pi G_1}\right)^{\frac{1}{2}} \int_0^\infty \frac{|S(i\omega)|\,|S(i\omega/n)|\,d\omega}{1+m+mT^2\omega^2/n^2}}{\left[\int_0^\infty \frac{(1+m+mT^2\omega^2)\,|S(i\omega/n)|^2\,d\omega}{(1+m+mT^2\omega^2/n^2)^2}\right]^{1/2}}, \qquad (1)$$

where $m = m(R_H) = G_2/G_1$.

Functions $n(R_H)$ at $\Delta\omega_T = \text{const}$ with other parameters of the reception system predetermined can be calculated by using an expression for the effective noise passband of the channel:

$$\Delta\omega_T = \frac{\int_0^\infty |K(i\omega)|^2 d\omega}{K^2(0)} = \frac{(1+m)^2}{S^2(0)} \int_0^\infty \frac{|S(i\omega/n)|^2 d\omega}{(1+m+mT^2\omega^2/n^2)^2}.$$

Next let us consider a gaussian signal $i_c(t) = A\varepsilon e^{-\pi(t/\tau)^2}$, where A is the amplitude of radiant power on the photodetector; τ is duration of the signal pulse on a level of ≈ 0.5max.

After rather lengthy integration and a number of transformations, we can get from expression (1)

$$\mu = \frac{A\varepsilon \left(\frac{2\sqrt{2}}{\sqrt{\pi}} \frac{n\tau^2}{1+n^2}\right)^{1/2} H(\beta_1)}{C\bar{e}_y \beta \left\{H(\beta)[1-2\beta^2+n^2(1+2\beta^2)] + \frac{2\beta^2}{\sqrt{\pi}}(1-n^2)\right\}^{1/2}}, \qquad (2)$$

where

$$\beta = \beta(R_\Sigma) = \frac{\tau}{T}[(1+m)/2\pi m]^{1/2} = (\tau/\sqrt{2\pi}\,\bar{e}_y C)\left(2eI_0 + 4KT^2/R_\Sigma + \bar{e}_y^2/R_\Sigma^2\right)^{1/2}, \qquad (3)$$

$$\beta_1 = \beta\left(\frac{n^2+1}{2}\right)^{1/2}, \quad H(x) = x[1-\operatorname{erf}(x)]e^{x^2}, \quad \operatorname{erf}(x) = \frac{2}{\sqrt{\pi}}\int_0^\infty e^{-x^2} dx.$$

With optimum filtration ($n = 1$) we get from (2)

$$\mu_{n=1} = M = A\varepsilon[\tau^2 H(\beta)]^{1/2}/\sqrt[4]{2\pi}\,C\bar{e}_y \beta.$$

The degree of relative reduction in signal-to-noise ratio due to departure from the optimum filtration conditions can be characterized by the expression

$$\alpha = \frac{\mu}{M} = \frac{2[n/(1+n^2)]^{1/2} H(\beta_1)}{H^{1/2}(\beta)\left\{H(\beta)[1-2\beta^2+n^2(1+2\beta^2)] + \frac{2\beta^2}{\sqrt{\pi}}(1-n^2)\right\}^{1/2}}.$$

Thus at a given value of $n \neq 1$ the quantity α depends only on the parameter β that gives a generalized characterization of the influence that the time lag of the photodetector circuit has on conditions of signal detection. Having determined function $n(\beta)$, we can find $\mu(\beta)$, $\alpha(\beta)$ and for other predetermined parameters with consideration of (3), we can find relations $\mu(R_H)$ and $\alpha(R_H)$.

For the width of the passband of the channel we can write the expression [Ref. 4]

$$\Delta\omega_T = \frac{\pi\sqrt{\pi}\,n}{2\sqrt{2}\,\tau}\left[H(\beta)(1-2\beta^2) + \frac{2}{\sqrt{\pi}}\beta^2\right]. \qquad (4)$$

At $n = 1$, formula (4) defines the optimum width of the channel passband. Let us assume that the quantity $\Delta\omega_T$ must be fixed from the condition

$$\Delta\omega_T = \Delta\omega_c/b = \pi\sqrt{2}/\tau b, \qquad (5)$$

where $\Delta\omega_c$ is the effective width of the signal spectrum, $b = \text{const}$. Then from (4) and (5) we find the required value of the coefficient of relative widening of the passband:

$$n = \frac{2b}{\sqrt{\pi}} \left[H(\beta)(1 - 2\beta^2) + \frac{2}{\sqrt{\pi}} \beta^2 \right]^{-1}.$$

Results of Calculations. Calculations were done as applied to the following initial parameters of the system:

$$\tau = 20 \text{ ns } (\Delta f_c = \Delta\omega_c/2\pi = 17.7 \text{ MHz}),\ I_0 = 10^{-7} \text{ A},\ C = 10 \text{ pF},$$

$$\bar{e}_y = 2.45 \cdot 10^{-9} \text{ V/Hz}^{1/2},\ b = 1,\ 2,\ 3\ (\Delta f_T = \Delta\omega_T/2\pi = 17.7 \text{ MHz},\ 8.85 \text{ MHz},\ 5.9 \text{ MHz}).$$

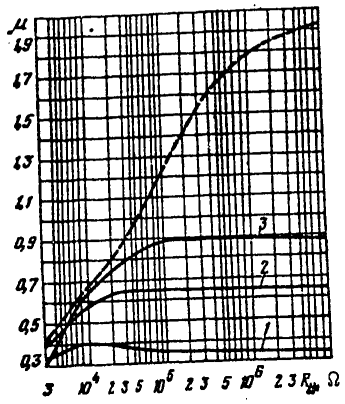

Fig. 2

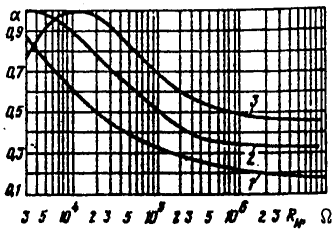

Fig. 3

Shown in Fig. 2 are curves for $\mu(R_H)$ for the three assumed values of Δf_T, and also the curve for $M(R_H)$ corresponding to optimization of the channel passband for each value of R_H (broken curve).

If the fixed passband of the channel is wide enough, curve $\mu(R_H)$ may have an extremum (curve 1), in which case an increase of R_H beyond some limit (here about 10^4 Ω) results in some reduction of signal-to-noise ratio. Even if the maximum of $\mu(R_H)$ is faint or nearly absent (curves 2, 3), the limits of effective increase in R_H at $\Delta f_T = \text{const}$ may be considerably displaced as compared with optimum filtration.

For example at $\Delta f_T = 8.85$ MHz (curve 2) the limit of practically feasible increase in R_H does not exceed $(2\text{-}3) \cdot 10^4$ Ω, whereas with optimum filtration this limit is approximately 10^7 Ω.

The resultant data also show the price paid for expansion of the channel passband from the standpoint of conditions of signal detection. For example increasing Δf_T from 5.9 MHz to 17.7 MHz reduces μ by a factor of approximately 2.2 (with the most favorable choice of R_H).

The loss in $[\alpha]$ as compared with optimum filtration is even greater, as shown by curves for $\alpha(R_H)$ in Fig. 3.

The results may be of use in development of pulsed lidar and optical communication systems with photodiode receivers.

REFERENCES

1. G. V. Voyshvillo, A. M. Romanov, Ye. G. Lebed'ko, RADIOTEKHNIKA, Vol 25, No 10, 1970.

2. V. A. Markin, OPTIKO-MEKHANICHESKAYA PROMYSHLENNOST', No 12, 1973.

3. F. I. Khaytun, Ye. G. Lebed'ko, OPTIKO-MEKHANICHESKAYA PROMYSHLENNOST', No 11, 1970.

4. R. B. Shemshedinov, F. I. Khaytun, Ye. G. Lebed'ko, OPTIKO-MEKHANICHESKAYA PROMYSHLENNOST', No 1, 1978.

[86-6610]

6610
CSO: 1860

UDC 535.8

LIGHT VALVE SYSTEMS WITH LASER LIGHT SOURCE

Leningrad PRIBOROSTROYENIYE in Russian Vol 23, No 9, Sep 80 pp 77-80

[Article by V. V. Khvalovskiy, S. N. Natarovskiy, Yu. V. Fedorov, Leningrad Institute of Precision Mechanics and Optics]

[Text] A study is made of the special operating characteristics of a light valve system with a coherent light source. Various versions of the construction of the optical system are investigated.

In modern light valve instruments most frequently powerful and superpowerful thermal sources, for example, superhigh pressure xenon tubes, are used as the light source for displaying nonabsorbing objects (for example, of the thermoplastic recording type). This arises, on the one hand, from the small admissible size of the source (restricted by the minimum angle of diffraction on the object) and, on the other hand, by the necessity for obtaining quite high illumination of the image.

The application of the indicated sources makes the heat balance of the instrument appreciably worse. In order to reduce the heating, the circuitry and the structural design of the instrument are complicated by introducing heat filters, thermal insulation and forced ventilation. In addition, the presence of a continuous radiation spectrum in the visible and infrared ranges of this type of source leads to the fact that the contrast transmission function of the projection objective on all spatial frequencies, in addition to zero, is less than one, that is, the image contrast of the fine details of the object is lowered [1]. All of this has a negative effect on the operating and technological characteristics of the instruments.

The use of a laser [2] with focusing lens of the light source in a light valve system permits the thermal heating characteristic of thermal sources and the reduction in image contrast to be avoided, but the grainy structure of the image in this case lowers its quality which is exhibited especially sharply in visual type instruments. Then the image consists of so-called aventurine dots. This deficiency is controlled by illuminating the object with the scattered laser light beam [3]. Frosted glass or liquid media with randomly moving particles (for example, a milk solution in water or liquid crystals) are used as the dispersing agent. However, these dispersion techniques lead to loss of coherent illumination and, consequently, to loss of image contrast of the small details of the object [4]. In addition, they have little advantage energywise.

The graininess of the image can be reduced significantly by installing a lens raster in the light valve projector system. The optical system can be built, as is shown

in Figure 1. It operates as follows: laser 1 emits a monochromatic light beam of essentially parallel rays which are scattered by the lens raster 2 in the volume of space limited by the raster aperture. The light beams completely fill the input aperture of the condenser 4 by means of the collector 3. After passage through the condenser, the light beams illuminate the nonabsorbing object 5 and reach the projection objective 6. The light beams which have passed through the object without refraction (diffraction) on its relief are screened out by the blank 7 and do not participate in the structure of the image. The light rays which undergo refraction (diffraction) on the object are not screened out by the blank 7 and construct the image of the viewed object on the screen 8.

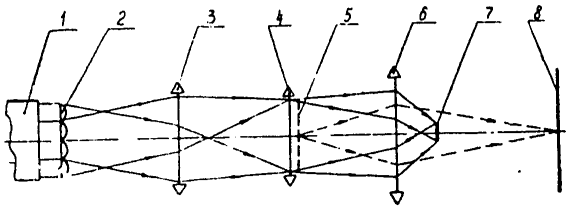

Figure 1.

In this system the viewing diaphragm (or blank) 7 is installed in the rear equivalent focal plane of the entire optical system including the condenser and the projection objective in itself, and the lens raster is installed in the plane conjugate to the entrance pupil of the illuminating part of the system. The installation of the lens raster in the indicated plane permits the interference conditions on the microunevennesses of the object to be altered in such a way that the grainy structure of the image is decreased to limits such that its influence becomes insignificant (it goes beyond the limits of resolution of the projection objective). Other versions of execution of this system can be used (see Figures 2, 3).

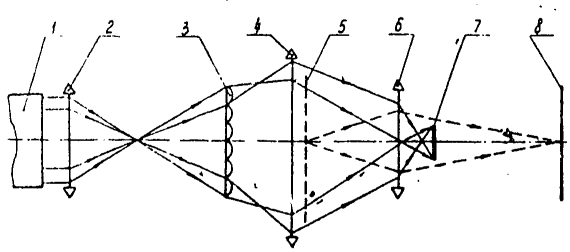

Figure 2.

The operation of the optical system shown in Figure 2 is analogous to the operation of the preceding one. The advantage of this optical system is that the lens raster 3 installed between the collector 2 and the condenser 4 operates in a wider light beam and, consequently, a larger number of lens elements of the raster 3 participate in the scattering of the light. Therefore, damage to one or several elements of the raster in practice does not disturb its properties as a light dispersing medium. Thus, it is possible to lower the technological requirements on manufacturing the lens raster.

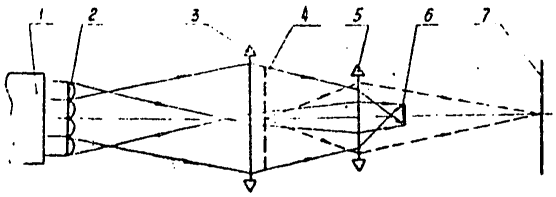

Figure 3.

The operation of the system presented in Figure 3 is also analogous to the one investigated above. A characteristic feature of this system is the fact that the lens raster 2 plays the role of a collector in addition to the role of the light beam dispersing medium. This simplifies the optical system (the total number of optical surfaces decreases), and it increases its physical lens speed, for the transmission coefficient of the system is increased somewhat.

The application of a laser as the light source insures coherence of the illumination for which the normalized contrast transmission function of the projection objective and all the remaining optical elements is constant with respect to the entire frequency pass band of the optical system, and it is equal to one. Thus, the image contrast of the viewed nonabsorbing object is undistorted (with small residual aberrations of the projection objective), and maximal with respect to magnitude. In addition, it is expedient to use a lens raster in the system which permits redistribution of the light beam energy to be obtained without loss of degree of coherence, for which the graininess of the image is significantly reduced, and the mode structure is entirely absent. In practice complete absence of heating of the elements of the optical system permits us not to use the heat protection means, which significantly simplifies the structural design of the light valve projector. In Figure 4,a [not reproduced], a photograph of the image of a phased test object is presented which was obtained on a mockup of a Schlieren projector constructed by the diagram in Figure 2, and an image of the same object illuminated directly by a laser light beam from which the lens raster has been taken out is presented for comparison in Figure 4,b [not reproduced].

BIBLIOGRAPHY

1. J. Goodman, VVEDENIYE V FUR'YE-OPTIKU (Introduction to Fourier Optics), Moscow, Mir, 1970.

2. V. M. Vaksman, G. V. Mikhaylik, "Mapping of Phased Images in a Schlieren Projector with a Coherent Light Source," ZHURNAL NAUCHNOY I PRIKLADNOY FOTOGRAFII I KINEMATOGRAFII (Journal of Scientific and Applied Photography and Kinematography), Vol 22, No 6, 1977.

3. L. M. Soroko, OSNOVY GOLOGRAFII I KOGERENTNOY OPTIKI (Fundamentals of Holography and Coherent Optics), Moscow, Nauka, 1971.

4. A. S. Toporets, "Interrelation of the Degree of Coherence of Diffusely Scattered Light Using the One Slit Method," OPTIKO-MEKHANICHESKAYA PROMYSHLENNOST' (Optical-Mechanical Industry), No 11, 1975.

Recommended by the Department of Optical Devices Theory

Manuscript received 11 April 1979

[8144/0258-10845]

10845
CSO: 8144/0258

PUBLICATIONS, INCLUDING COLLECTIONS OF ABSTRACTS

UDC 621.396.029.64:621.753.001.24

CALCULATING PRODUCTION TOLERANCES OF MICROWAVE DEVICES

Leningrad RASCHET PROIZVODSTVENNYKH DOPUSKOV USTROYSTV SVCh in Russian 1980 signed to press 14 Jan 80 pp 2, 145-147

[Annotation and table of contents from book "Calculating Production Tolerances of Microwave Devices", by Yevgeny Aleksandrovich Vorob'yev, Izdatel'stvo "Sudostroyeniye", 3700 copies, 148 pages]

[Text] The book examines methods of calculation and rational designation of production tolerances for microwave components, microwave assemblies and standard microwave devices most extensively used at the present time in ground-based, shipborne and airborne radar and radionavigation facilities as well as in microwave monitoring and measurement instrumentation.

The main thrust of the book is to present up-to-date methods of calculating production tolerances and studying the most successful engineering design decisions that ensure high technical quality of electronic equipment in the microwave band.

The book is intended for radio engineers and technologists working in the area of developing and producing microwave devices, and also for instructors, graduates and undergraduate students in the electronics departments of colleges and universities.

Contents

6610
CSO: 1860

UDC 681.883.67(075.3)

HYDROACOUSTIC TRANSDUCERS AND ANTENNAS

Leningrad GIDROAKUSTICHESKIYE PREOBRAZOVATELI I ANTENNY in Russian 1980 signed to press 24 Apr 80 pp 228-230

[Annotation and table of contents from book "Hydroacoustic Transducers and Antennas", by Gregoriy Mikhaylovich Sverdlin, Izdatel'stvo "Sudostroyeniye", 3800 copies, 232 pages]

[Text] This is a textbook for intermediate special academic institutions in specialty No 0649. It outlines the principles of operation of hydroacoustic transducers of the types most extensively used in hydroacoustic antennas, the theory of directionality and the theory of calculating and designing hydroacoustic transducers.

Methods of calculating and constructing hydroacoustic transducers and antennas are presented.

The book contains examples of calculation of typical hydroacoustic transducers and antennas, and data in the form of reference tables and graphs.

The book is intended for students of technical schools and may be of use to those attending colleges and universities with major in applied hydroacoustics, as well as to engineers working in this field.

Contents

[88-6610]

6610
CSO: 1860

UDC 621.3.049.77:681.518.3

INTEGRATED ELECTRONICS IN MEASURING INSTRUMENTS

Leningrad INTEGRAL'NAYA ELEKTRONIKA V IZMERITEL'NYKH USTROYSTVAKH in Russian 1980 signed to press 22 Apr 80 pp 2, 246-247

[Annotation and table of contents from book "Integrated Electronics in Measuring Instruments", by Valentin Sergeyevich Gutnikov, Izdatel'stvo "Energiya", 40,000 copies, 248 pages]

[Text] The book deals with the use of series-produced analog and logic ICs for making standard functional units of measurement devices. Particular attention is given to methods of designing various measurement transducers (including precision amplifiers) based on integrated opamps. An examination is made of the particulars of using integrated switches, multipliers, comparators and so on. Varieties of logic ICs are described as well as their use for realizing logic functions, making registers, counters, code-to-frequency converters and the like. The presentation of the material is accompanied by a condensed theoretical analysis. The examples that are given are based on up-to-date Soviet ICs.

The book is intended for a wide class of specialists and studnets engaged in the development and investigation of electronic measurement equipment.

Contents

6610
CSO: 1860

UDC 681.84.083.8:534.14

MEASURING INSTABILITY OF THE SPEED OF A RECORDING MEDIUM

Moscow IZMERENIYE NESTABIL'NOSTI SKOROSTI NOSITELYA ZAPISI in Russian 1980 signed to press 12 May 80 pp 2, 102-103

[Annotation and table of contents from book "Measuring Instability of the Speed of a Recording Medium", by Mark Vladimirovich Laufer, Izdatel'stvo "Svyaz'", 2450 copies 104 pages]

[Text] An analysis is made of the instability of the speed of a recording medium based on the time scale function. An examination is made of the influence that this instability has on recording-playback processes for different kinds of data. Methods and devices are given for measurements of speed instability in the record-playback mode.

The book is intended for engineering and technical workers engaged in the development and application of various devices for information recording and playback.

Contents

[89-6610]

6610
CSO: 1860

UDC 621.396.62:[623.61:455.40]+621.317.757

PANORAMIC RECEIVERS AND SPECTRUM ANALYZERS

Moscow PANORAMNYYE PRIYEMNIKI I ANALIZATORY SPEKTRA in Russian 1980 signed to press 15 Dec 79 pp 2, 348-350

[Annotation and table of contents from book "Panoramic Receivers and Spectrum Analyzers", by Valentin Alekseyevich Martynov and Yuriy Ivanovich Selikhov, Izdatel'stvo "Sovetskoye radio", second revised and enlarged edition, 10,000 copies, 352 pages]

[Text] An examination is made of the principal methods of spectral analysis and the fundamentals of design of panoramic receivers and spectrum analyzers. The purpose and areas of application of panoramic devices are defined, and the requirements are formulated for their major characteristics. An analysis is made of physical processes in the main channels of these devices, and recommendations are given on optimizing their design under realistic operating conditions. Block diagrams of panoramic devices are considered as well as design variations and problems of displaying, recording and processing the results of analysis. Descriptions are given of some panoramic receivers and spectrum analyzers presently being used (the first edition was published in 1964).

The book is intended for specialists working on development of the pertinent equipment or using it to analyze radio emissions. It may be of use to instructors and students in colleges and universities specializing in appropriate fields.

Contents

[87-6610]
6610
CSO: 1860

UDC 621.313.13:537.228.1

PIEZOELECTRIC MOTORS

Moscow P'YEZOELEKTRICHESKIYE DVIGATELI in Russian 1980 signed to press 12 Mar 80 pp 2, 109-110

[Annotation and table of contents from book "Piezoelectric Motors", by Vyacheslav Vasil'yevich Lavrinenko, Igor' Aleksandrovich Kartashev and Vladimir Sergeyevich Vishnevskiy, Izdatel'stvo "Energiya", 7000 copies, 112 pages]

[Text] A study is made of the structural designs and the mechanism of the operation of various piezoelectric motors; their specifications are presented. Recommendations are made with respect to the engineering design of the indicated motors. The problems connected with the development of power supply for piezoelectric motors and also the problems of the manufacturing technology for such motors and the problems of measuring their characteristics are investigated.

The book is designed for engineers working in the field of building and using electric motors and also for engineering-technical workers involved with the design of radioelectronic equipment.

Contents

10845
CSO: 1860

UDC 621.391.037.372

DIGITAL DATA TRANSMISSION IN RADIO COMMUNICATIONS

Moscow TSIFROVAYA PEREDACHA INFORMATSII V RADIOSVYAZI in Russian 1980 signed to press 6 Feb 80 pp 2, 254-255

[Annotation and table of contents from book "Digital Data Transmission in Radio Communications", by Mikhail Semenovich Nemirovskiy, Izdatel'stvo "Svyaz'", 6500 copies, 256 pages]

[Text] This book contains a brief discussion of the problems of constructing digital data transmission systems. The paper consists of several parts, each of which is devoted to a group of closely related problems and devices.

The first part of the book discusses the problems of analog-to-digital and digital-to-analog conversions during data transmission. Admissible accuracies of conversion of analog data to digital form with PCM modulation and Δ-conversions, means of optimizing the parameters of the corresponding devices, methods of achieving conversion accuracies close to the potentially possible accuracies are analyzed. A description is also presented of methods of converting digital data to an analog signal designed for transmission over communication channels with restricted pass band.

The second part of the book discusses the problems of demodulation of digital radio signals in the presence of interference. The noiseproofness of the basic keying methods is defined considering signal distortions in the filter sections of the receiver. A description is given of the structure of the corresponding receivers, and the noiseproofness losses caused by nonidealness of individual sections of the structure are estimated.

In the third part of the book a study is made of the problems pertaining to the noise-proof encoding of digital data. The structure of block and super-precise codes and the principles of constructing economical decoders are described. The effectiveness of the various codes is estimated as a function of the keying method used in the radio line, the amount of instability of the carrier frequency and other parameters.

The fourth part of the book is devoted to the study of the noiseproofness of automatic frequency control systems and cadence synchronization systems widely used in the receivers of digital communication lines. Recommendations are made with respect to optimizing the parameters of these systems.

In the fifth part of the book a description is presented of the basic methods of time multiplexing and sharing of digital signal; known methods of asynchronous input are analyzed; the characteristics insured by them and the efficient areas of use of each of these methods are defined.

The sixth part of the book is on the specific problem of multistation access occurring when building prospective communication lines with the radio relay on an artificial earth satellite. The basic methods of multistation access are described, and their energy efficiency is defined.

Thus, the book material familiarizes the reader with the basic ideas of the corresponding areas of engineering, the results achieved and the prospects for further development. The discussion is carried to the calculation relations suitable for use in engineering practice and includes a number of original results.

The book is intended for scientific workers involved with the development of communications equipment.

There are 99 illustrations, 15 tables and 67 references.

Contents

10845
CSO: 1860

UDC 621.3.0853:532.783

LIQUID CRYSTAL DISPLAYS

Moscow INDIKATORNYYE USTROYSTVA NA ZHIDKIKH KRISTALLAKH in Russian 1980
signed to press 16 Jan 80 pp 2, 239-240

[Annotation and table of contents from book "Liquid Crystal Displays", by Zenon Yur'yevich Gotra, Eduard Pavlovich Dzisyak, Leonard Kazimipovich Vistin', Lyubomir Mikhaylovich Smerklo, Valentin Vasil'yevich Parkhomenko, and Vasiliy Teodorovich Fechan, Izdatel'stvo "Sovetskoye radio", 10,000 copies, 240 pages]

[Text] A discussion is presented of the state of the art in the development of liquid crystal displays. The basic physical properties and electrooptical effects in liquid crystals are investigated. Process-design recommendations are made with respect to the execution of the displays.

The book is designed for a broad class of engineering and technical workers and students involved with the problems of the investigation, development, production and application of liquid crystal displays.

Contents

[59-10845]

10845
CSO: 1860

UDC 621.391.1

FUNDAMENTALS OF THE THEORY AND DESIGN OF INFORMATION SYSTEMS

Moscow OSNOVY TEORII I RASCHETA INFORMATSIONNO-IZMERITEL'NYKH SISTEM in Russian 1980 signed to press 25 Dec 79 pp 2, 278-280

[Annotation and table of contents from book "Fundamentals of the Theory and Design of Information Systems", by Oleg Nikolayevich Novoselov and Aleksey Fedorovich Fomin, Izdatel'stvo "Mashinostroyeniye", 9000 copies, 280 pages]

[Text] A discussion is presented of the fundamentals of the theory and design of measurement data gathering, representation and transmission means. The data processing problems pertaining to the reproduction of continuous transmissions and improvement of their reliability at the system output are investigated, and standard examples of the calculations are given.

The book is designed for engineering-technical and scientific workers dealing with the planning, design, operation and maintenance of information measuring systems and automated control systems (ASU).

Contents

10845
CSO: 1860

UDC 621.397.61

TELEVISION TRANSMITTING STATIONS

Moscow PEREDAYUSHCHIYE TELEVIZIONNYYE STANTSII in Russian 1980 signed to press 5 Mar 80 pp 2, 327-328

/Annotation and table of contents from book "Television Transmitting Stations", by Aleksandr Mikhaylovich Varbanskiy, Izdatel'stvo"Svyaz'", 7000 copies, 328 pages/

[Text] A study is made of the structure of the television transmitting network and methods of planning the placement of television transmitting stations. A description is given of the equipment of standard television transmitters, television relays and antenna-feeder devices. The problems of the design and organization of the operation of television transmitting stations are discussed.

The book is designed for engineering and technical workers involved with the development, operation and maintenance of television transmitting stations, and it can also be useful to students of the higher institutions of learning specializing in the field of television transmission engineering.

Contents

10845
CSO: 1860

UDC 621.372.8

WAVEGUIDE DIELECTRIC FILTERS

Moscow VOLNOVODNYYE DIELEKTRICHESKIYE FILTRY in Russian 1980 signed to press 20 Mar 80 pp 2, inside back cover

[Annotation and table of contents from book "Waveguide Dielectric Filters", by Boris Yulianovich Kapilevich, Izdatel'stvo "Svyaz'", 3400 copies, 136 pages]

[Text] A study is made of the problems of the calculation and design of small microwave filters based on waveguide-dielectric structures with evanescent couplings. Examples of the practical realization of multisection filters are presented. FORTRAN-IV programs for analyzing the frequency characteristics of evanescent resonators and filters are described in the appendices.

The book is designed for engineering and technical workers involved with the calculation, design and construction of microwave equipment, and it can also be useful to postgraduate students and students in the advanced courses at the institutions of higher learning.

Contents

[56-10845]

10845
CSO: 1860

END